IMPLICATIONS FOR VOLCANIC HAZARDS IN THE CENTRAL AND SOUTHERN CASCADES BASED ON GAS EMISSIONS DURING EXPLOSIVE CINDER CONE ACTIVITY

by

LUCY KATHLEEN WALSH

A THESIS

Presented to the Department of Geological Sciences
and the Graduate School of the University of Oregon
in partial fulfillment of the requirements
for the degree of
Master of Science

December 2012

THESIS APPROVAL PAGE

Student: Lucy Kathleen Walsh

Title: Implications for Volcanic Hazards in the Central and Southern Cascades Based on Gas Emissions During Explosive Cinder Cone Activity

This thesis has been accepted and approved in partial fulfillment of the requirements for the Master of Science degree in the Department of Geological Sciences by:

Dr. Paul Wallace	Chair
Dr. A. Dana Johnston	Member
Dr. Katharine Cashman	Member

and

Kimberly Andrews Espy	Vice President for Research & Innovation/Dean of the Graduate School

Original approval signatures are on file with the University of Oregon Graduate School.

Degree awarded December 2012

THESIS ABSTRACT

Lucy Kathleen Walsh

Master of Science

Department of Geological Sciences

December 2012

Title: Implications for Volcanic Hazards in the Central and Southern Cascades Based on Gas Emissions During Explosive Cinder Cone Activity

Volatile emissions from Cascades cinder cone eruptions have been well-documented; however the implications for understanding the effects that volcanic gases have on surrounding communities have not been addressed. This study examines the hazards from volatile degassing during explosive activity by (1) analyzing S, Cl, and F concentrations dissolved in olivine-hosted melt inclusions and matrix glass from cinder cones located in central Oregon and northern California, (2) estimating the mass of volcanic gas degassed during these eruptions, and (3) predicting gas concentrations downwind of the vent. Analyses reveal that the magmas degassed >88% S, <49% Cl, and <50% F during eruption, equating to a release of ≤4.5 Mt SO_2, ≤0.2 Mt HCl, and ≤0.2 Mt HF. Predictions of gas concentrations downwind of the vent provides reassurance that the levels of volcanic gases were not high enough at the time of eruption to present acute or severe health hazards to nearby residents.

CURRICULUM VITAE

NAME OF AUTHOR: Lucy Kathleen Walsh

GRADUATE AND UNDERGRADUATE SCHOOLS ATTENDED

University of Oregon, Eugene, OR
University of Washington, Seattle, WA
Gonzaga University, Spokane, WA

DEGREES AWARDED:

Master of Science, Geological Sciences, 2012, University of Oregon
Bachelor of Science, Earth and Space Sciences, 2009, University of Washington

AREAS OF SPECIAL INTEREST:

Physical volcanology
Geochemistry

PROFESSIONAL EXPERIENCE:

Graduate Teaching Fellow, University of Oregon, 2010 to present

Research Assistant, Pacific Northwest Seismic Network, 2007-2010

Teaching Assistant, Department of Earth and Space Sciences, University of Washington, 2009

GRANTS, AWARDS, AND HONORS:

Graduate Teaching Fellowship, Geological Sciences, 2010 to present

Johnston Scholarship, University of Oregon, Department of Geological Sciences, 2011

PUBLICATIONS:

Walsh, L.K., Wallace, P.J., and Cashman, K.V. (2012), Volatile emissions from Cascade cinder cone eruptions: Implications for future hazard assessments in the Central and Southern Cascades, abstract V53C-2854, 2012 Fall Meeting.

Walsh, L.K., Wallace, P.J., and Cashman, K.V. (2011), Volatile budget for an unusual central Oregon Cascades cinder cone and implications for future activity, abstract NH13B-1378, 2011 Fall Meeting.

Bodin, P., Vidale, J.E., Luetgert, J.H., Malone, S.D., Delorey, A.A., Steele, W.P., Gibbons, D.A., Walsh, L.K., Wallace, P.J., and Cashman, K.V. (2011), Seismic Monitoring with Netquakes: The First in the Pacific Northwest, abstract S53C-01, 2011 Fall Meeting.

ACKNOWLEDGMENTS

I wish to express my sincerest gratitude to Paul Wallace for granting me the opportunity to contribute research to a topic that I truly care about. I would also like to thank Paul for his guidance over the last two years- I am a better scientist because of his efforts. Thank you to Kathy Cashman, Dana Johnston, and Daniele McKay for their invaluable insight and their commitment to the success of my Masters Thesis. I owe special thanks and appreciation to Marli Miller and Dave Blackwell. Thank you Marli for being the first faculty member that made me feel like a peer. Your willingness to share your own graduate experiences will forever be of value to me as it taught me to take setbacks with grace and confidence. A very big thank you to Dave Blackwell, for whom I hold the greatest respect for. Dave, you have been such a tremendous mentor. You taught me the importance of teaching- the importance of caring about students and peers such that you give them a better chance at success. Thank you for your confidence in my teaching abilities and your tireless efforts on the behalf of your students and GTFs.

To my family, who has never ceased to amaze me in their support of everything I do, even during times I can't muster up my own self-confidence. I would not be the woman I am today without your love. Thank you for trusting in my decisions and being there for me every day- I love you. Thanks to Mike for also being there every step of the way and for acting as my rock and my reason for both perseverance and procrastination. I would also like to thank many graduate students, and more importantly, my good friends who made these last two years so enjoyable. Thank you to my officemate Ryan who's fro-yo runs, late night pump up sessions, and kind words help define my graduate experience. Thank you to Stan, Angie, and Dana for Bachelor nights, caring for

inebriated field camp students, epic dodgeball birthdays, excuses to chat instead of work, and your irreplaceable friendships. Finally, I would like to thank Cindie Judy and her Rec team for providing me with no t-shirt, but a great set of memories with my fellow grads.

To Grandpa Joe and Grandaddy Walsh, whose endless love and support lives within me.

TABLE OF CONTENTS

Chapter Page

LIST OF FIGURES

Figure Page

LIST OF TABLES

Table Page

CHAPTER I

INTRODUCTION

The relationship between magmatic volatiles and the hazards they pose to surrounding communities is one of the least understood aspects of explosive cinder cone eruptions. The main focus of studies concerning magmatic volatiles erupted at cinder cones has been on volatile recycling by subduction, formation of arc magmas, and the effects of shallow degassing on eruption styles (Leeman et al., 1990; Conrey et al., 1997; Johnson et al., 2008; Keating et al., 2008; Vigouroux et al., 2008; Di Traglia et al., 2009; Pioli et al., 2009; Ruscitto et al., 2010). Along the central and southern Cascade Arc, magmatic volatiles like H_2O, CO_2, S, and Cl have been studied at mafic cinder cones to better understand the geochemical and geophysical processes listed above (e.g. Wallace, 2005; Le Voyer et al., 2010; Ruscitto et al., 2010). However, the implications for understanding the effects that volcanic gases can have on surrounding communities during eruption, especially the effects of fluorine, have not been addressed.

During eruption, typical gas species emitted include water vapor (H_2O), carbon dioxide (CO_2), sulfur dioxide (SO_2), hydrogen chloride (HCl), hydrogen fluoride (HF), hydrogen sulfide (H_2S), carbon monoxide (CO), radon (Rn), and heavy metals including lead and mercury (Hansell and Oppenheimer, 2004). Health hazards from the emission of water vapor are minimal, so most research on gas exposure to date has focused on exposure to CO_2, H_2S, and SO_2 from degassing of volcanic and geothermal sources (Hansell et al., 2006). For this reason, I concentrate on the health effects from degassing

of the more poorly understood gases HCl and HF. I include SO_2 in my analyses as well so I can better compare gas contents in the Cascades to other volcanic centers worldwide.

A wide array of hazardous effects have been documented at active volcanic centers (e.g. Auckland Volcanic Field, New Zealand; Coote et al. 1997; Rhoades et al. 2002; Bebbington and Cronin 2011). These effects have also been inferred using tools such as geologic mapping and geochemical analyses of erupted materials for prehistoric eruptions (e.g. Cerro Negro, Nicaragua; Hill et al. 1998; McKnight and Williams 1997). Real-time measurements of gas composition and flux released from actively erupting volcanic centers have been measured using ground-based remote sensing methods. For example, Correlation Spectrometry (COSPEC) can measure SO_2 concentrations in tons/day. Cinder cone eruptions in the Cascades are all prehistoric, and because the most recent cinder cone eruptions in the Cascades occurred long before modern instrumentation, real-time measurement cannot be employed. Instead, volatile fluxes from these past eruptions can be estimated by analyzing melt inclusions trapped within olivine phenocrysts and rapidly quenched tephra matrix glass.

Studies on cinder cone degassing suggest such eruptions can produce volatile emissions at concentrations high enough to pose significant health hazards (e.g. Stoiber and Rose, 1973; Cronin and Sharp, 2002; Delmelle et al., 2002). However, the majority of these studies focused on inhalation or ingestion of volcanic gases and aerosols by livestock and flora; therefore not much is known of the effects on humans. This emphasizes the importance of such a study in a volcanically active and populous region such as the Cascades. Cinder cones are also the most common volcanic landform on Earth, and the relatively short recurrence rates of cinder cone volcanism in some regions

(e.g. Michoacán-Guanajuato volcanic field, 2 x10^{-3} vents/year; Connor and Conway, 2000) increase the probability of human experience with cinder cone hazards. The central and southern Cascade arc is an ideal study site because it has a wealth of geochemical and geophysical data already in existence, it has relatively young, numerous, and well-preserved cinder cones, and it is host to major urban population centers.

Data presented in this thesis from analysis of dissolved volatiles in olivine-hosted melt inclusions and quenched matrix glass are used to address the following questions:

(1) What are the pre- and post-eruptive volatile concentrations of S, Cl, and F in the magmas erupted from cinder cones located in central Oregon and northern California?

(2) How do S, Cl, and F concentrations in the central and southern Cascades arc magmas compare to those from other arcs worldwide?

(3) What are the concentrations of SO_2, HCl, and HF likely to be experienced at ground level in communities downwind of the vent during a sustained explosive cinder cone eruption?

(4) Are these concentrations of SO_2, HCl, and HF elevated above World Health Organization (WHO) and Occupational Safety and Health Administration (OSHA) maximum exposure limits?

(5) Knowing the gas concentration downwind of the vent, will city governments in central Oregon and northern California need to prepare for hazardous effects to agriculture or human life?

Substantial work on across-arc volatile concentrations has been carried out in the central and southern Cascades. Extensive melt inclusion analyses and bulk lava analyses

were performed by Ruscitto et al. (2010) and Ruscitto (2011) at the University of Oregon. However, the fluorine analyses had relatively large analytical errors, and therefore were not considered to be reliable. For this study, I developed a modified procedure for F analysis with considerably less error using a LTAP diffraction crystal on the Cameca SX100 in the CAMCOR facility on the University of Oregon campus. A secondary basaltic glass standard with low F concentration was used to assess accuracy of F detection. The goal of this dissertation is to use this increased precision to modify current expectations of cinder cone hazards to human, livestock, and agricultural industries for surrounding communities in the central and southern Cascades.

CHAPTER II

OVERVIEW OF CINDER CONE VOLCANISM, TECTONIC SETTING, AND MAGMA GEOCHEMISTRY IN THE CASCADES ARC

2.1. Cinder cone eruptions

A cinder cone is a mafic volcanic structure that forms by the eruption of low-viscosity basaltic magma (Vespermann and Schmincke, 2000). It is comprised of unconsolidated walls formed from ballistic deposition and subsequent slumping as the angle of repose is exceeded. The walls are composed of scoria, a mafic eruption product ejected from the vent as gas within the magma rises, expands, and bursts. Internal to a cinder cone is a central vent and a welded core (Wohletz and Heiken, 1992). Cinder cones have relatively simple magmatic plumbing systems consisting typically of a central feeder dike and radial dikes that transport magma from the lower crust to the surface (Keating et al., 2008; Hintz and Valentine, 2012). Cinder cones are commonly monogenetic (single eruptive episode), however polygenetic eruptions from a single vent have been documented (e.g. Cerro Negro, Nicaragua). Eruptions can last weeks to years, as seen at Parícutin, Mexico, which continuously erupted from 1943 to 1952. Eruptions vary between Hawaiian-type eruptions (no ash column; lava flows and fire fountaining) to Violent Strombolian-type eruptions (≤ 10 km high ash columns and lava flows) (Vergniolle and Mangan, 2000; Pioli et al., 2008).

Cinder cones erupt a variety of material that ranges in size, composition, and physical properties. Tephra is defined as magmatic fragments erupted from a cinder cone and can range in coarseness from bomb- (>64 mm) to ash-size (<2 mm). Tephra is

ejected from the vent during periods of explosive activity. Depending on the explosivity of an eruption, tephra can travel 100's of kilometers away from the vent. Tephra cools quickly as ambient air temperatures are much cooler than magmatic temperatures. This large temperature gradient causes very rapid quenching and creates a glass matrix that retains some dissolved volatiles, typically less than the concentration in the parent magma. Lava is fluid magma released during periods of effusive eruption. Lava is transported to the surface by radial dikes and is erupted at the base of cinder cones. Lava crystallizes slowly when it reaches the surface as heat is lost through the top of the flow allowing volatiles to readily escape.

2.2. Olivine-hosted melt inclusions

The mineral olivine is transported from depth and erupted simultaneously with tephra and lava. Olivine is commonly the first mineral, along with Cr-spinel, to crystallize from a basaltic melt. Olivine-hosted melt inclusions commonly form during pulses of rapid crystal growth, and data for suites of melt inclusions often show evidence for polybaric crystallization of the rising magma. The pulses of rapid growth create embayments that can subsequently trap melt as the olivine crystal continues to grow (Roedder, 1984; Metrich and Wallace, 2008). These small volumes of silicate melt trapped within the olivine crystals are known as olivine-hosted melt inclusions. A melt inclusion is relatively unaffected by external changes once it is formed and therefore records a snapshot in time of magma composition at depth. Changes to major element and volatile concentration can occur within a melt inclusion if the melt inclusion is allowed to cool slowly. During cooling, post-entrapment crystallization of the melt

inclusion can increase concentrations of incompatible elements, including volatiles (Roedder, 1984; Sisson and Layne, 2003). Segregation of the melt into a separate liquid and gas phase can also occur inside the melt inclusion when the pressure in the melt inclusion drops below the vapor saturation pressure of the melt contained at a certain temperature. These shrinkage bubbles, or vapor bubbles, greatly decrease the concentration of volatiles with low solubility (e.g. CO_2) as they diffuse from the trapped melt into the bubble (Roedder, 1984; Metrich and Wallace, 2008). However, it is unlikely the shrinkage bubbles will affect S, Cl, or F as these volatiles have high solubilities within the melt. Lastly, hydrogen is susceptible to diffusion into and out of the olivine after entrapment, which can affect overall H_2O concentrations (Portnaygin et al., 2007), but again, no evidence suggests such effects with S, Cl, or F concentrations.

During eruption, volatiles are initially released into the atmosphere as gases, but depending on the time spent within the plume, the density of ash particles, and temperature, a gas can transition into an aerosol – a fine solid or liquid particle suspended in gas (Mather et al., 2003). Formation of aerosols can occur in a variety of ways, most commonly as volcanic gases cool and condense to form particles, adsorb onto surfaces of existing particles, and dissolve into pre-existing aqueous phases (e.g. water droplets). Scavenging by silicates can be an important sink for volcanic volatiles during eruption as documented at Fuego Volcano where up to 33% S and 17% Cl were rapidly deposited to the ground after adhering to ash with the convective plume (Mather et al., 2003). Aerosols that adhere to the surface of such tephra grains can be deposited great distances from the vent (Oskarsson, 1980). Acidic gases undergo acid-base reactions within the plume that can enhance gas uptake in an aqueous phase. An aqueous phase is likely

already present in the ambient air that mixes with the plume, and the high solubility of HCl and HF, and moderate solubility of SO_2 and H_2S makes it easy for these gas species to dissolve into that aqueous phase (Mather et al., 2003; Textor et al., 2003). Modeling of stratospheric volcanic gas scavenging by water droplets in the Laacher See eruptive plume by Textor et al. (2003) suggested almost complete depletion of HCl in the plume with insignificant scavenging of SO_2. However, gas scavenging models from Aiuppa et al. (2006) in the troposphere show only minor HCl dissolution into an aqueous phase or adsorption onto a particle surface during short-term transport (e.g. traverse of several kilometers in tens of minutes). SO_2 and H_2S were also conserved during short-term transport. It is unclear why the process of gas scavenging in the stratosphere differs from the troposphere, but Textor et al. (2003) and Mather et al. (2003) propose the differences may be due to the percent water and temperatures necessary to drive reactions within the plume. Since Strombolian to Violent Strombolian plume heights rarely extend past the troposphere, it is unlikely that the volatiles released from these cones transitioned into an aerosol phase. For the sake of clarity, I will refer to the volatiles released from the vent into the eruptive plume as gases.

2.3. Tectonic setting

The Cascades volcanic arc extends 1,250 km from northern California to southern British Columbia. The arc consists of well-separated, NNW trending volcanic vents that have erupted basaltic to rhyolitic lava compositions since the onset of volcanism at 40 Ma when the ancient, oceanic Farallon Plate docked with North America. Broken into three segments, Quaternary volcanism occurs today as the Explorer Plate (north), the Juan de

Fuca Plate (central), and the Gorda Plate (south) actively subduct beneath the North American plate (Figure 1).

Seismic tomography, geochemical, and geodetic studies of the Cascadian arc have constrained the slab dip angle, the crustal thickness of the arc, the convergence rate, and convergence angle of subduction and suggest the Cascadian subduction zone is relatively warm, young, and slow (Kirby et al., 2002; Stern, 2002). A warm slab environment is one in which young oceanic lithosphere subducts at slow to moderate rates (Kirby and Wang, 2002). The Cascades volcanic arc is a global end-member of warm-slab subduction resulting from the slow subduction (35 mm/yr) of the young Juan de Fuca plate beneath Western North America (Ruscitto et al., 2010). The dip of the Juan de Fuca plate is calculated to be <20°, with conservative constraints of 13-16° (Trehu et al., 1994; Kirby et al., 2002). Estimates of North American crustal thickness above the subducting plate vary from 15 km off the coast of Oregon to 40 km beneath the High Cascades (Trehu et al., 1994). The basement beneath the Cascades from central Oregon to southern Washington consists of an oceanic terrain known as "Siletzia", which is believed to have accreted to northern Oregon at ~50 Ma (Trehu et al., 1994). Accretion of Siletzia to present day Oregon has induced a clockwise rotation of the Oregon forearc. The rotation of this rigid block is thought to be responsible for the intra arc E-W extension along the crest of the Cascades and in the back arc (Taylor, 1990; Ruscitto, 2011).

Along with western encroachment of the Basin and Range extension in the Cascadian backarc, the central and southern segments of the Cascade arc have an estimated extension rate of 1 mm/yr (Schmidt and Grunder, 2009). Most of the extension in the back arc is accommodated in the form of either linear normal faults or horst and

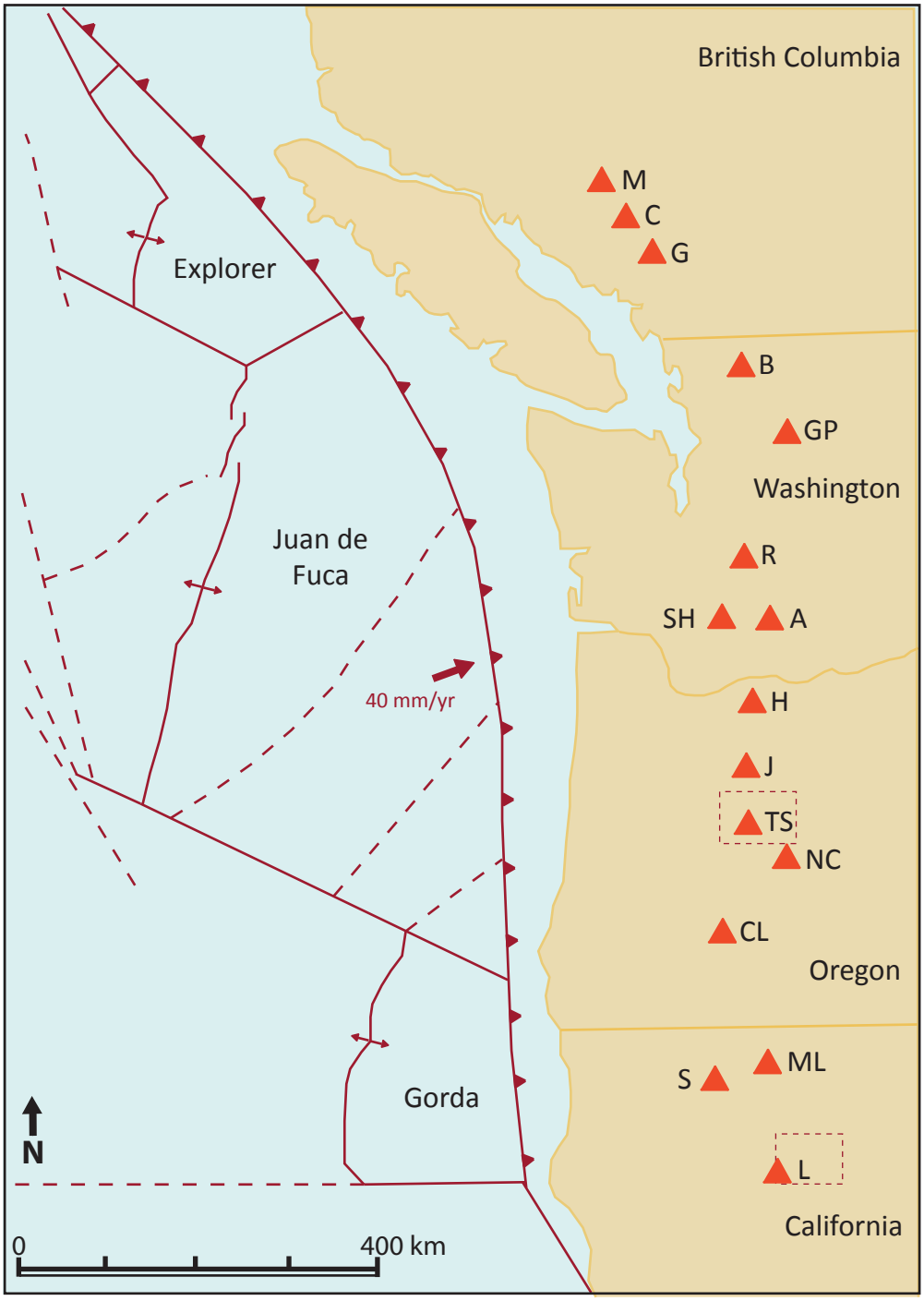

Figure 1: Location map of the Cascadian subduction zone adapted from Bacon et al., 1997. Surface expression of faulting (red line) and active stratovolcanoes (orange triangle) associated with subduction. Abbreviations for volcanoes include: (M) Meager Mountain; (C) Mount Cayley; (G) Mount Garibaldi; (B) Mount Baker; (GP) Glacier Peak; (R) Mount Rainier; (SH) Mount St. Helens; (A) Mount Adams; (H) Mount Hood; (J) Mount Jefferson; (TS) Three Sisters; (NC) Newberry Crater; (CL) Crater Lake; (ML) Medicine Lake; (S) Mount Shasta; (L) Lassen Peak. Dashed red boxes indicate areas of focus within this study.

graben structures. The central Oregon Cascades is bounded to the west and east by a continuous arc-parallel graben known as the High Cascades Graben (Conrey et al. 1997). In central Oregon the majority of volcanism occurs within this High Cascades Graben. To the south in northern California a similar graben exists and is referred to as the Hat Creek Graben. Like the High Cascades Graben, Hat Creek Graben is defined by similar extensional regimes and houses the majority of extension-related volcanism within the region. Opening of the Cascadian back arc has produced prolific mafic volcanism in central Oregon and northern California.

Holocene volcanic activity in areas of the Cascades undergoing extension has formed small, isolated batches of basaltic and basaltic-andesite magmas erupted from extensive chains of cinder cones, small shields, and fissure-fed lava flows along pre-existing faults (Hughes & Taylor, 1986; Sherrod et al., 2004; Ruscitto, 2011). The focus of my research includes both the central Oregon Cascades (Three Sisters Volcanic Field) and the northern California Cascades (Lassen Volcanic Field). The density of Quaternary volcanoes in the central Oregon Cascades alone is extraordinary (1,054 vents in ~9500 km^2; Hildreth 2007) (Figure 2). Only Michoacán, Mexico, southern Washington and northern California are comparable in terms of volcano density (Hildreth 2007). In the Three Sisters Volcanic segment alone, 466 Quaternary volcanoes cover the 90 km long landscape. In northern California, the Lassen Volcanic Field is distinguishable from other fields within the southern Cascades arc, most notably the Shasta field, by a 50 km gap along the arc crest that contains no Quaternary volcanic edifices. The Lassen Volcanic Field contains approximately 476 volcanoes that cover a ~6500 km^2 area.

Greater than 85% of all Quaternary volcanic edifices in the Three Sisters Volcanic Field and the Lassen Volcanic Field erupted basaltic to andesitic lavas (Hildreth, 2007).

The types of mafic lavas in the central and southern segments of the Cascades arc include low-K tholeiites (LKT), ocean island basalts (OIB), and calc-alkaline basalts (CAB). Each type indicates heterogeneity in mantle compositions and melting processes. LKTs probably form by a high degree of decompression melting of a depleted magma source. LKT magmas are also synonymous with high-Al olivine tholeiites (HAOT) and have some similarities to mid-ocean ridge basalts (MORB) (Ruscitto et al. 2010). OIBs are derived from an enriched mantle source that has high concentrations of high field strength elements such as Zr and Nb (e.g. Münker et al., 2004; Rowe et al., 2009). CABs represent mantle wedge melting with contributions from slab-derived fluids (Miyashiro, 1974; Leeman et al., 1990; Bacon et al., 1997; Leeman et al., 2005; Ruscitto et al., 2010). The combination of subduction and intra-arc extension along and off the arc axis has resulted in the eruption of LKTs, OIBs, and CABs in central Oregon and northern California.

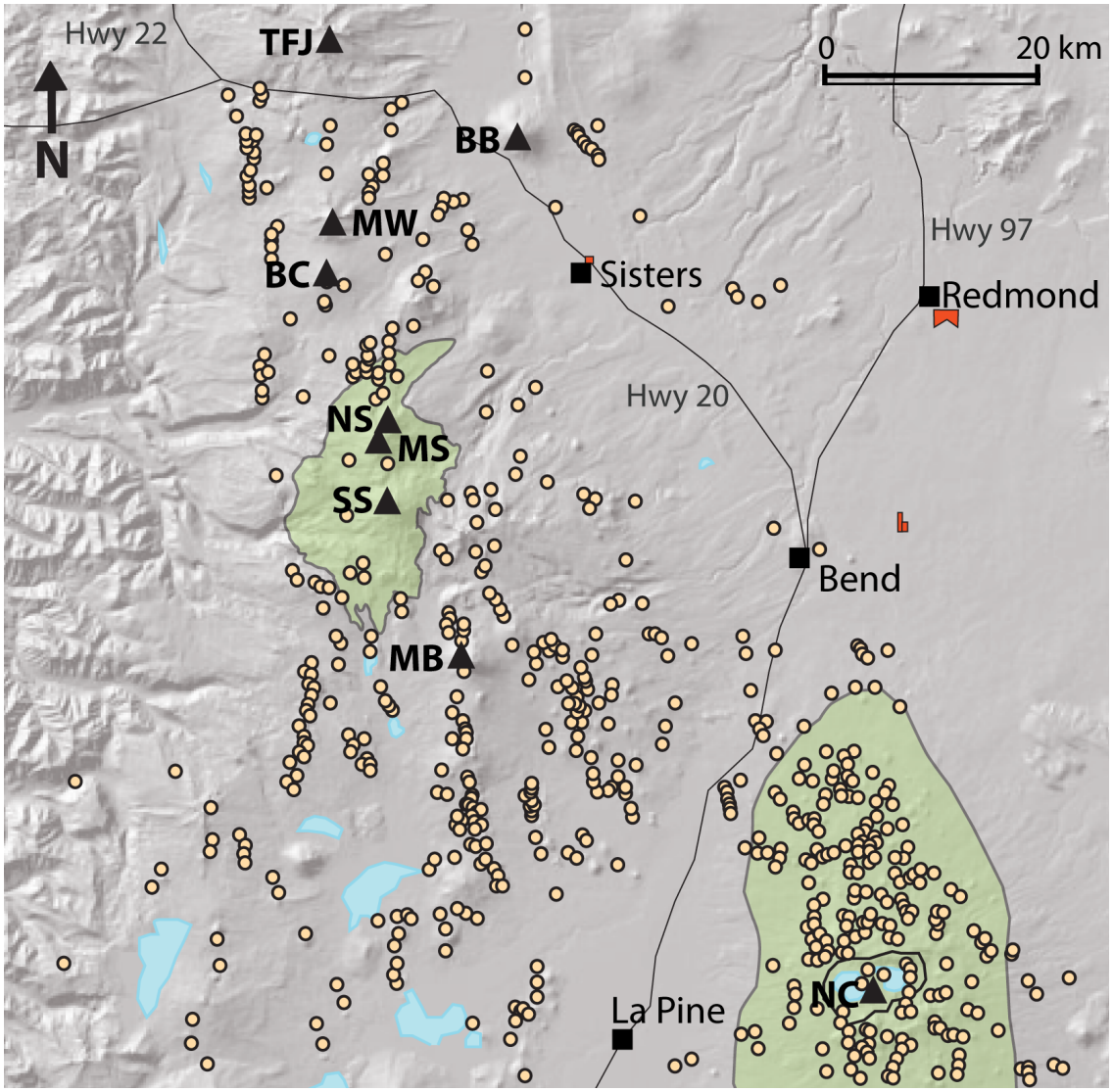

Figure 2: Cinder cone density map for the central Oregon Cascades adapted from Schmidt and Grunder, 2009. Yellow circles denote single cinder cone vents, black triangles denote volcanic edifices, green shaded areas represent the extents of volcanic depositsred shapes denote airports, black squares represent the location of popular central Oregon cities, and black lines denote major highways. Abbreviations for volcanic edifices include: (TFJ) Three Fingered Jack; (BB) Black Butte; (MW) Mount Washington; (BC) Belknap Crater; (NS) North Sister; (MS) Middle Sister; (SS) South Sister; (MB) Mount Bachelor; (NC) Newberry Crater. The dissected topography to the west represents the western edge of the High Cascades Graben. Within the graben cinder cones erupt along chains associated with normal fault rifting of the back-arc basin.

CHAPTER III

SAMPLE LOCATIONS AND DESCRIPTIONS

3.1. Sample characteristics

I selected tephra samples from cinder cones in the central Oregon and northern California Cascades based on the following criteria: (1) previous geochemical work by Ruscitto (2011) showing that many cones in central Oregon had a relatively simple magmatic history, allowing for simple mass-balance calculations, (2) a range of basaltic compositions throughout the arc, (3) eruption deposits of relatively young age (late Holocene) such that the tephra deposit was relatively intact, allowing for accurate estimate of eruptive volume and eruption characteristics, and (4) location of the cone within a critical distance of large populations centers or busy tourist communities. A detailed summary of each cone can be found in Appendix A.

The cinder cones included in this study are Collier Cone, Yapoah Crater, Four-in-One Fissure, Garrison Butte, Cinder Cone, Basalt of Old Railroad Grade (BORG), and Basalt of Highway 44 (BAS44). Figures 3 and 4 show the geographical locations of these cinder cones. Most of the cones studied erupted basaltic to basaltic andesite tephra and lava. The style of eruption ranges from Strombolian to Violent Strombolian, with the exception of Four-In-One Fissure, which is thought to have periods of Hawaiian-style eruptions (Marks, 2012; McKay, 2012). Dense rock equivalent (DRE) eruptive volumes range from 0.03-0.36 km^3 (Clynne, 2011; Muffler et al., 2011; Marks, 2012; McKay, 2012 ;), however these are minimum estimates as weathering has mostly likely eroded the deposits. Cone height is trimodal- all cones are roughly 40 m, 80 m, or 150 m in height.

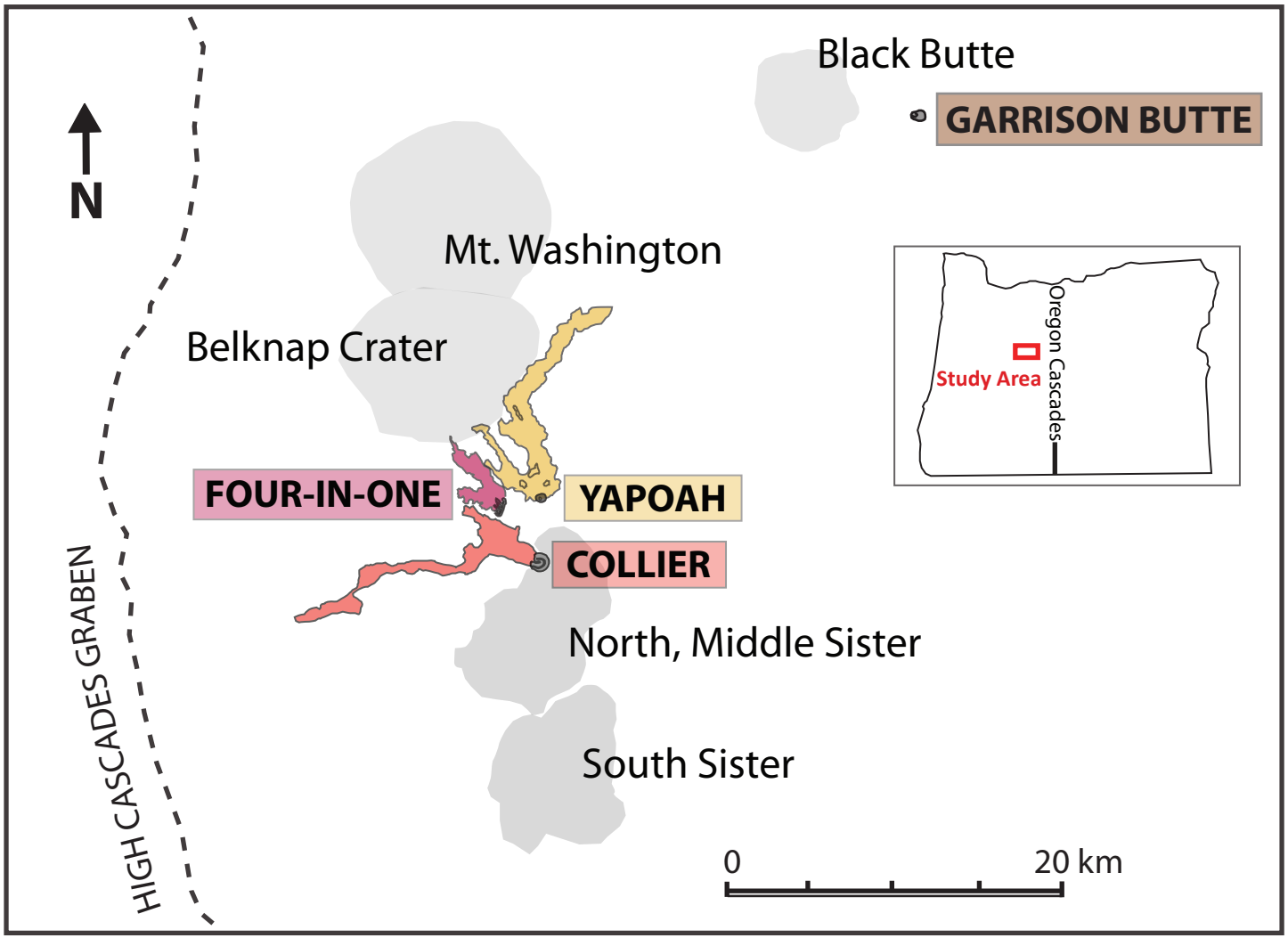

Figure 3: Location map of Collier Cone, Yapoah Crater, Four-In-One Fissure, and Garrison Butte. Grey shaded areas outline the cone (or volcanic) edifice; lava flows of each cone are outlined in color. Lava flows associated with Garrison Butte are highly vegetated and the extent of the flows has not been mapped. Dashed line traces the western edge of the High Cascades Graben.

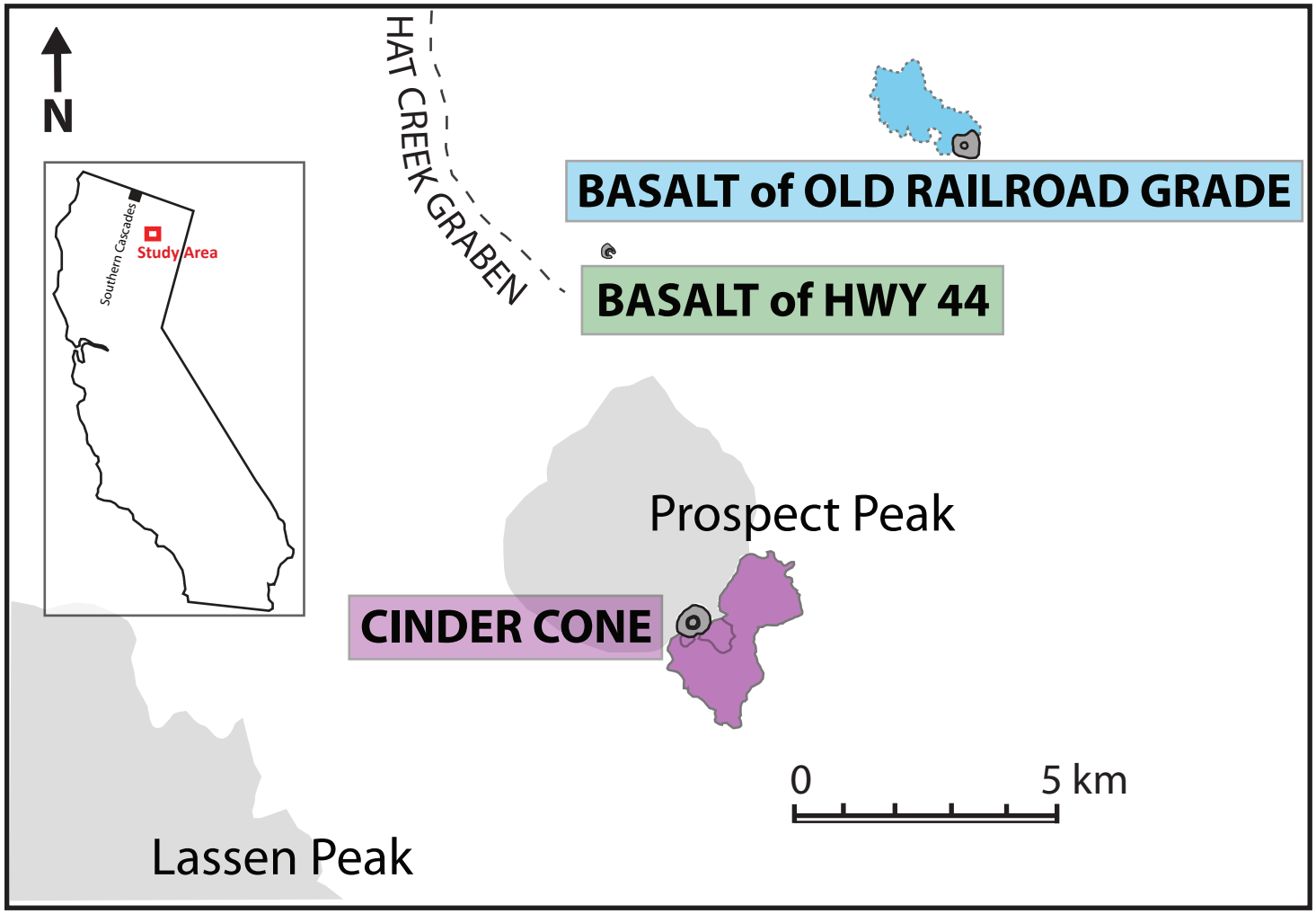

Figure 4: Location map of Cinder Cone, Basalt of Old Railroad Grade (BORG), and Basalt of Highway 44 (BAS44). Grey shaded areas outline the cone (or volcanic) edifice; lava flows of each cone are outlined in color. The small dashed line around the lava flow of BORG indicates an unknown flow boundary. The lava flow of BAS44 is highly vegetated and partially covered by younger flows from a cinder cone that sits on the SE flank of West Propect Peak shield volcano. Dashed line traces the eastern edge of the Hat Creek Graben.

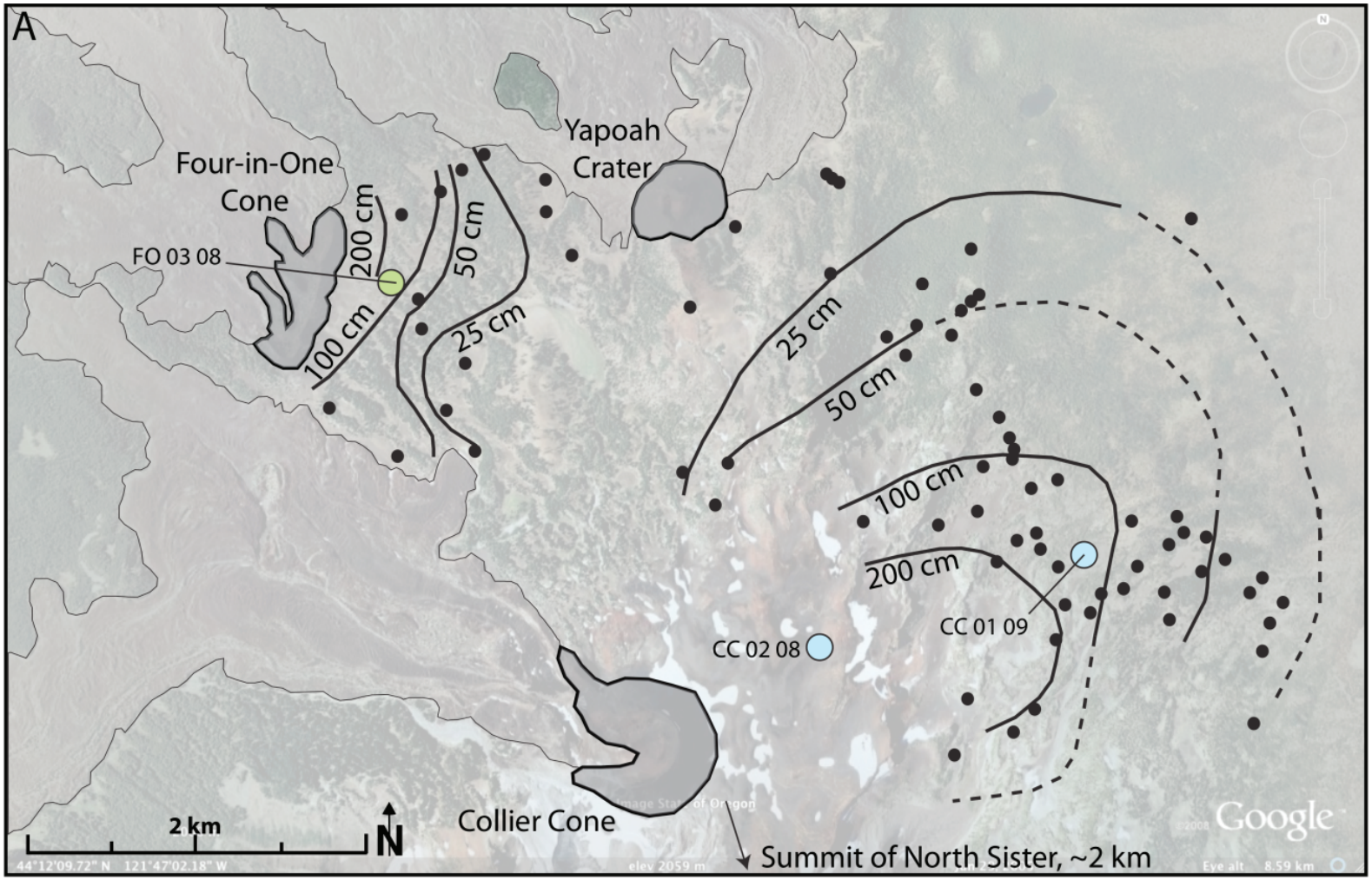

Figure 5: Isopach maps of Collier Cone and Four-In-One Fissure from McKay, 2012. Dashed lines indicate inferred tephra isopachs locations. Black circles represent locations where tephra thickness measurements were made; colored circles are locations where complete statigraphy was described. Grey shaded areas outline the cone edifice. Underlay is provided by Google Maps.

Most of the tephra samples contain phenocrysts of olivine, plagioclase, and pyroxene with the exception of Garrison Butte. Tephra from Garrison Butte contains only olivine. Spinel occurs as mineral inclusions in most of the olivines and is also sometimes present within olivine-hosted melt inclusions. The lavas of Collier Cone contain silicic xenoliths similar in composition to the Obsidian Cliffs, a dacitic to rhyolitic flow originating from Middle Sister (Schick, 1994). Lavas at Cinder Cone also have entrained quartz xenocrysts and granitic xenoliths that are suggested to be from a Mesozoic(?) granite, possibly akin to the Sierra Nevadas, buried beneath the Lassen region. The granitic xenoliths have major and trace element compositions that are typical of the Sierra Nevada granitoids (Borg and Clynne, 1998). Geographical and geological characteristics of each cinder cone analyzed in this study can be found in Table 1. Major and minor element concentrations for the silicic xenoliths can be found in Table 2.

Extensive mapping and lithologic descriptions of Holocene tephra deposits from Collier Cone and Four-in-One Fissure have been completed by McKay (2012) (Figure 5). Before the research of McKay (2012), many of the central Oregon cinder cone tephra deposits had yet to be mapped. McKay (2012) presented tephra isopachs along with estimates of erupted volume of each deposit from Collier Cone and Four-in-One Fissure. Work by McKay (2012) is fundamental in understanding the total tephra thickness deposited by these cinder cones and the distances the tephra traveled within the buoyant eruption plume.

Table 1: Geographical and geological characteristics of cinder cones in the central Oregon Cascades and northern California

	lat/lon	landform type	age (yr BP)*	DRE erupted volume (km^3)**	reference
central Oregon					
Collier Cone	44.18°N, 121.78°W	cinder cone	1600±100 ^{14}C	0.154 (0.037 tephra; 0.154 lava; 0.024 cone)	*Sherrod et al. (2004) **McKay (2012)
Yapoah Crater	44.22°N, 121.78°W	cinder cone	Stratigraphically below Collier and Four-in-One	unknown	*Sherrod et al. (2004)
Four-in-One Fissure	44.2°N, 121.82°W	fissure	1980±160 ^{14}C	0.032 (0.002 tephra; 0.036 lava; 0.004 cone)	*Sherrod et al. (2004) **McKay (2012)
Garrison Butte	44.38°N, 121.54°W	cinder cone	unknown	unknown	
northern California					
Cinder Cone	40.54°N, 121.32°W	cinder cone	264±28 ^{14}C	0.36 (0.043 tephra; 0.08 lava)	*Clynne et al. (2008) **Clynne AGU (2011); Marks (2012)
BORG	40.65°N, 121.22°W	cinder cone	102.4 ± 11.4 to 46.3 ± 3.4 $^{40}Ar/^{39}Ar$	0.07 (0.059 lava; 0.009 cone)	*Muffler et al. (2011) ** Muffler et al. (2011)
BAS44	40.63°N, 121.34°W	cinder cone	unknown	unknown	

Table 2: Major and minor element concentrations for central Oregon and northern California granitic inclusions; wt% (Schick, 1994; Borg and Clynne, 1998)

	K_2O	SiO_2	TiO_2	Al_2O_3	FeO^T	MgO	CaO	Na_2O	MnO	P_2O_5
North Sister	3.62	73.00	0.27	13.70	1.92	0.35	0.60	3.79	0.09	0.10
Lassen Peak	3.62	75.56	0.14	13.88	0.89	0.25	1.57	3.97	0.03	0.08

3.2. Sand Mountain: An unusual mafic eruption in the central Cascades

Sand Mountain is a cinder cone located in the Sand Mountain Volcanic Field (SMVF) of the central Oregon Cascades. The SMVF includes the Sand Mountain chain of vents, Nash and Little Nash craters, the Lost Lake chain of vents, and associated lava flows and tephra blankets (Deligne, 2012). Previous physical analysis on Sand Mountain by McKay (2012) has shown the occurrence of a phreatomagmatic eruption, with explosive behavior similar to what has been described as Subplinian, ~3000 ybp. McKay (2012) suggested that magmas interacted with ground water during eruption (the High Cascades is a groundwater-dominated system; Deligne, 2012), fragmenting the magma and allowing deposition of a 25 cm isopach ~20 km from the vent (Figure 6). For reference, Collier Cone's 25 cm isopach was deposited only ~5 km from the vent (Figure 5). McKay (2012) estimated the maximum eruptive volume of Sand Mountain to be 1.13 km^3. This estimate includes trace deposits (<25 cm) that are not definitively correlated to Sand Mountain. However, McKay relates thinning trends of Sand Mountain tephra to that of the 1943-1952 eruption at Paricutin and the two deposits match surprisingly well. McKay concludes that until the trace deposits of Sand Mountain are definitely identified, Paricutin's thinning trend is a reliable estimate for Sand Mountain's maximum eruptive volume. This unusual widespread tephra deposit appears to represent the maximum probable tephra hazard for mafic activity in central Oregon.

I conducted preliminary analyses on Sand Mountain olivine-hosted melt inclusions and matrix glass for four units of the eruption deposit using the methods outlined in the following chapter and found higher concentrations of S, Cl, and F than in any of the other central Oregon and northern California cinder cones in this study (Figure

7). The analysis also revealed a complex system of melt inclusion formation by differing processes at variable depths (Ruscitto, 2011). I was unable to match melt inclusion compositions to tephra compositions because it appears that multiple olivines with different magmatic histories were erupted at the same time.

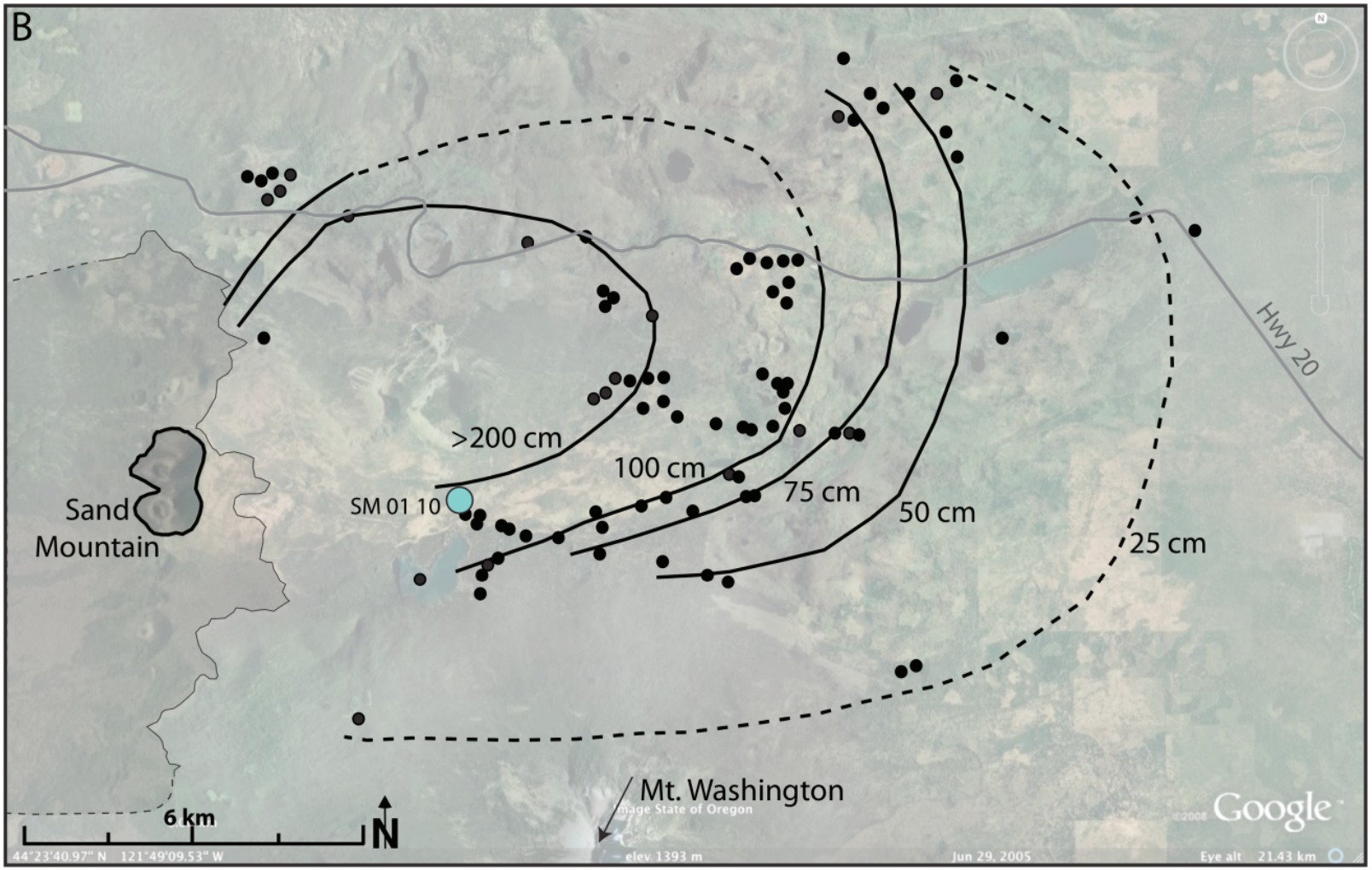

Figure 6: Isopach map of Sand Mountain from McKay, 2012. Dashed lines indicate inferred tephra isopachs locations. Black circles represent locations where tephra thickness measurements were made; colored circles are locations where complete statigraphy was described. Grey shaded areas outline the cone edifice. Underlay is provided by Google Maps.

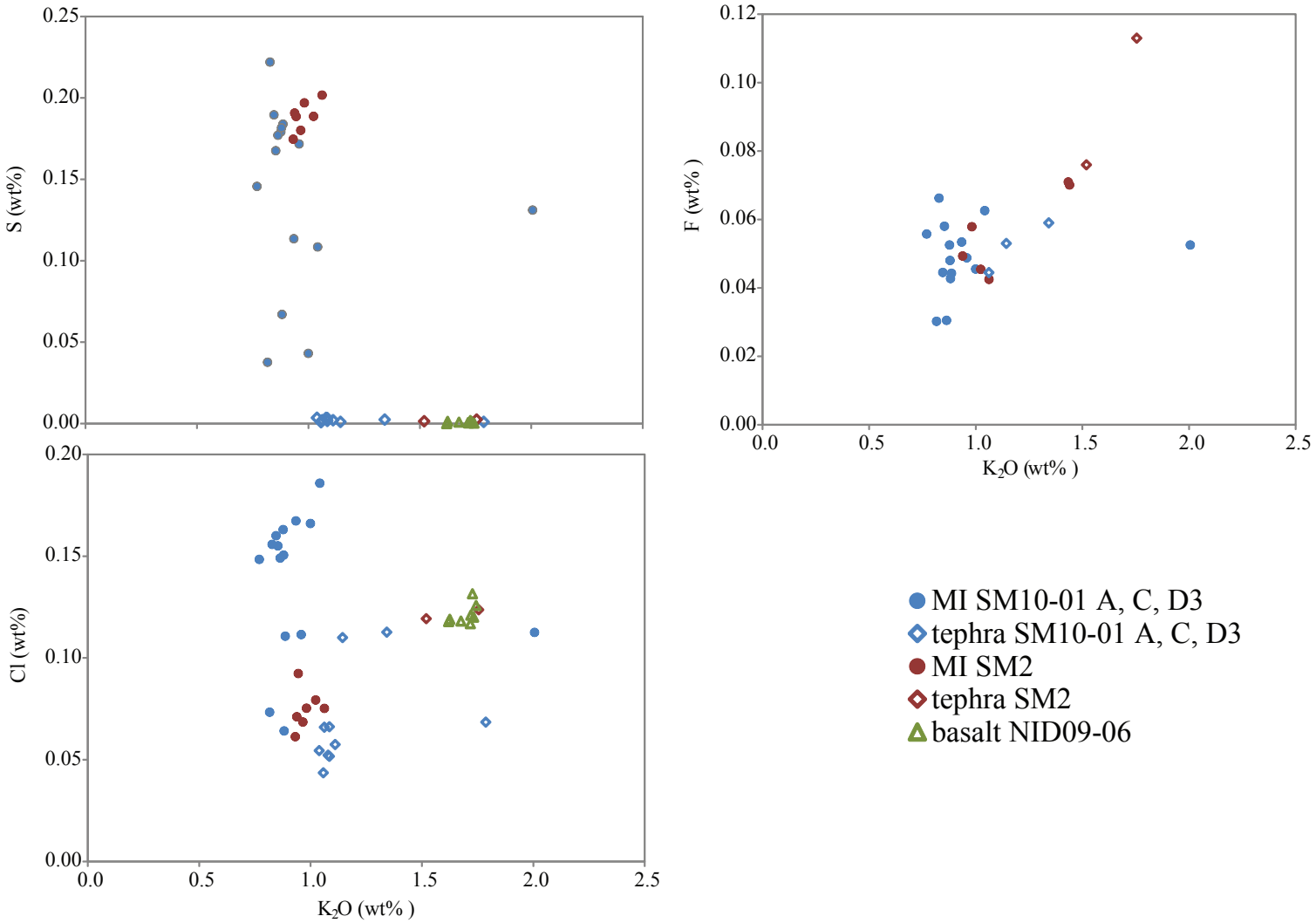

Figure 7: Volatile concentrations in olivine-hosted melt inclusions (filled circle), matrix glass (open diamond), and lava glass (open triangle) erupted from Sand Mountain, located in the central Oregon Cascades. Sand Mountain has an unusually large tephra deposit (maximum DRE eruptive volume is ~1.13 km^3) and the S, Cl, and F concentrations are elevated above those of the cinder cones analyzed in this study.

CHAPTER IV

METHODS

To test whether cinder cone eruptions in the central and southern segments of the Cascade arc pose a significant hazard to adjacent communities I (1) analyzed olivine-hosted melt inclusions and matrix glass to determine the pre-and post-eruptive concentrations of dissolved sulfur, chlorine, and fluorine, (2) calculated a total atmospheric release (in Megatons) of S, Cl, and F using a method modified from Thordarson et al. (1996) and, (3) calculated the maximum downwind gas concentrations for a steady-state eruption using a Gaussian plume advection-dispersion-diffusion model.

Tephra samples from proximal vent deposits from the cinder cones described in Chapter III were collected by Dan Ruscitto, Paul Wallace, Katharine Cashman, and Michael Clynne. Loose olivine grains were picked from the tephra samples. Using a refractive index oil of 1.657 and a binocular microscope, olivine grains containing enclosed melt inclusions >40 μm were selected for analysis. The olivine grains were mounted with crystal bond on glass slides and sanded with fine grit paper until the melt inclusion(s) were intersected. The olivines were then then mounted onto 2.5 cm circular pucks and polished to obtain optimal surface smoothness. Tephra clasts of 2-4 mm size were also selected along with the olivine grains. These clasts were mounted in 2.5 cm circular pucks, impregnated with Buehler epoxy, and then polished. The types of samples selected for analysis are shown schematically in Figure 8.

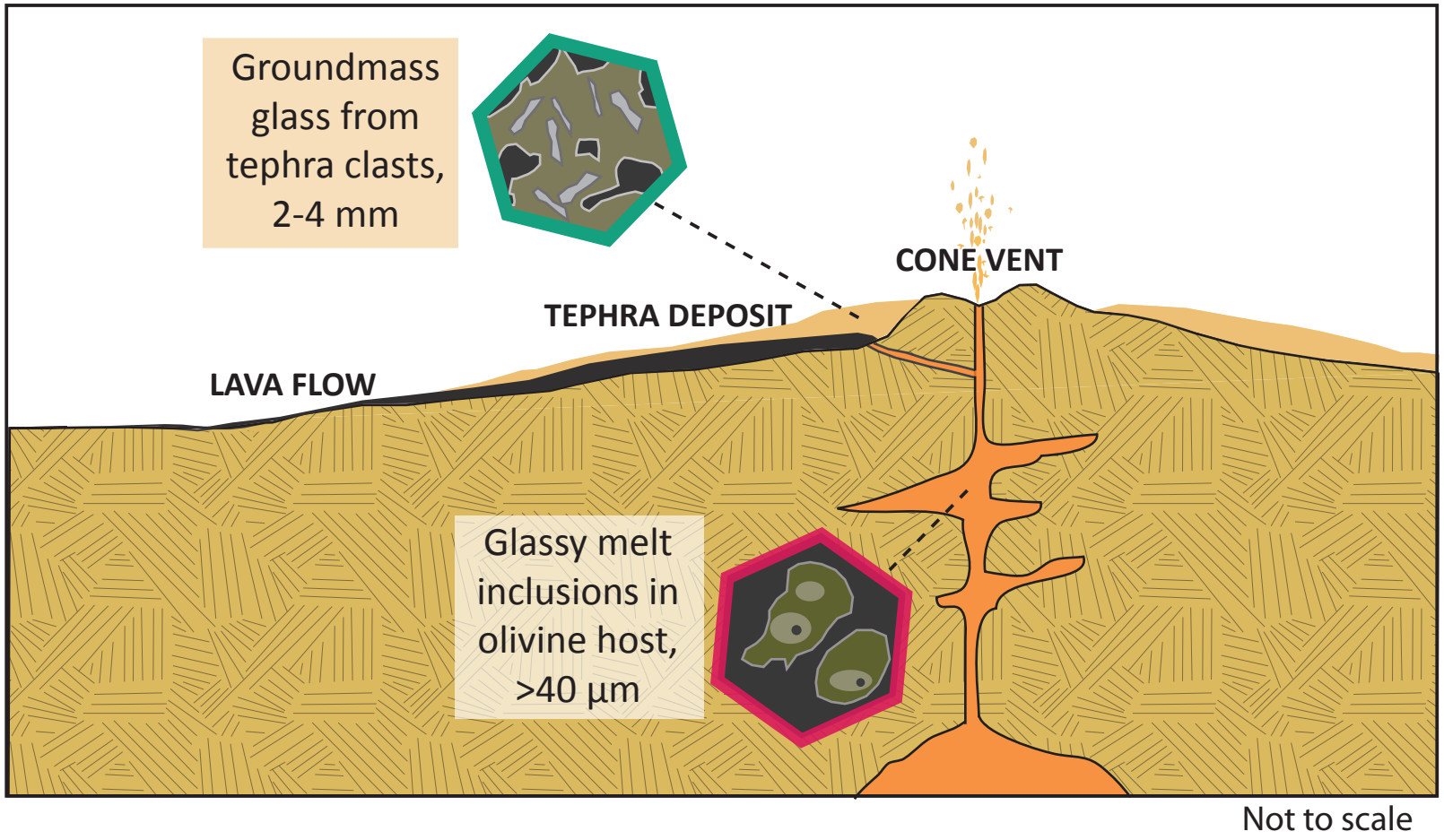

Figure 8: Illustration showing the types of samples collected for analysis; adapted from Thordarson et al., 1996. Pre-eruptive volatiles are measured using olivine-hosted melt inclusions, formed within the magmatic chamber at depth. The olivines are erupted along with tephra during explosive activity. Glassy melt inclusions with no accessory phases (e.g. titanomagnetite) were picked from the erupted tephra to be analyzed. Tephra groundmass glass records post-eruptive volatile concentrations. Golden-colored tephra, with a high percentage of glassy matrix, was chosen to be analyzed. By comparing pre- and post-eruptive volatiles concentrations the total concentration of volatiles released during an eruption can be determined.

4.1. Analytical procedures

Melt inclusion and matrix glass compositions were determined using the Cameca SX100 electron microprobe (EPMA) housed in the CAMCOR facility at the University of Oregon. The Cameca SX100 is equipped with five wavelength dispersive spectrometers and for this study I used a LTAP, a LPET, and three PET diffraction crystals. The elements K, Si, Ti, and S were analyzed using PET diffraction crystals, while Cl and F were analyzed using LPET and LTAP diffraction crystals, respectively. Concentrations of Al_2O_3, FeO^T, MnO, MgO, CaO, Na_2O, and P_2O_5 were necessary for matrix corrections for the probe analyses. I used the average analyzed melt inclusion values from each cone from Ruscitto et al. (2011) for the central Oregon Cascades (Appendix B, C) and from unpublished work by Walowski et al. and Rasmussen et al. for cinder cones in northern California (Appendix B, C). Ruscitto et al., (2011) and Clynne (2011) provided the average analyzed matrix glass values, respectively. Because of the small K-α peak produced by fluorine, the LTAP diffraction crystal was chosen to measure fluorine as it provides more surface area, resulting in a higher count rate and narrower F peak that does not overlap with larger, adjacent peaks such as P. The single element per spectrometer set up that I used on the SX100 electron microprobe yields less variance between point analysis of individual melt inclusions and greater reproducibility of volatile concentrations within one cinder cone than the analytical procedures used by Ruscitto (2011).

The standards that I used were orthoclase MAD-10 for K, NBS K-411 glass for Si, TiO_2 synthetic for Ti, pyrite UC #21334 for S, chlor-apatite for Cl, and fluor-phlogopite for F. Standard VG-2 USNM 111240/52 was used to check the accuracy of

fluorine analyses using the fluor-phlogopite standard. Operating conditions for the standards were a 10 µm diameter beam, 50 nA beam current, and 15 kV accelerating voltage. A mean atomic number (MAN) background intensity correction was applied to Si (standard and unknown), thus no high or low off-peak background was measured. On peak (and background high, low) counting times were as follows: K: 40 s (5,5); Si: 40 s (none); Ti: 40 s (10,10); S: 40 s (10,10); Cl: 40 s (10,10); and F: 40 s (10,10).

All olivine-hosted melt inclusions and matrix glasses were analyzed using a 10 µm diameter beam, 50 nA beam current, and 15 kV accelerating voltage. Major and minor elements for melt inclusion and matrix glass samples were analyzed as unknowns for the following on peak (and background high, low) counting times: K 80 s (10, 10); Si 40 s (none); Ti 160 s (80, 80) ; S 160 s (80, 80) ; Cl 160 s (80, 80) ; F 160 s (80, 80). Two to three data points were collected for each individual melt inclusion. Three to five data points were analyzed for matrix glass samples. Time dependent intensity (TDI) element concentrations were applied to Si, Ti, S, Cl, and F to correct the effects of element migration during analysis as the high beam current may have been responsible for minor shifts in the element concentration. An S K-α shift was applied to the run to account for the difference in the S Kα value between the standard and the unknown (Wallace and Carmichael, 1994).

Detection limits for the elements analyzed were calculated for a 95% confidence interval using a single point detection limit equation adapted from Love and Scott (1983) (Donovan et al., 2011):

$$CDL = ZAF * \frac{n}{IS} * \sqrt{IB} * 100 \quad (1)$$

where n is equal to the standard score (1=68%, 2=95%, 3=99.7%), IS, or the raw counts on the analytical (pure element) standard, is equal to:

$$IS = STCT * C_t * B_c \quad (2)$$

and, IB, or the raw background counts on the unknown sample, is equal to:

$$IB = UNBG * C_t * B_c \quad (3)$$

ZAF is a method for the matrix correction of x-rays emitted from a sample. The method outputs a value that quantifies the effects of atomic number (Z), absorption (A) and characteristic (and sometimes continuum) fluorescence (F) separately (Donovan et al., 2011). STCT are the standard counts/sec for a specific element, UNBG are the unknown counts/sec for a specific element, C_t is the count time for a specific element, and B_c is the background counts for a specific element. Since the standards used in these analyses are not pure, IS was divided by the K-factor to normalize to a pure standard concentration.

4.2. Volcanic degassing calculations

Research by Thordarson et al. (1996) on the historical Laki fissure eruption in Iceland from 1783 to 1784 AD presented a mass balance approach for calculating the total SO_2, HCl, and HF degassed during the eruption. This calculation assumes a relatively simple magmatic plumbing system such that the olivine-hosted melt inclusions and matrix glass are cogenetic and therefore, closely related. By analyzing olivine-hosted melt inclusions, tephra matrix glass, and lava matrix glass they estimated pre-eruptive and post-eruptive volatile concentrations in Laki magmas. These estimates are minimum values, in that the calculation assumes that there was no pre-erupted vapor phase. Their

findings indicate that a greater release of volatiles occurred during eruption than had been previously estimated. The technique developed by Thordarson et al. (1996) served as model for the analytical and modeling research presented here, but was modified to include the effects of variable fractional crystallization and assimilation in the magmatic systems that I studied.

The total mass of a volatile species in a given erupted volume of magma (C) is estimated using total DRE eruptive cone and tephra volume (V_T), melt density (ρ_m) (taken to be 2750 kg/m^3; Thordarson et al. 1996), calculated concentration of the volatile of interest from a melt inclusion that represents the evolved melt concentration due to fractional crystallization, crustal assimilation, and no degassing (C_{adj}; in weight fraction), volatile species' molecular weight (M) (e.g. SO_2; 64.064 g/mol), volatile atomic weight (A) (e.g. S; 32.066 g/mol), and fraction of crystals in the groundmass (x) :

$$C = \frac{V_T * \rho_m * C_{ol} * \left(\frac{M}{A}\right)}{10^9} * (1 - x) \quad (4)$$

The volatile mass fraction released (F) during eruption is calculated by:

$$F = 1 - \left[c_{matrix} * \left(\frac{1}{1 - f_A * \left(\frac{c_{ol}}{1 - f_M}\right) + f_A * c_{i,A}} \right) \right] \quad (5)$$

where c_{ol} is the measured volatile concentration in the least evolved melt inclusion, c_{matrix} is the measured volatile concentration in the matrix glass, $c_{i,A}$ is the concentration of the volatile species within the assimilant, and f_M is the extent of fractional crystallization, and f_A is the extent of crustal assimilation that together relate the bulk composition of the

least evolved melt inclusion and the matrix glass. By combining equation (4) and equation (5) the total mass of a volatile species lost to degassing is calculated by:

$$m_T = C * F \quad (6)$$

This method (Eq. 4-6) converts the wt% of each volatile lost from the magma into a mass, in Mt, of a gaseous compound released into the troposphere during the explosive phase of the eruption. The formula also takes into account the size of the eruption. This applies an inherent "scaling" for each eruption. Eruptive volumes for Yapoah Crater, Garrison Butte, and BAS44 are not known, so I calculated the mass of volatiles released during eruption based on an eruptive volume of Collier Cone (i.e. 0.04 km^3). BORG's estimated eruptive volume does not include the tephra deposit, only the cone.

No analysis of the volatile content in the silicic contaminants near North Sister or Lassen Peak has been performed. Therefore to proceed with the degassing calculations, I used average S, Cl, and F concentrations in the upper continental crust from studies by Hartman and Wedepohl (1993), Wedepohl (1995), and Rudnick and Gao (2003) for the variable $c_{i,A}$. A more detailed explanation can be found in the Volatile Evolution and Degassing section in the Discussion chapter.

4.3. Gaussian plume dispersal model

To calculate the concentration of hazardous volcanic gases downwind from the vent during a sustained eruption I employ a Gaussian plume model from a point source. The point source Gaussian plume model is a simplified steady-state plume model that assumes a Gaussian distribution of particle concentration or species concentration in a gas phase, a constant flux of material, a constant wind speed, a constant eddy diffusivity,

and conservation of mass (Figure 9). This equation has mainly been applied to chemical pollutants within a smoke stack plume, but here I apply the equation to volcanic plumes and volcanic gases. The gas concentration can be determined as a function of a 3-dimensional plane {x, y, z} (Hanna et al., 1981):

$$C_0(x,y,z) = \frac{Q}{2\pi u \sigma_y \sigma_z}\left\{exp\left(\frac{-(z-h)}{2\sigma_z^2}\right) + exp\left(\frac{-(z+h)}{2\sigma_z^2}\right)\right\}\left\{exp\left(\frac{-(y^2)}{2\sigma_y^2}\right)\right\} \quad (7)$$

where x is the distance downwind from the vent, y is the horizontal distance away from the plume centerline, and z is the vertical distance away from the plume centerline. Q is the mass eruption rate of a volatile, h is the "center point" height of the plume, and u is the wind speed. The spatial coordinates x, y, and z define locations along a trajectory downwind of the vent. I focused on values of x that corresponded to average distances between central Oregon and northern California cinder cones and major population or tourist centers. By defining y and z as zero, I calculated the concentration of volcanic gases (ppm) at ground level directly below the plume, a set distance downwind from the vent. Q was determined by converting the weight fraction of a volatile dissolved in the melt into a volatile mass eruption rate (VMER) using the maximum and minimum volatile mass released during eruption from Equation (6). I used the total DRE mass of the cone and tephra erupted (kg) and a magmatic mass eruption rate MER (kg/s) to calculate the total eruption time (s), and with this value I converted the Mt released of S, Cl, and F in an eruption rate for each volatile (kg/s). Estimates of MER were adapted from Pioli et al. (2008, 2009) who concluded that MER drives eruption styles and Violent Strombolian eruptions occur with 10^3 < MER <10^5 kg/s. For this model, I estimated a

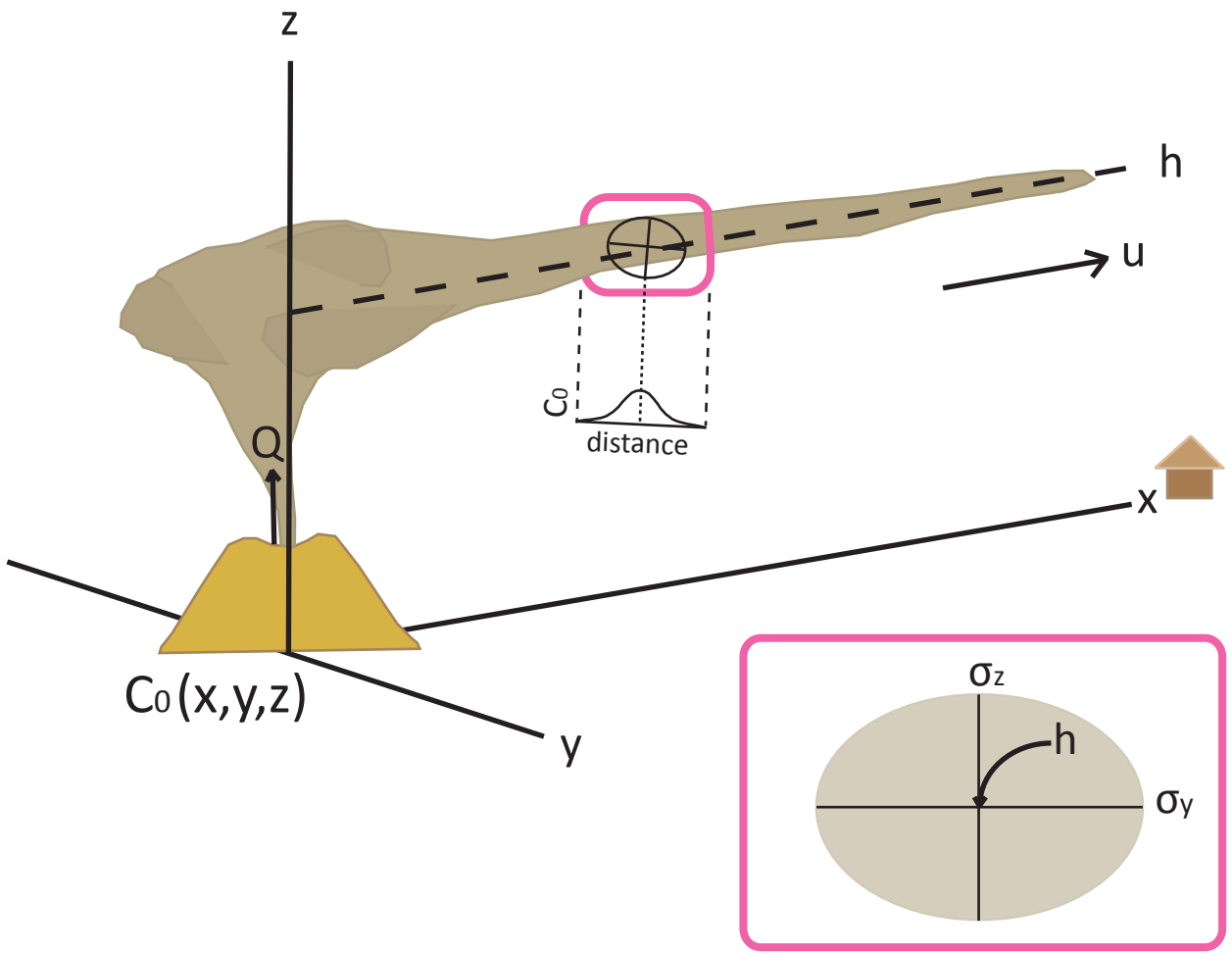

Figure 9: Schematic of the point source Gaussian plume model implemented for cinder cone eruptions to predict volatile concentrations downwind from the vent. The model assumes a Guassian distribution of volatile concentration within the plume and assumes the plume reaches a steady state. The variables in the model includes: (x) downwind spreading distance; (y) horizontal spreading distnce; (z) vertical spreading distance; (C_0) initial volatile concentration in the parental melt; (Q) magmatic flux; (h) centerline height of the plume; (u) wind speed; (σ_Z) cross-sectional concentration in the vertical spreading direction; (σ_Y) cross-sectional concentration in the horizontal spreading direction.

magmatic MER of 10^4 kg/s as it is the average MER for Violent Strombolian cinder cone eruptions found by Pioli et al. (2009). A wind speed of 9 mph (0.004 km/s) was estimated for the annual average wind speed in the central Oregon Cascades from historical databases, and I used an average plume centerline height of 1.5 m. σ_z and σ_y are the cross-sectional concentrations of a gas within the plume in the vertical and horizontal directions, respectively. σ_z and σ_y are defined by the stability of the plume and are calculated by:

$$\sigma_y = 465.11628x(tan\theta) \quad (8)$$

where,

$$\theta = 0.017453293\big(c - dln(x)\big) \quad (9)$$

and,

$$\sigma_z = ax^b \quad (10)$$

The variables a, b, c, and d are assigned values that are a function of plume stability and x, the downwind distance (Appendix E). The stability of the plume can be described as "unstable", "slightly stable", "moderately stable", "neutral", "slightly stable", or "stable" (Hanna et al., 1981). The stability of the plume is defined by its shape (or its vertical response), which is a function of atmospheric stability. After assessment of historic mafic eruption plumes of similar eruption styles (e.g. Parícutin, Cerro Negro, Etna; Figure 10) and descriptions of plume stability from Hanna et al. (1981), Guenther (2010), and EPA (2012), I chose a plume stability rating from "unstable" to "neutral" to assess volatile concentration within the plume downwind of the vent for a range of plume behavior.

Figure 10: Examples of unstable plume stability in historic eruptions of Paricutin (top) and Cerro Negro (bottom).

CHAPTER V

RESULTS

5.1. Melt inclusion compositions

The K_2O, SiO_2, TiO_2, S, Cl, and F concentrations for olivine-hosted melt inclusions and matrix glass analyzed in this study are listed in Tables 3 and 4. The concentrations of these elements (except for F) in the melt inclusions analyzed in this study are similar to the measured compositions reported by Ruscitto (2011), Rasmussen (unpublished), and Walowski (unpublished) for the same cones. Melt inclusions from the central Oregon and northern California Cascades trapped mostly basalt (45-53 wt% SiO_2) to basaltic-andesite (53-57 wt% SiO_2) melt compositions: Collier Cone (51.5-56.1 wt% SiO_2); Yapoah Crater (49.9-53.3 wt% SiO_2); Four-In-One Fissure (51.4-55.1 wt% SiO_2); Garrison Butte (47.4-51.0 wt% SiO_2); Cinder Cone (50.9-60.6 wt% SiO_2); BORG (49.9-53.4 wt% SiO_2); BAS44 (49.0-50.5 wt% SiO_2). Melt inclusions from these cinder cones are medium-K calc-alkaline in composition, but the melt inclusions with the highest SiO_2 contents from Cinder Cone extend into the high-K field (Figure 11). BAS44 displays a transition to a LKT type magma, a signature distinguished by low (<0.5 wt%) K_2O and a high (>2.2) TiO_2/K_2O ratio (Leeman et al., 2005). BORG and Garrison Butte also display a slight transition into a LKT type magma, yet Garrison Butte has slightly elevated K_2O (0.33-0.87 wt%) and BORG has a slightly lower TiO_2/K_2O ratio (1.37-.2.28) in comparison to BAS44. Interestingly, Garrison Butte, BORG, and BAS44 lie ~10 km farther east of the Cascadia trench than Collier Cone, Yapoah Crater, Four-In-One Fissure, and Cinder Cone. Collier Cone, Yapoah Crater, Four-In-One Fissure, and

Table 3: Major and minor element concentrations for melt inclusions of cinder cones from the central Oregon Cascades and northern California; in wt%. Major and minor elements not analyzed in this study (italic) are provided by Ruscitto (2011) (OR), Walowski et al. (unpublished) (CA); and Rasmussen et al., (unpublished) (CA)

	K_2O	SiO_2	TiO_2	S	Cl	F	Al_2O_3	FeO^T	MgO	CaO	Na_2O	MnO	P_2O_5
Collier Cone													
Collier33B-1	0.884	53.837	0.945	0.077	0.071	0.012	*19.50*	*6.77*	*5.27*	*8.82*	*4.09*	*0.10*	*0.13*
Collier33B-3	0.716	52.548	0.886	0.076	0.059	0.011	*19.50*	*6.77*	*5.27*	*8.82*	*4.09*	*0.10*	*0.13*
Collier33B-7	0.591	52.544	1.020	0.076	0.068	0.009	*19.50*	*6.77*	*5.27*	*8.82*	*4.09*	*0.10*	*0.13*
Collier33D-5	0.566	52.341	0.939	0.085	0.068	0.006	*18.76*	*7.00*	*4.40*	*8.28*	*4.57*	*0.11*	*0.14*
Collier33D-5.2	0.642	55.047	1.036	0.079	0.079	0.012	*18.76*	*7.00*	*4.40*	*8.28*	*4.57*	*0.11*	*0.14*
Collier33D-6	0.505	51.561	0.969	0.077	0.065	0.015	*18.76*	*7.00*	*4.40*	*8.28*	*4.57*	*0.11*	*0.14*
Collier33D-3	0.641	54.108	1.027	0.076	0.070	0.004	*18.76*	*7.00*	*4.40*	*8.28*	*4.57*	*0.11*	*0.14*
Collier33D-3.2	0.580	53.309	1.133	0.073	0.063	0.011	*18.76*	*7.00*	*4.40*	*8.28*	*4.57*	*0.11*	*0.14*
Collier33D-4	0.894	56.135	1.087	0.024	0.070	0.077	*18.76*	*7.00*	*4.40*	*8.28*	*4.57*	*0.11*	*0.14*
Yapoah Crater													
Yo016E-1	0.700	52.211	1.077	0.017	0.089	0.099	*18.61*	*7.44*	*5.25*	*8.83*	*4.13*	*0.09*	*0.16*
Yo016E-3	0.625	49.955	1.197	0.012	0.100	0.103	*18.61*	*7.44*	*5.25*	*8.83*	*4.13*	*0.09*	*0.16*
Yo016E-6	0.614	50.835	0.958	0.015	0.093	0.080	*18.61*	*7.44*	*5.25*	*8.83*	*4.13*	*0.09*	*0.16*
Yo016E-8	0.583	51.538	0.904	0.017	0.093	0.080	*18.61*	*7.44*	*5.25*	*8.83*	*4.13*	*0.09*	*0.16*
Yo016E-7	0.713	51.406	1.241	0.024	0.117	0.095	*18.61*	*7.44*	*5.25*	*8.83*	*4.13*	*0.09*	*0.16*
Yo016E-10	0.956	53.330	1.439	0.016	0.135	0.055	*18.61*	*7.44*	*5.25*	*8.83*	*4.13*	*0.09*	*0.16*
Yo016E-12	0.722	50.907	1.077	0.021	0.101	0.083	*18.61*	*7.44*	*5.25*	*8.83*	*4.13*	*0.09*	*0.16*
Four-In-One Fissure													
Fo0803D3-2	0.831	55.095	1.166	0.025	0.066	0.012	*17.44*	*8.42*	*5.91*	*9.12*	*3.21*	*0.13*	*0.25*
Fo0803D3-1	0.749	51.594	1.089	0.014	0.071	0.101	*17.44*	*8.42*	*5.91*	*9.12*	*3.21*	*0.13*	*0.25*
Fo0803D3-5	0.609	51.456	1.068	0.017	0.067	0.095	*17.44*	*8.42*	*5.91*	*9.12*	*3.21*	*0.13*	*0.25*

Table 3 (continued)

	K_2O	SiO_2	TiO_2	S	Cl	F	Al_2O_3	FeO^T	MgO	CaO	Na_2O	MnO	P_2O_5
Four-In-One Fissure													
Fo0803D3-7	0.734	52.623	1.169	0.020	0.072	0.107	*17.44*	*8.42*	*5.91*	*9.12*	*3.21*	*0.13*	*0.25*
Fo0803D3-8	0.751	52.218	1.088	0.017	0.072	0.083	*17.44*	*8.42*	*5.91*	*9.12*	*3.21*	*0.13*	*0.25*
Fo0803D3-14	0.870	54.783	1.104	0.025	0.072	0.005	*17.44*	*8.42*	*5.91*	*9.12*	*3.21*	*0.13*	*0.25*
Fo0803D3-9	0.938	54.426	1.492	0.026	0.087	0.023	*17.44*	*8.42*	*5.91*	*9.12*	*3.21*	*0.13*	*0.25*
Garrison Butte													
GB072-2	0.660	50.260	1.580	0.025	0.046	0.108	*17.16*	*10.49*	*7.17*	*9.84*	*3.24*	*0.16*	*0.39*
GB072-2.2	0.461	48.660	1.442	0.027	0.050	0.143	*17.16*	*10.49*	*7.17*	*9.84*	*3.24*	*0.16*	*0.39*
GB072-1	0.597	49.326	1.481	0.032	0.043	0.142	*17.16*	*10.49*	*7.17*	*9.84*	*3.24*	*0.16*	*0.39*
GB072-5	0.868	51.041	2.046	0.038	0.055	0.017	*17.16*	*10.49*	*7.17*	*9.84*	*3.24*	*0.16*	*0.39*
GB072-8	0.439	48.510	1.508	0.027	0.044	0.151	*17.16*	*10.49*	*7.17*	*9.84*	*3.24*	*0.16*	*0.39*
GB072-6	0.334	43.830	0.763	0.016	0.024	0.069	*17.16*	*10.49*	*7.17*	*9.84*	*3.24*	*0.16*	*0.39*
GB072-9	0.475	48.764	1.475	0.024	0.049	0.134	*17.16*	*10.49*	*7.17*	*9.84*	*3.24*	*0.16*	*0.39*
GB072-12	0.418	47.715	1.460	0.027	0.038	0.107	*17.16*	*10.49*	*7.17*	*9.84*	*3.24*	*0.16*	*0.39*
Cinder Cone													
LCC9-7	1.360	53.833	0.796	0.022	0.038	0.074	*16.21*	*6.65*	*9.27*	*9.75*	*2.98*	*0.09*	*0.15*
LCC9-7.2	1.585	56.735	0.768	0.026	0.041	0.005	*16.21*	*6.65*	*9.27*	*9.75*	*2.98*	*0.09*	*0.15*
LCC9-6	0.829	51.348	0.869	0.013	0.039	0.101	*16.21*	*6.65*	*9.27*	*9.75*	*2.98*	*0.09*	*0.15*
LCC9-6.2	0.814	50.921	0.850	0.021	0.039	0.101	*16.21*	*6.65*	*9.27*	*9.75*	*2.98*	*0.09*	*0.15*
LCC9-11	1.419	55.953	0.835	0.033	0.041	0.009	*16.21*	*6.65*	*9.27*	*9.75*	*2.98*	*0.09*	*0.15*
LCC2-2	2.033	58.441	0.882	0.020	0.040	0.017	*18.10*	*5.12*	*5.59*	*9.85*	*3.16*	*0.09*	*0.21*
LCC2-3	0.784	51.619	1.050	0.016	0.043	0.110	*18.10*	*5.12*	*5.59*	*9.85*	*3.16*	*0.09*	*0.21*
LCC2-3.2	2.168	57.113	1.031	0.037	0.044	0.034	*18.10*	*5.12*	*5.59*	*9.85*	*3.16*	*0.09*	*0.21*

Table 3 (continued)

	K_2O	SiO_2	TiO_2	S	Cl	F	Al_2O_3	FeO^T	MgO	CaO	Na_2O	MnO	P_2O_5
Cinder Cone													
LCC2-7	1.502	60.675	1.189	0.030	0.052	0.068	*18.10*	*5.12*	*5.59*	*9.85*	*3.16*	*0.09*	*0.21*
LCC2-5	0.664	50.847	1.001	0.021	0.043	0.104	*18.10*	*5.12*	*5.59*	*9.85*	*3.16*	*0.09*	*0.21*
LCC2-5.2	1.522	53.677	1.058	0.036	0.040	0.016	*18.10*	*5.12*	*5.59*	*9.85*	*3.16*	*0.09*	*0.21*
Basalt of Old Railroad Grade													
BORG12-3	0.350	49.973	0.740	0.013	0.048	0.133	*19.01*	*6.49*	*5.41*	*10.94*	*3.06*	*0.12*	*0.11*
BORG12-2	0.263	53.474	0.597	0.012	0.058	0.138	*19.01*	*6.49*	*5.41*	*10.94*	*3.06*	*0.12*	*0.11*
BORG12-4	0.111	47.168	0.254	0.007	0.008	0.022	*19.01*	*6.49*	*5.41*	*10.94*	*3.06*	*0.12*	*0.11*
BORG12-6	0.350	52.968	0.723	0.012	0.058	0.158	*19.01*	*6.49*	*5.41*	*10.94*	*3.06*	*0.12*	*0.11*
BORG12-8	0.504	51.261	0.734	0.005	0.052	0.175	*19.01*	*6.49*	*5.41*	*10.94*	*3.06*	*0.12*	*0.11*
BORG12-10	0.531	50.889	0.838	0.009	0.040	0.177	*19.01*	*6.49*	*5.41*	*10.94*	*3.06*	*0.12*	*0.11*
BORG12-12	0.521	50.839	0.715	0.011	0.053	0.152	*19.01*	*6.49*	*5.41*	*10.94*	*3.06*	*0.12*	*0.11*
Basalt of Highway 44													
BAS44-1	0.333	50.579	1.130	0.018	0.033	0.165	*17.68*	*7.84*	*7.60*	*11.21*	*3.00*	*0.13*	*0.26*
BAS44-7.2	0.309	49.079	1.002	0.020	0.031	0.131	*17.68*	*7.84*	*7.60*	*11.21*	*3.00*	*0.13*	*0.26*
BAS44-5.2	0.305	49.133	1.011	0.014	0.028	0.134	*17.68*	*7.84*	*7.60*	*11.21*	*3.00*	*0.13*	*0.26*
BAS44-3	0.400	50.403	1.057	0.009	0.030	0.059	*17.68*	*7.84*	*7.60*	*11.21*	*3.00*	*0.13*	*0.26*
BAS44-3.2	0.403	49.988	1.017	0.015	0.027	0.078	*17.68*	*7.84*	*7.60*	*11.21*	*3.00*	*0.13*	*0.26*
BAS44-8	0.401	50.044	1.037	0.014	0.030	0.096	*17.68*	*7.84*	*7.60*	*11.21*	*3.00*	*0.13*	*0.26*
BAS44-11	0.304	49.978	0.947	0.015	0.031	0.076	*17.68*	*7.84*	*7.60*	*11.21*	*3.00*	*0.13*	*0.26*
BAS44-8.2	0.384	50.518	1.072	0.029	0.025	0.039	*17.68*	*7.84*	*7.60*	*11.21*	*3.00*	*0.13*	*0.26*

Table 4: Major and minor element concentrations for matrix glass of cinder cones from the Central Oregon Cascades and northern California; in wt%. Major and minor elements not analyzed in this study (italic) are provided by Ruscitto (2011) (OR) and Clynne (2011) (CA)

	K_2O	SiO_2	TiO_2	S	Cl	F	Al_2O_3	FeO^T	MgO	CaO	Na_2O	MnO	P_2O_5
Collier Cone													
Collier33B-t3	1.549	62.552	1.492	0.016	0.052	0.002	*18.93*	*6.53*	*4.87*	*7.33*	*3.94*	*0.12*	*0.13*
Collier33D-t1	1.416	62.729	1.680	0.024	0.063	0.003	*18.50*	*7.44*	*3.78*	*7.27*	*4.27*	*0.13*	*0.15*
Collier33D-t3	0.709	61.787	1.361	0.001	0.065	0.001	*18.50*	*7.44*	*3.78*	*7.27*	*4.27*	*0.13*	*0.15*
Yapoah Crater													
Yo016E-t1	1.843	61.328	1.657	0.025	0.104	0.000	*20.00*	*6.85*	*5.88*	*8.29*	*3.37*	*0.12*	*0.15*
Yo016E-t4	1.591	61.488	1.583	0.025	0.099	0.000	*20.00*	*6.85*	*5.88*	*8.29*	*3.37*	*0.12*	*0.15*
Four-In-One Fissure													
Fo0803D3-t1	0.981	58.073	1.587	0.026	0.065	0.000	*17.44*	*19.25*	*5.52*	*8.96*	*3.62*	*0.14*	*0.23*
Fo0803D3-t2	1.038	57.726	1.612	0.030	0.061	0.003	*17.44*	*19.25*	*5.52*	*8.96*	*3.62*	*0.14*	*0.23*
Fo0803D3-t2.2	0.904	57.745	1.432	0.020	0.059	0.001	*17.44*	*19.25*	*5.52*	*8.96*	*3.62*	*0.14*	*0.23*
Garrison Butte													
GB072-t1	1.099	58.520	1.639	0.019	0.063	0.006	*16.42*	*10.30*	*9.09*	*9.33*	*2.80*	*0.18*	*0.29*
GB072-t2	0.868	53.159	2.159	0.032	0.043	0.008	*16.42*	*10.30*	*9.09*	*9.33*	*2.80*	*0.18*	*0.29*
GB072-t3	0.858	52.858	2.122	0.031	0.045	0.010	*16.42*	*10.30*	*9.09*	*9.33*	*2.80*	*0.18*	*0.29*
Cinder Cone													
LCC2-t1	2.092	62.790	1.196	0.025	0.038	0.046	*16.52*	*6.37*	*7.34*	*7.84*	*3.28*	*0.12*	*0.19*
LCC2-t2	2.379	61.191	1.127	0.024	0.037	0.040	*16.52*	*6.37*	*7.34*	*7.84*	*3.28*	*0.12*	*0.19*
LCC9-t1	2.135	60.566	1.182	0.028	0.036	0.007	*16.14*	*6.49*	*8.24*	*8.31*	*3.08*	*0.12*	*0.18*
LCC9-t2	2.100	60.117	1.162	0.024	0.034	0.000	*16.14*	*6.49*	*8.24*	*8.31*	*3.08*	*0.12*	*0.18*
Basalt of Old Railroad Grade													
BORG12-t3	1.197	59.001	1.533	0.039	0.079	0.000	*16.86*	*7.56*	*10.64*	*10.00*	*2.52*	*0.14*	*0.13*
BORG12-t3.2	0.620	57.319	1.547	0.030	0.069	0.002	*16.86*	*7.56*	*10.64*	*10.00*	*2.52*	*0.14*	*0.13*

Table 4 (continued)

	K_2O	SiO_2	TiO_2	S	Cl	F	Al_2O_3	FeO^1	MgO	CaO	Na_2O	MnO	P_2O_5
Basalt of Highway 44													
BAS44-t3	0.533	53.267	1.267	0.016	0.026	0.001	*17.74*	*8.59*	*0.15*	*10.58*	*2.86*	*0.13*	*0.19*
BAS44-t2	0.589	53.542	1.344	0.020	0.026	0.003	*17.68*	*8.59*	*0.15*	*10.58*	*2.86*	*0.13*	*0.19*
BAS44-t1	0.442	53.010	1.199	0.011	0.026	0.004	*17.68*	*8.59*	*0.15*	*10.58*	*2.86*	*0.13*	*0.19*

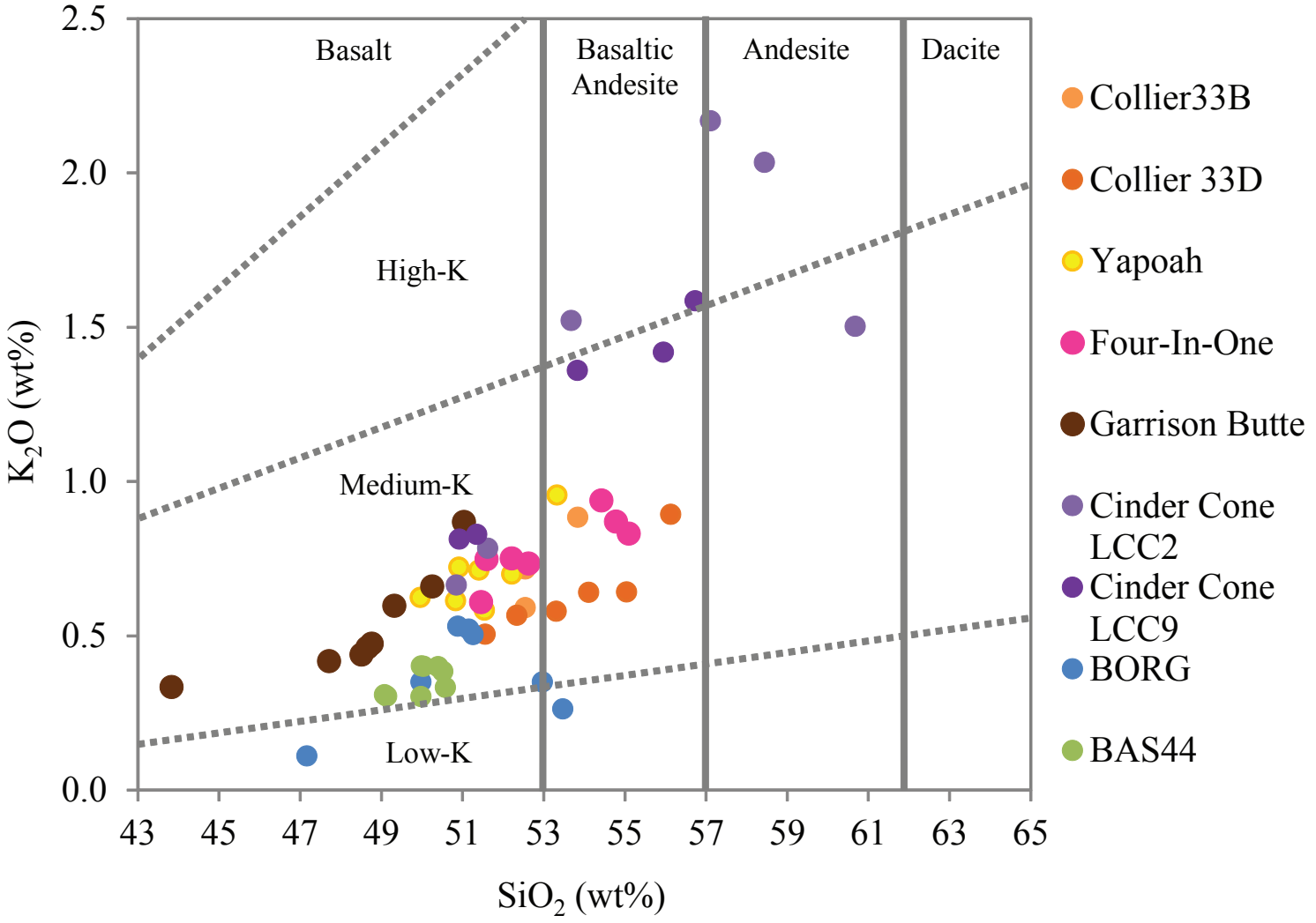

Figure 11: Melt inclusion K_2O and SiO_2 concentrations. Most central and southern Cacades melt inclusions plot in the medium-K basalt and basaltic andesite fields. Garrison Butte, BORG, and BAS44 inclusions are slighly less alkalic, with lower SiO_2 concentrations. Contaminated melt inclusions from Cinder Cone plot in basaltic andesite to andesite fields and contain higher K_2O contents.

Cinder Cone all display typical subduction zone chemical characteristics (calc-alkaline basalt, or CAB) signatures, with elevated (>0.6-2.2 wt%) K_2O. See Table 5 for a summary on central and southern Cascades magma compositions.

5.2. Tephra bulk compositions

Tephra erupted from central Oregon and northern California cinder cones is mostly basaltic andesite to andesitic (54-62 wt% SiO_2) in composition – Collier Cone (61.7-62.7 wt% SiO_2); Yapoah Crater (61.3-61.5 wt% SiO_2); Four-In-One Fissure (57.7-58.1 wt% SiO_2); Garrison Butte (52.8-58.5 wt% SiO_2); Cinder Cone (60.1-62.7 wt% SiO_2); BORG (57.3-59.0 wt% SiO_2); BAS44 (53.0-53.5 wt% SiO_2).

5.3. Dissolved volatiles

Sulfur contents in the melt inclusions are highly variable, ranging from below detection (50 ppm) to a maximum of 1750 ppm at BORG. However, most melt inclusions contain >700 ppm S. The highest concentrations of S occur in the melt inclusions that have compositions transitional to LKT. The concentrations of chlorine range from 240 to 1350 ppm, with the lowest Cl concentrations found in melt inclusions from BAS44. The Cl contents found in melt inclusions from Yapoah Crater plot well above Cl concentrations of the other central and southern Cascades cones. Measured fluorine contents range from below detection (90 ppm) to 380 ppm. No systematic difference in F between the LKT transitional and CAB magma types is distinguishable.

The matrix glass from all cones has low concentrations of S compared to the melt inclusions, in contrast to the data for Cl and F (Table 4; Figure 12). Measured S contents

range from below detection (50 ppm) to 450 ppm, with the majority of data points hovering near the detection limit. Chlorine concentrations remain constant from melt inclusions to tephra matrix glass, with the minimum and maximum concentrations being 260 ppm and 1040 ppm, respectively. Fluorine contents also remain constant within the melt, ranging in concentration from 115-385 ppm.

Table 5: Magma type of erupted mafic lavas in central Oregon and northern California

low-K tholeiite transition	Garrison Butte
	BORG
	BAS44
calc-alkaline basalt	Collier Cone
	Yapoah Crater
	Four-In-One Fissure
	Cinder Cone

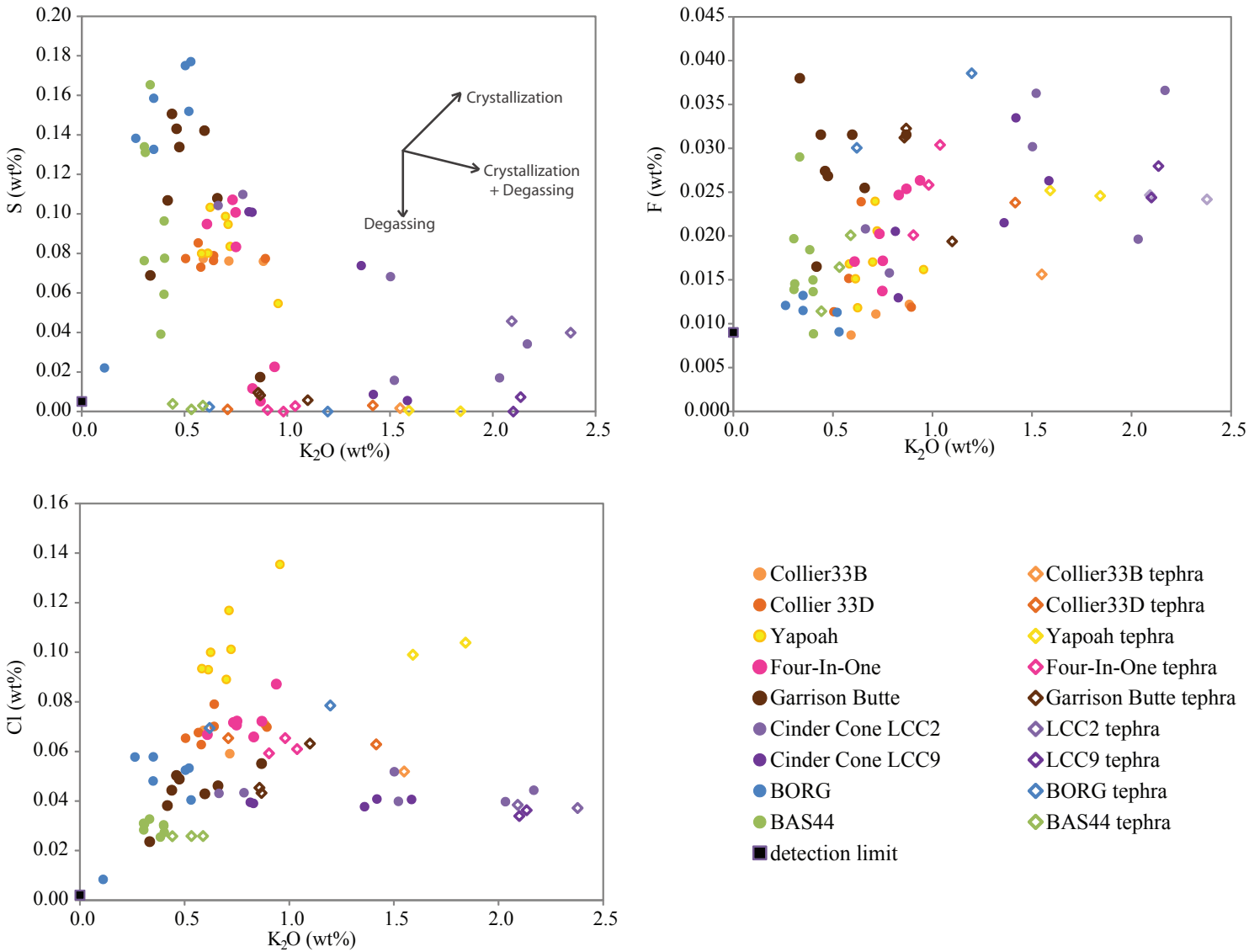

Figure 12: Dissolved volatile contents in olivine-hosted melt inclusions (filled circles) and matrix glass (open diamonds). Sulfur evolution is dominated by degassing, where Cl and F evolution is predominately dominated by a moderate degree of crystallization with degassing.

CHAPTER VI

DISCUSSION

6.1. Melt evolution- The importance of fractional crystallization and crustal assimilation during ascent

Systematic variations of incompatible element concentrations (K_2O, TiO_2) in the melt inclusions and matrix glass define distinct trends that are generated by similar melt evolution processes. Melt components not incorporated into crystallizing minerals become increasingly concentrated in the residual melt as crystallization proceeds and are referred to as "incompatible". K_2O and TiO_2 are commonly used as an index of fractional crystallization in mafic melts because both behave systematically with crystallization of mafic minerals. K_2O is not incorporated into the structure of crystallizing mafic minerals (i.e., olivine, plagioclase, spinel, pyroxene). The covariance of K_2O and TiO_2 that is commonly seen in many data suites of cinder cone magmas suggests there has not been substantial crystallization of titanomagnetite (Erlund et al., 2010; Johnson et al., 2010). K_2O and TiO_2 can also be used as an index of crustal assimilation in mafic magmas. Crustal materials are enriched in K_2O, therefore increasing the concentration of K_2O during assimilation. TiO_2 however, will decrease in concentration with the addition of a crustal contaminant because granitic and silicic volcanic rocks generally have very low TiO_2 contents (Erlund et al., 2010).

Crystallization via Rayleigh fractionation, or the removal and separation of minerals from a melt, is identified by a linear trend of incompatible element concentrations (e.g. K_2O, TiO_2) along a fractionation line (Figures 13, 14). Assimilation

of more silicic material, such as the proposed granitic country rock adjacent to Lassen Peak, can be identified using a diagram of TiO_2/K_2O vs. SiO_2 (Figures 15, 16). If data points lie along a hyperbolic mixing line between a primitive magma composition and a more evolved crustal contaminant, the magma is interpreted to be contaminated. Figures 13 and 14 show the effects of fractional crystallization, both with and without assimilation. The data for the crustal contaminant used in these figures, as well as for the mixing curves in Figures 15 and 16 come from Table 2. Based on melt inclusion and matrix glass data variations, only a few of the magmas experienced pure fractional crystallization as they ascended from the lower crust. Instead, each parental magma has experienced a combination of crystal fractionation and crustal assimilation from the lower crust to the surface. Figures17 and 18 show a comparison among all cones of the effects of fractional crystallization and crustal assimilation, respectively.

The spread in melt inclusion data points from Yapoah Crater and Garrison Butte can be explained by a magmatic history of pure fractional crystallization (Figure 13). Yapoah Crater magma fractionated up to 36% crystals. The parent magma at Garrison Butte fractionated up to 28% crystals. The melt inclusion recording the lowest K_2O and TiO_2 concentrations at Garrison Butte is conceivably a xenocryst as fractionation lines emanating from this melt inclusion do not describe the evolution of the other inclusions. It is also possible that the spread in melt inclusion data represents the simultaneous evolution of two similar, but compositionally distinct magmas. Work by Strong and Wolff (2003) in the southern segment of the Cascades suggests scoria cones can tap magmas from different mantle sources as melts can travel through the crust without storage within a magma chamber or because of inefficient mixing within a magma

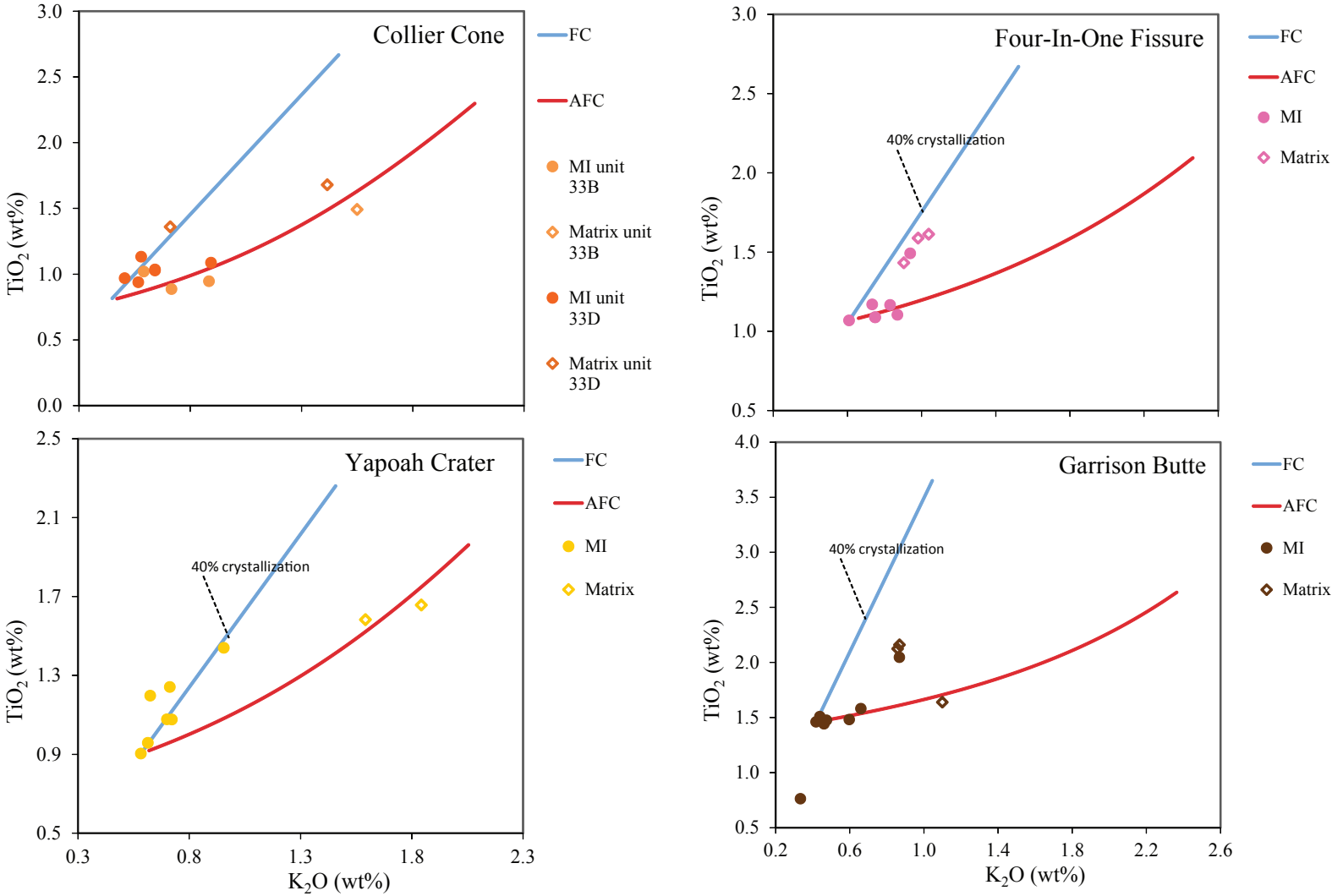

Figure 13: Evolution of the melt through crystal fractionation and crustal assimilation recorded by olivine-hosted melt inclusions (filled circles) and matrix glass (open diamonds) in central Oregon. The lowest K_2O and TiO_2 concentration melt inclusion was chosen as the best representative of the parental magma composition. Melt inclusions from Collier Cone do not represent the most primitive melt and therefore a hypothetical parent melt was used to calculate crystal fractionation and assimilation. FC denotes pure fractionation of crystals; AFC denotes crystal fractionation with assimilation.

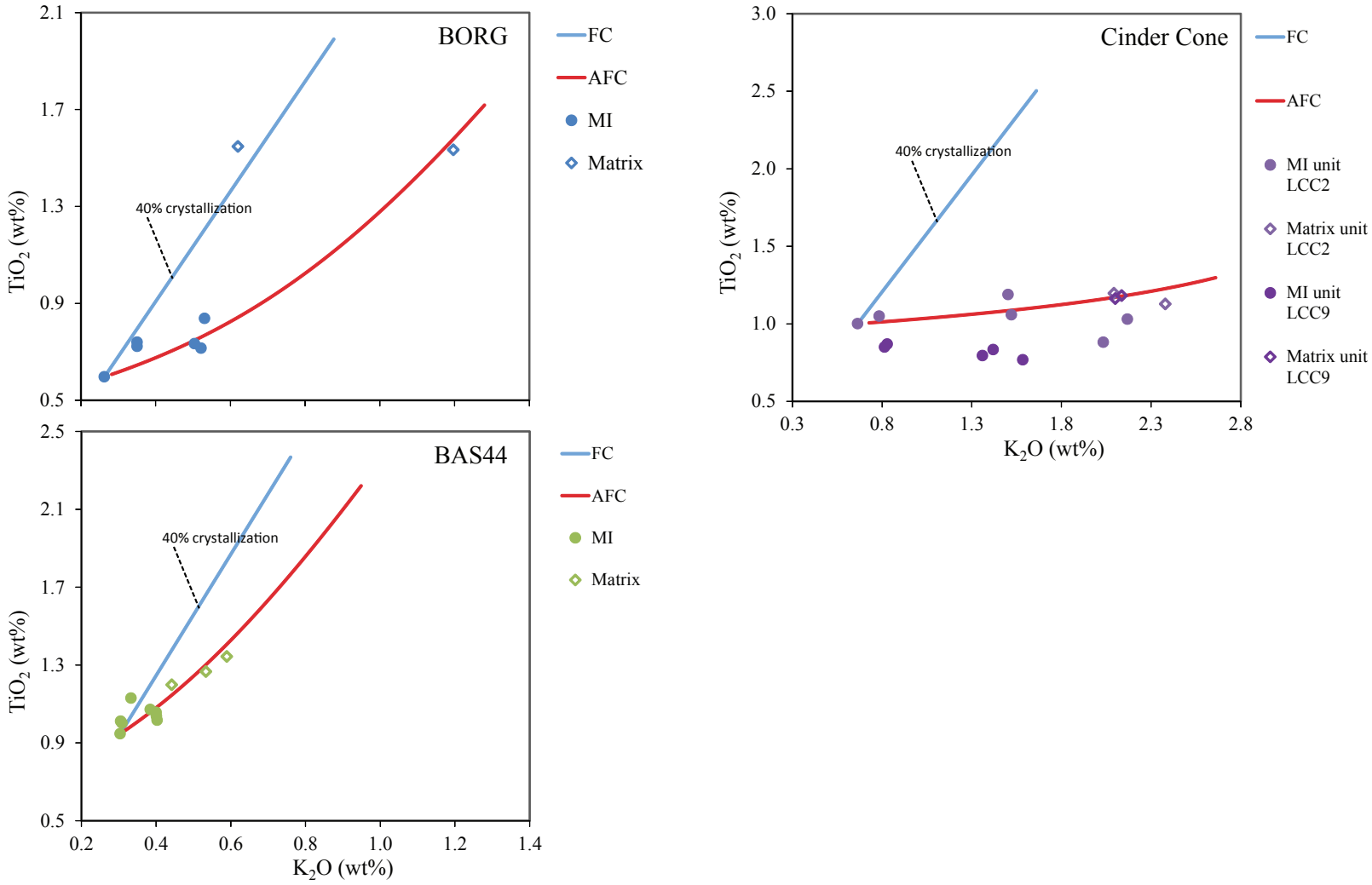

Figure 14: Evolution of the melt through crystal fractionation and crustal assimilation recorded by olivine-hosted melt inclusions (filled circles) and matrix glass (open diamonds) in northern California. The lowest K_2O and TiO_2 concentration melt inclusion was chosen as the best representative of the parental magma composition. FC denotes pure fractionation of crystals; AFC denotes crystal fractionation with assimilation.

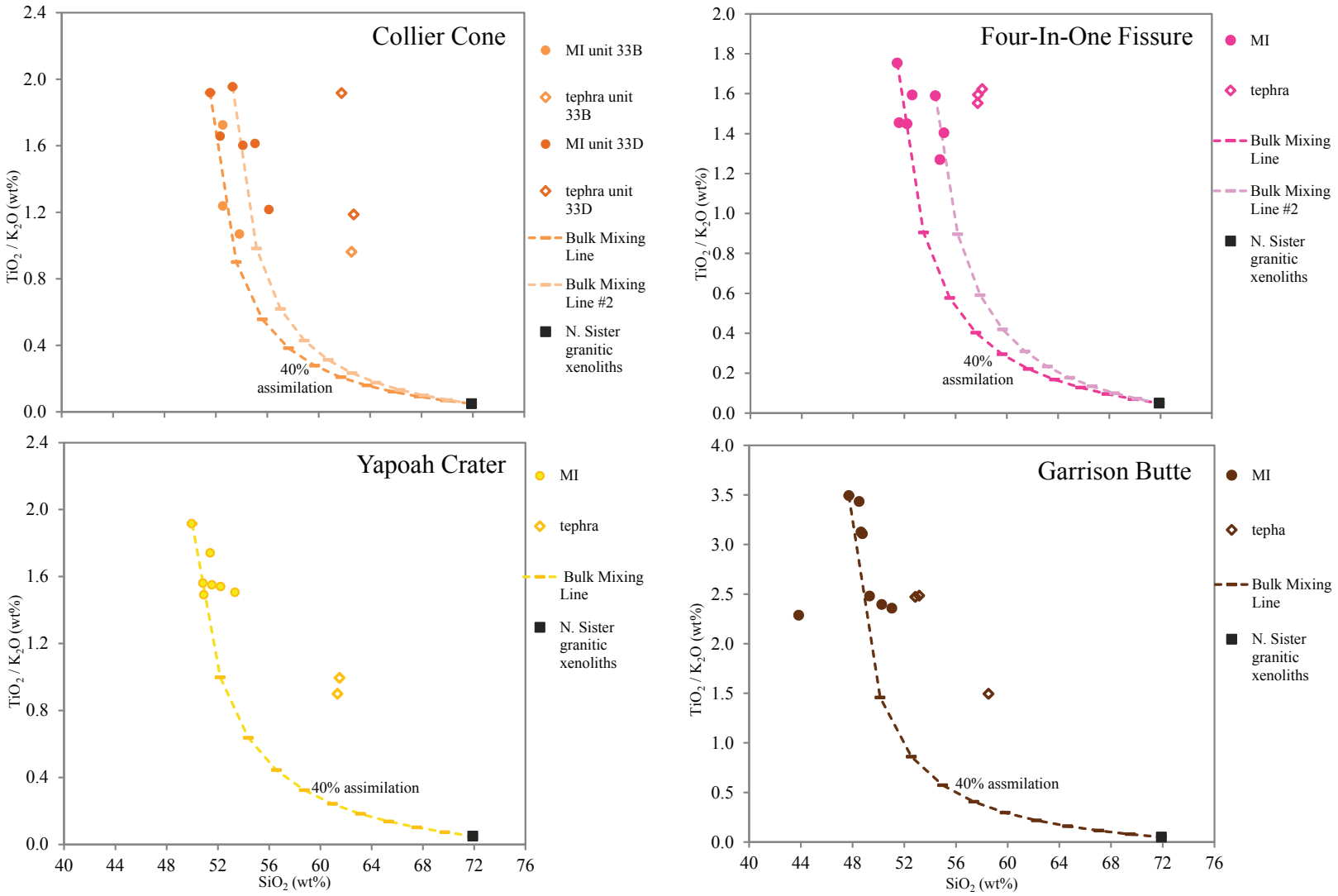

Figure 15: Individual TiO_2/K_2O and SiO_2 contents of olivine-hosted melt inclusions (filled circles) and matrix glass (open diamonds) for the central Oregon Cascades cinder cones.

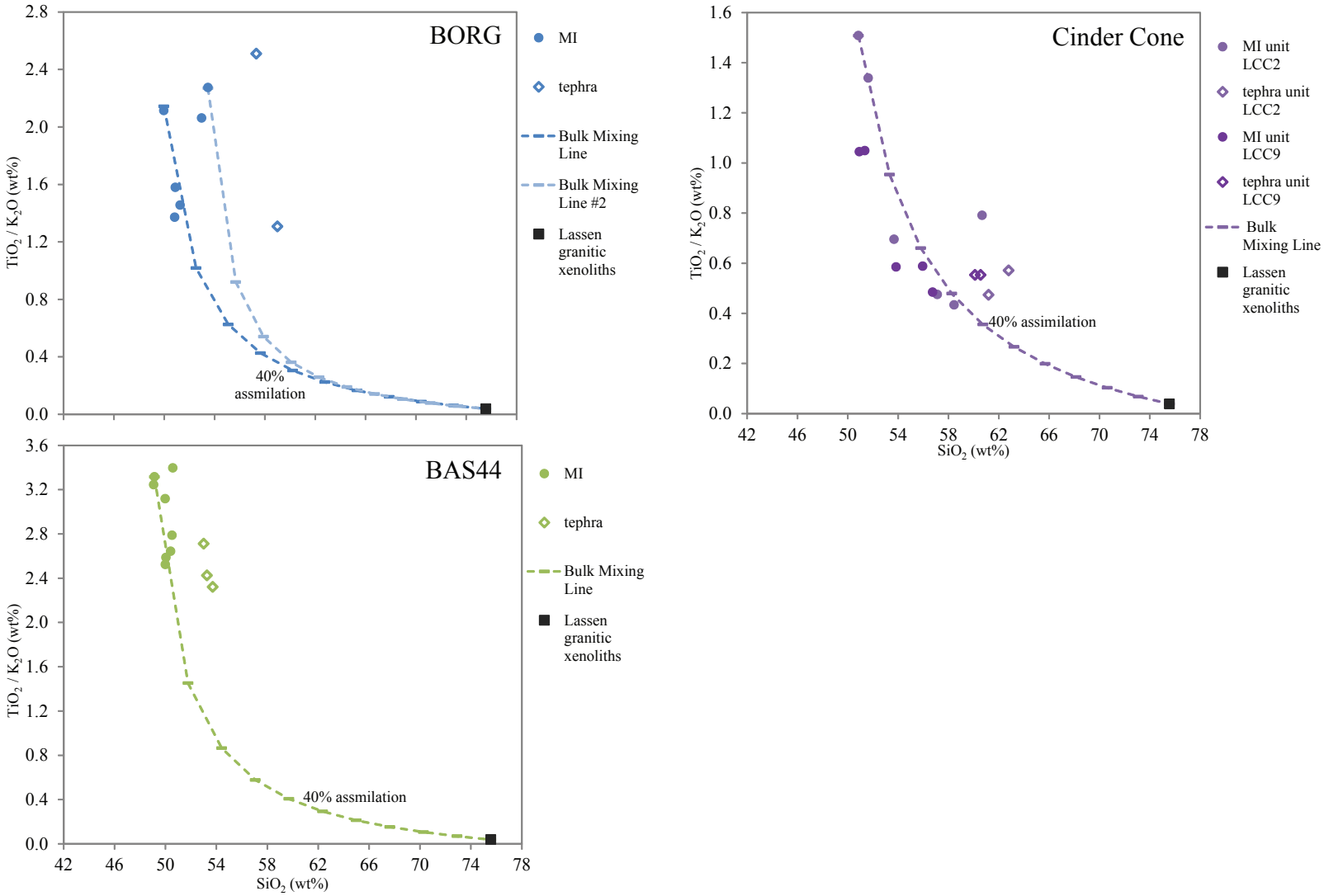

Figure 16: Individual TiO_2/K_2O and SiO_2 contents of olivine-hosted melt inclusions (filled circles) and matrix glass (open diamonds) for northern California cinder cones.

chamber. Starting from a magma that is represented by the lowest K_2O inclusion, the matrix glass from Yapoah Crater suggests the magma fractionated up to 52% crystals with as much as 13% assimilation of silicic material similar to the granitic xenoliths erupted by Collier Cone. The spread of matrix glass data points from Garrison Butte can be explained by end-member models requiring 32% fractional crystallization or fractionation up to 22% with as much as 4% silicic assimilation.

Cinder Cone is the only cone to show fractionation with a high percentage of crustal assimilation in both the melt inclusions and the matrix glasses (Figure 14). Using the melt inclusion with the lowest K_2O content the range of values recorded by melt inclusions can be explained by fractionation of up to 44% crystals with as much as 37% assimilation of a silicic contaminant like that of granitic country rock near Lassen Peak. Matrix glass compositions require up to 50% crystals with as much as 43% silicic assimilation from a magma represented by the lowest K_2O concentrations.

The melt inclusions from Collier Cone, Four-In-One Fissure, BORG, and BAS44 record the evolution of magma that can either be explained by crystal fractionation or crustal assimilation (Figures 13, 14). I suggest the melt inclusions of Collier Cone show entrapment of an evolved melt such that the actual parent magma of Collier Cone is composed of lower K_2O and TiO_2 concentrations than those shown by the melt inclusions. Using this hypothesized parent magma, magma from Collier Cone fractionated up to 28% crystals or fractionated up to 28% of crystals with as much as 6% assimilation with the granitic xenoliths. Four-in-One Fissure magma fractionated up to 28% crystals or fractionated up to 10% crystals with as much as 4% silicic assimilation. Melt inclusions from BORG show that the magma fractionated up to 18% crystals or

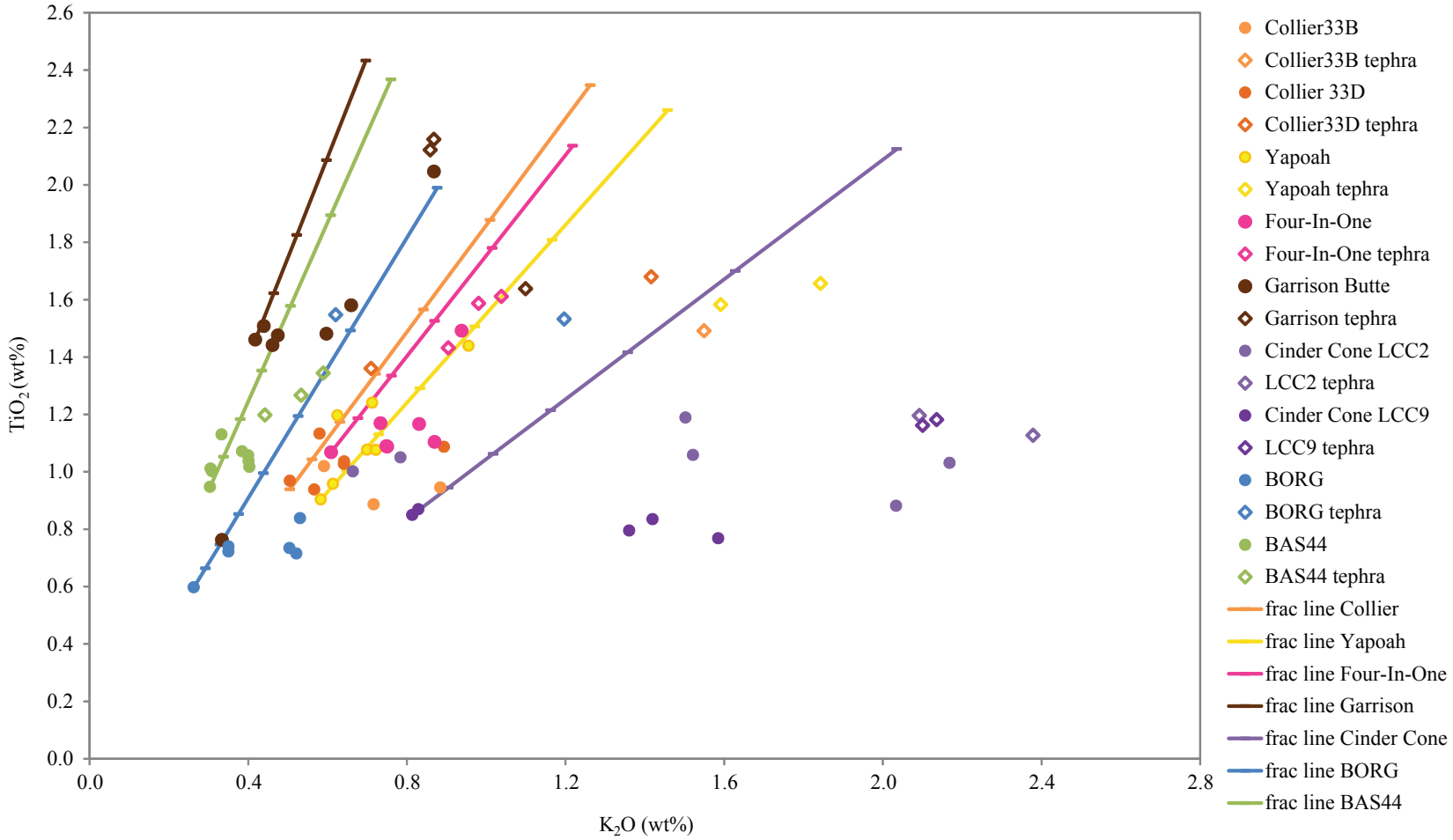

Figure 17: TiO_2 and K_2O contents of melt inclusions (filled circles) and matrix glass (open diamonds) from central Oregon and northern California. Melt inclusions show evolution by crystal fractionation with coupled assimilation. Yapoah Crater shows significant fractionation, with tephra appearing to assimilate with a granitic-like body. TiO_2 and K_2O diagrams for individual cones are found in Figures 13 and 14.

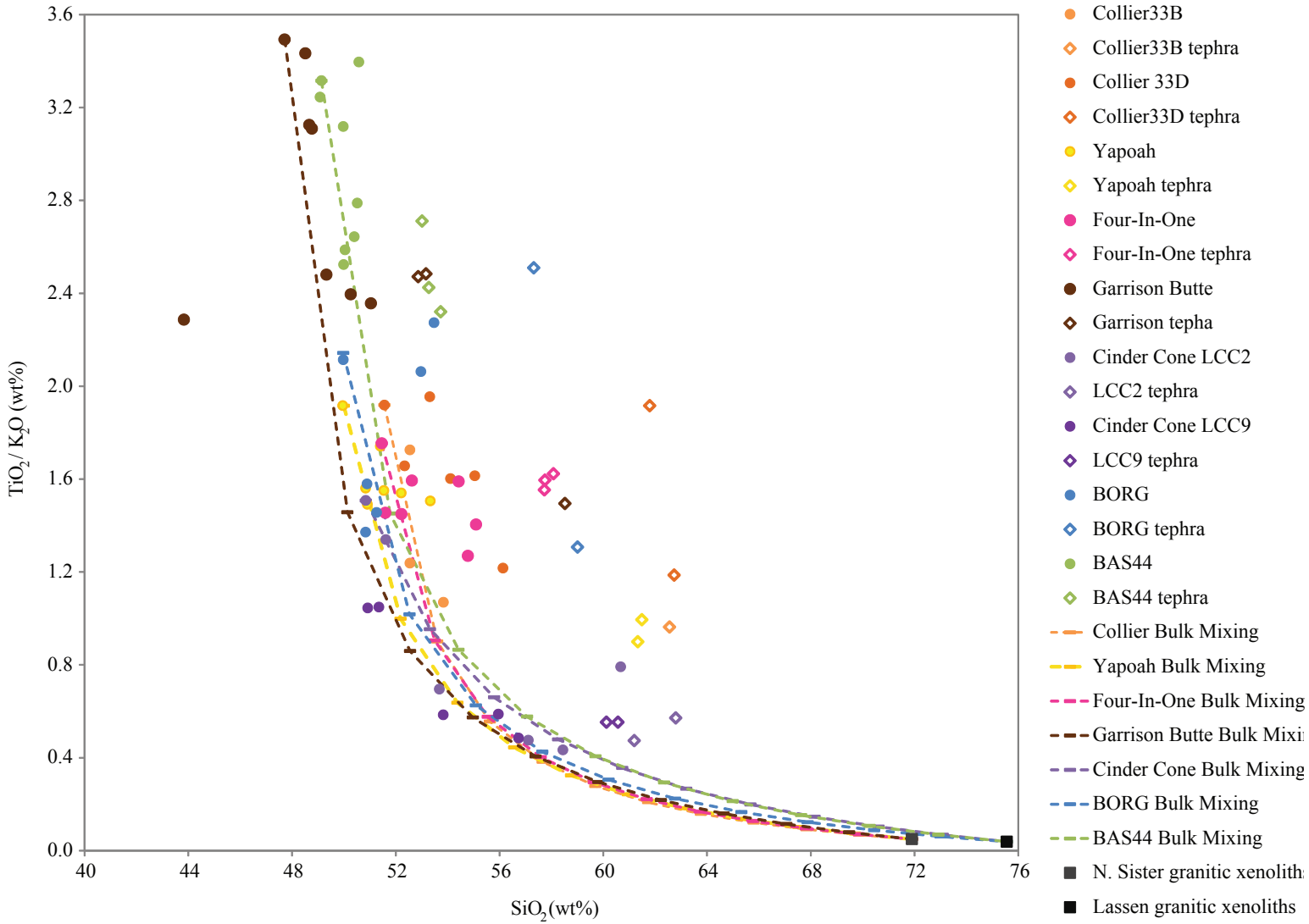

Figure 18: TiO_2 /K_2O and SiO_2 contents of melt inclusions (filled circles) and matrix glass (open diamonds) from central Oregon and northern California. The majority of the melt inclusions follow an assimilation path toward a depleted granitic contaminant, most notably melt inclusions from Cinder Cone. TiO_2 /K_2O vs. SiO_2 diagrams for individual cones are found in Figures 15 and 16.

fractionated up to 28% with as much as 6% silicic assimilation. At BAS44, the magma fractionated up to 12% crystals or fractionated up to 12% crystals with as much as 1% assimilation of a silicic contaminant like that of granitic country rock near Lassen Peak. The evolution in the matrix glass of these four cinder cones varies. Four-in-One Fissure records fractionation only of the melt (up to 32% crystals), BAS44 matrix glass record up to 32% crystal fractionation with as much as 4% silicic assimilation, and matrix glasses of Collier Cone and BORG magmas can be explained by either fractionation up to 40% and 62% crystals, respectively or fractionation up to 54% and 66% crystals with as much as 12% and 14% silicic assimilation, respectively.

6.2. Volatile evolution and degassing

When a melt fractionates, the concentration of incompatible elements will increase. Volatile elements can also behave incompatibly if they have relatively high solubility and are not entering other solid or immiscible liquid phases (e.g., sulfide minerals). Melting of an assimilant can also increase or decrease the concentration of highly soluble elements, such as S, Cl, and F, in the melt, depending on the volatile content of the assimilant. The controls of fractional crystallization or crustal assimilation on dissolved volatiles vary with each cinder cone. Some cones are more affected by fractional crystallization whereas others are more affected by crustal assimilation. Figure 19 shows the controls on S, Cl, and F evolution. A decrease in volatile concentration with an increase in K_2O can be attributed to partial degassing or interaction with a contaminant that contains a very low concentration of the volatile. Where assimilation is minimal, Cl concentrations follow along a crystal fractionation line. Yapoah Crater

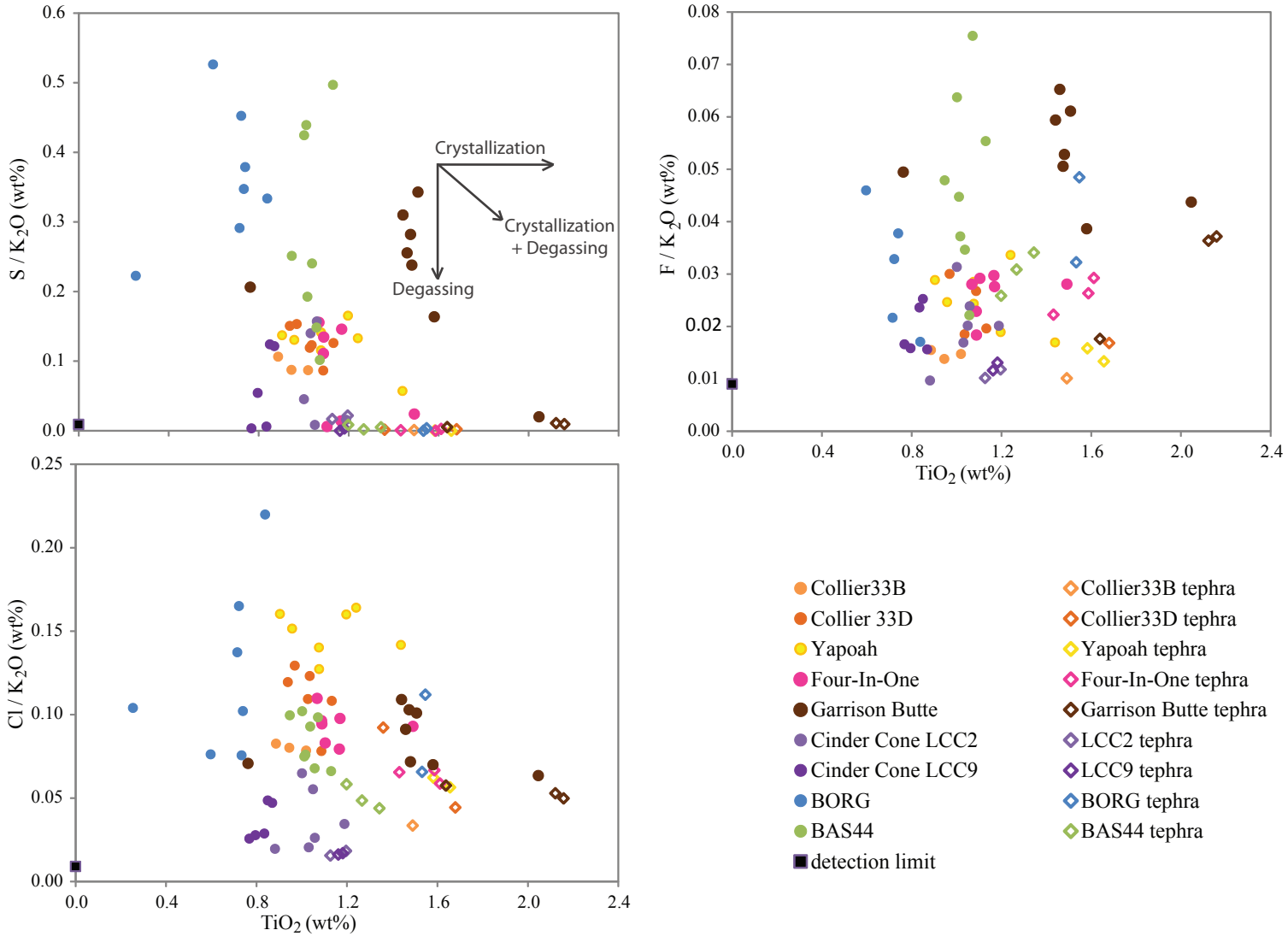

Figure 19: Volatile/K_2O and TiO_2 contents of olivine-hosted melt inclusions (filled circles) and matrix glass (open diamonds) for central Oregon and northern California cinder cones. As incompatible elements (K_2O, TiO_2) increase, volatile concentrations decrease strongly through degassing, decrease moderately through simultaneous crystallization and degassing, or display concentrations similar to the most primitive melts.

displays a typical fractional crystallization trend. Chlorine increases with K_2O as the melt fractionates 36% crystals. Melt inclusions of BAS44 collapse onto a fractional crystallization line as Cl increases with 12% crystallization. Fluorine should also follow a fractionation line as it is an element with high melt solubility. In general, F appears to increase at a faster rate than K_2O. However, given the relatively large uncertainties on the F measurements, I conclude that F increases at the same rate as K_2O, consistent with fractional crystallization. Detection of S evolution within each melt is more difficult due to sulfur's strong ability to exsolve into a vapor phase and degas from the system at lower pressures. Controls on S evolution in the melt inclusions and matrix glass at all cones are masked by strong degassing and therefore are not discernable. Averages of major, minor, and volatile concentrations for each cone can be found in Figures 20 and 21.

No volatile analyses have been performed on the silicic xenoliths near North Sister or Lassen Peak, so to account for effects on volatile concentration due to assimilation, I used upper crustal compositions of S, Cl, and F compiled by Hartman and Wedepohl (1993), Wedepohl (1995), and Rudnick and Gao (2003). By using upper crustal averages I calculated the original S, Cl, and F concentrations in the magma with varying degrees of fractional crystallization and assimilation before any degassing had occurred. By assuming a non-zero volatile concentration in the silicic contaminants near North Sister and Lassen Peak I can make a reliable estimate of volatile evolution within the melt and the quantity of gas released during eruption.

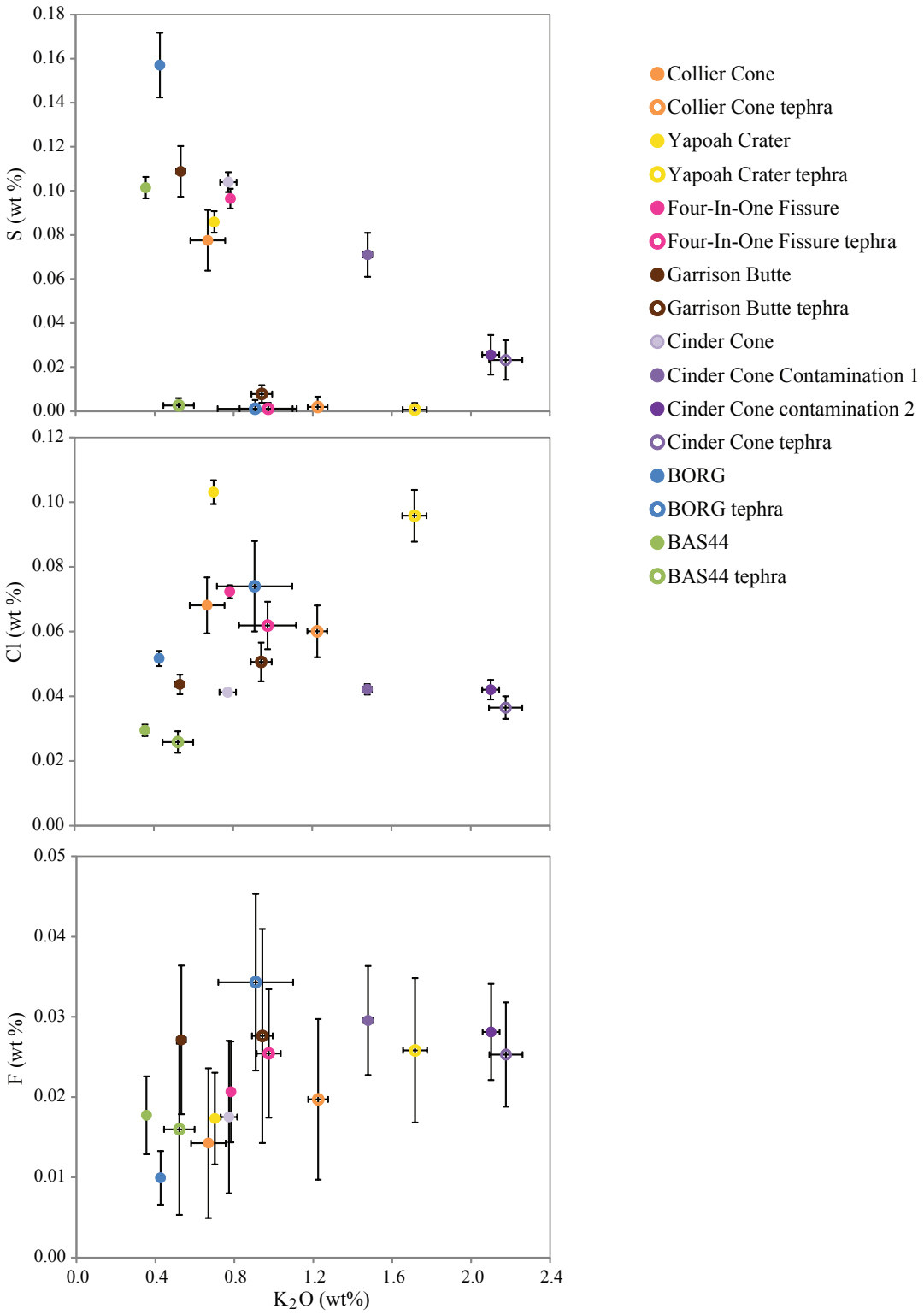

Figure 20: Averaged volatile and K_2O concentrations for cinder cones in the central and southern Cascades. Error bars represent 2 standard deviations. Filled circles represent averaged olivine-hosted melt inclusions; open circles represent averaged matrix glass. Cinder Cone melt inclusions were separated into 3 distinct groups based on their K_2O content. An average was created for each grouping.

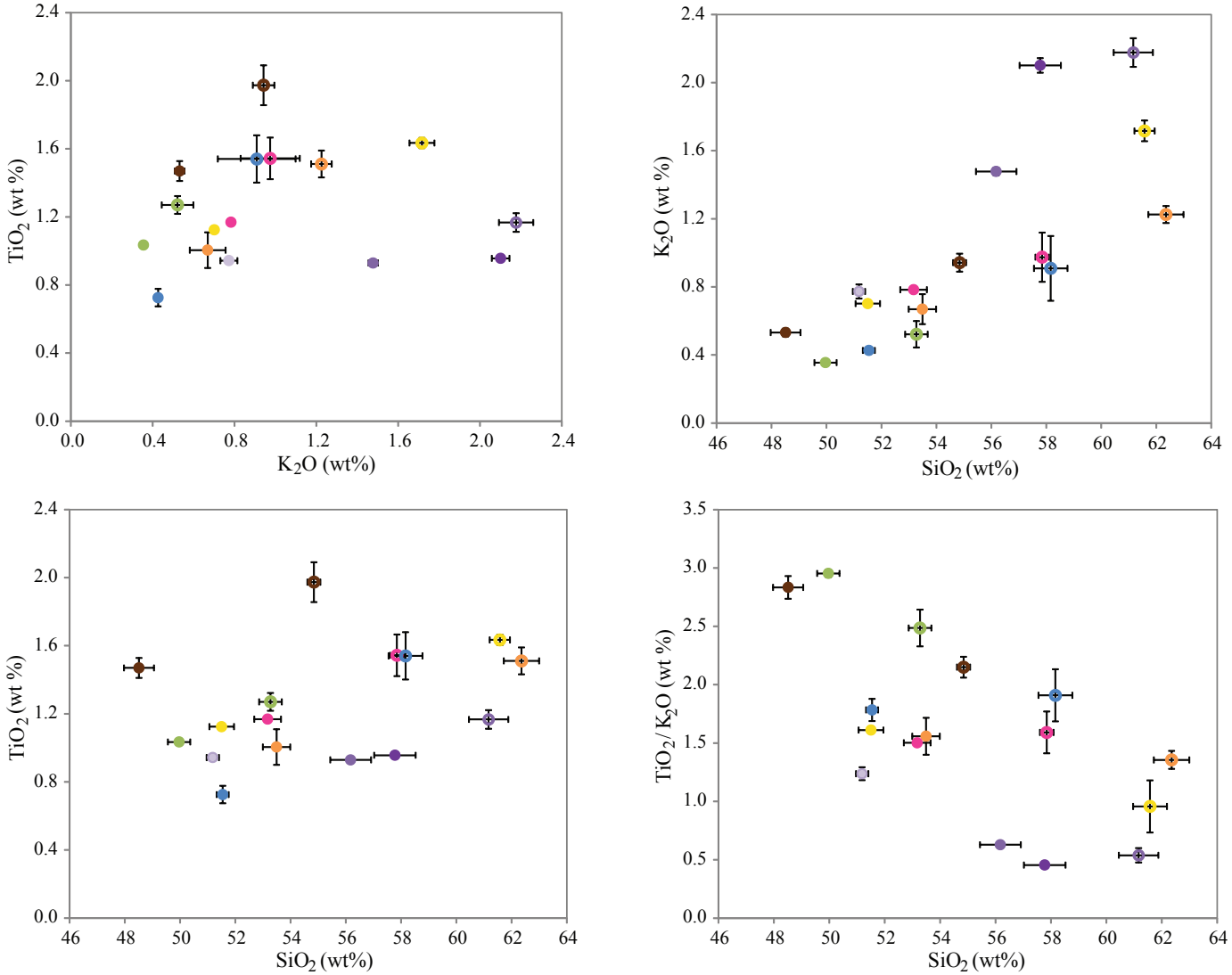

Figure 21: Averaged TiO_2, K_2O, and SiO_2 concentrations for cinder cones in the central and southern Cascades. Error bars represent 2 standard deviations. Filled circles represent averaged olivine-hosted melt inclusions; open circles represent averaged tephra groundmass glass. Cinder Cone melt inclusions were separated into 3 distinct groups based on their K_2O content. An average was created for each grouping. Legend for symbol colors is the same as in Figure 24.

6.3. Comparison of volatile concentrations in Cascades magmas to other global mafic eruptions

Mid-ocean ridge basalts have S, Cl, and F values on average of ~1000 ppm, ~100 ppm, and ~140 ppm, respectively (Jambon, 1994; Wallace, 2005). Values for S, Cl, and F concentrations in mafic arc magmas are higher in comparison to MORB because of fluid fluxing from the subducted slab into the mantle wedge (Wallace, 2005; Ruscitto, 2011). Evolved melts contain low concentrations (≤200 ppm) of S due to sulfur's strong preference to partition into a vapor phase or precipitate in sulfide or sulfate minerals, such as anhydrite, during crustal storage (Wallace and Anderson, 2000; Wallace, 2003; Wallace and Edmonds, 2011). The incompatibility of Cl and F at high pressure causes their concentrations to increase in the melt with increasing differentiation, in contrast to S (Metrich and Wallace, 2008). Chlorine concentrations can reach up to 2000 ppm in silicic magmas with the addition of NaCl-rich fluid, such as seawater, or a Cl-rich vapor (Wallace, 2005; Metrich and Wallace, 2008). Volcanic locales such as Etna, Arenal, and Ruapehu record F levels over 1000 ppm (Cronin et al., 2003; Spilliaert et al., 2006; Wade et al., 2006).

Volatile concentrations in magmas erupted from central Oregon and northern California are elevated above MORB values and are comparable to mafic magmas from other volcanic arcs (Wallace, 2005). Most notably, volatile contents of central Oregon and northern California have considerable overlap with eruptive centers such as Cerro Negro (Roggensack et al., 1997; Portnyagin et al., 2012) (Figure 22). Volatile concentrations at Etna, La Sommata, and at the highly potassic cones in the Trans-Mexican Volcanic Belt (TMVB) are significantly elevated above the volatile contents of

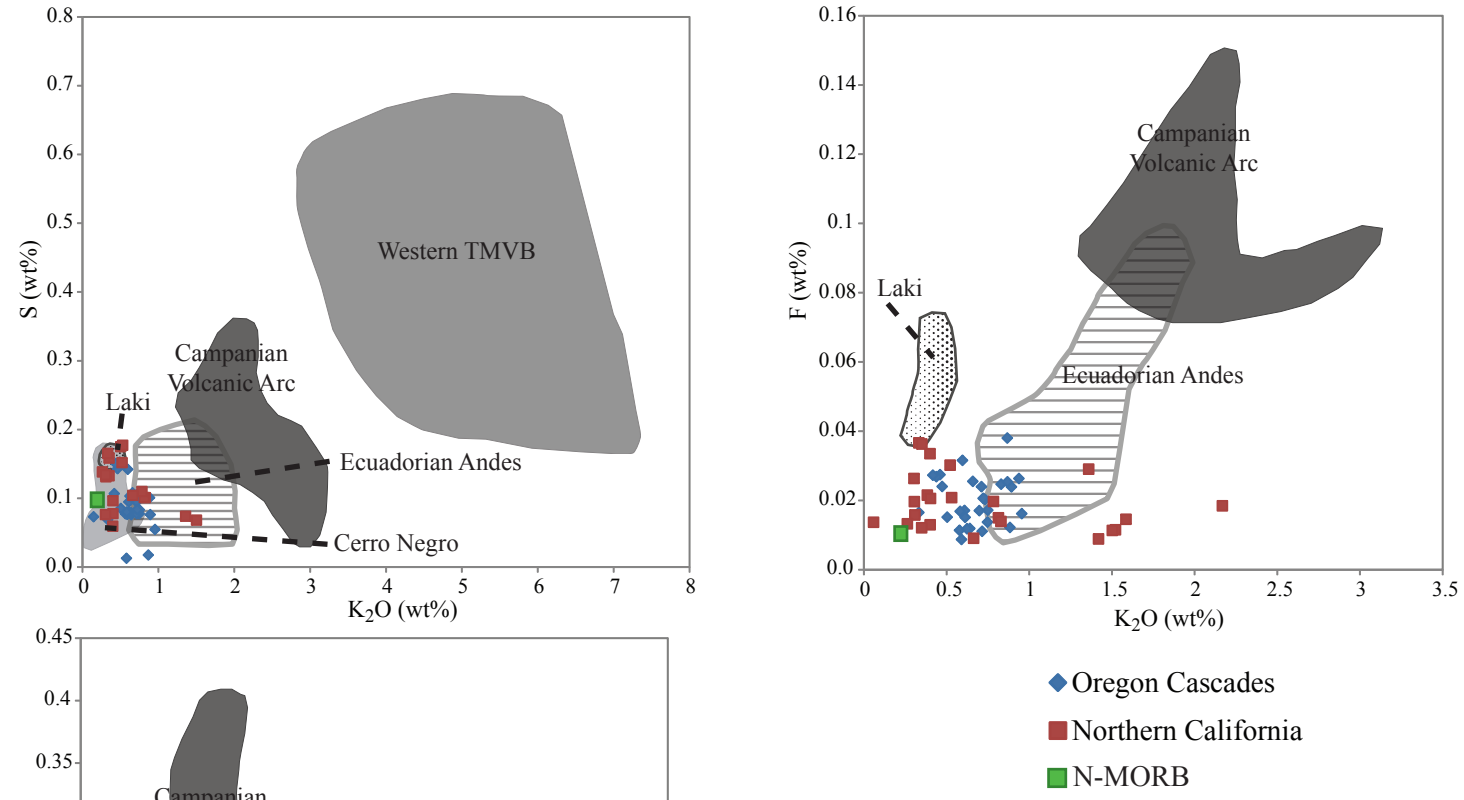

Figure 22: Comparison of Cascades arc volatile contents to other global arc volatile contents. Filled in areas represent melt inclusion values for the Campanian Arc (La Sommata, Mt. Etna; dark grey), the Western Trans-Mexican Volcanic Belt (medium grey), Cerro Negro (light grey), the Ecuadorian Andes (stripped), and Laki (speckled). Melt inclusions from the central Oregon Cascades and northern California have significant overlap with volatile concentrations from Cerro Negro and Laki. MORB data from Jambon, 1994; Wallace, 2005. Global data from Thordarson et al., 1996; Le Voyer et al., 2008; Vigouroux et al., 2008; Le Voyer, 2009; Portnyagin et al., 2012.

the Cascades cones, indicating a dissimilar magmatic source and magmatic evolution. Vigouroux et al. (2008) suggested that the highly potassic magmas erupted in the TMVB involved melting of a metasomatized phlogopite-apatite-rich mantle source. Interestingly, with the exception of F (of which no F melt inclusion data currently exists in publication for Cerro Negro), S and Cl concentrations match well with those of Cerro Negro. Much work has documented the hazards associated with historical eruptions at Cerro Negro and the dangers they have presented for human populations and ecosystems (McKnight and Williams, 1997; Hill and Connor, 1998; Connor, 2001). The upper limits of volatile concentrations in the central and southern Cascades also match well with the 1783-1784 fissure eruption at Laki. The eruption at Laki is a significant event in volcanic history because it became known as one of the greatest atmospheric pollutants in prehistoric and historic records. Thordarson et al. (1996) calculated a release of 75% of the dissolved volatiles over the entire eruption. Such large degassing events affect both atmospheric and ground/surface water chemistry. Granted, the sheer eruptive volume of the Laki eruption (~0.5-2.0 km^3 for each eruptive episode, 15.1 km^3 total; Thordarson et al., 1996) sets it apart from the Cascades, but it is important to note as a possible eruptive outcome for central Oregon and northern California.

6.4. Release of SO_2, HCl, and HF into the troposphere

Volatile exsolution is a critical driving force for volcanic eruptions as the expansion of bubbles accelerates magmatic froth upward through the conduit, eventually causing it to exit the vent as a gas-rich jet (Parfitt and Wilson, 1995). When the vesicularity reaches ~75% by volume, fragmentation occurs (Cashman et al., 2000).

Volatiles also control the eruption style exhibited by a cinder cone through a dependence on the regime of gas bubble transfer (e.g. Belien, 2011) and the magma supply and ascent rates (e.g. Pioli et al., 2008). It has been documented that high volatile fluxes can sustain lava fountains and play a major role in the transition from an effusive eruption into a Strombolian-type eruption (Wallace and Anderson, 2000).

Following the methods outlined in Chapter IV for calculating the masses of volatiles released into the troposphere during the explosive phase of an eruption, I estimate volatile emissions for SO_2, HCl, and HF (Table 6) using calculated melt inclusion values representative of the melt at time of eruption following fractional crystallization with some assimilation (c_{adj}) and their corresponding matrix glass compositions. An example of this procedure can be seen in Figure 23, where data from Yapoah Crater reveals a minimum and maximum of degassing from the calculated evolved melt. Examples for the remaining six cones can be found in Appendix F. Given the relatively elevated oxygen fugacities of the magmas involved (Ruscitto et al., 2010), I assume that all S was released as SO_2 (e.g. Wallace and Carmichael, 1994), though it is possible that some H_2S was also involved. Based on the low concentrations of S in the matrix glass samples, it appears that nearly all the dissolved S was released during eruption. Cinder Cone released the largest mass of SO_2, but all cones released 88-100% of their initial S content. Collier Cone, Yapoah Crater, and Cinder Cone released 31-49% of their initial Cl in the form of HCl, whereas Four-In-One Fissure, BORG, and BAS44 lost 14-32% Cl. Garrison Butte efficiently retained Cl and lost only 0-10% of its initial Cl concentration. Like Chlorine, moderate F was degased during eruption. Yapoah Crater, Garrison Butte, Cinder Cone, and BAS44 lost 6-50% of the initial F

Table 6: Mass of SO_2, HCl, and HF degassed during explosive activity of cinder cones in the central Oregon Cascades and northern California

	% groundmass crystals	% Crystal Fractionation	C_{adj} (wt%)	C_{matrix} (wt%)	V_T (km^3)	m_T SO_2 (Mt)	% degassed
Collier Cone	30	54	0.20 - 0.33	0.001	0.04	0.51 - 0.31	100
Yapoah Crater	25	52	0.33 - 0.37	0.0	0.04	0.62 - 0.54	100
Four-In-One Fissure	20	32	0.26 - 0.27	0.0 - 0.002	0.004	0.05	99 - 100
Garrison Butte	20	68	0.31 - 0.30	0.005 - 0.008	0.04	0.54 - 0.51	97 - 98
Cinder Cone	10	50	0.32	0.007 - 0.04	0.29	4.45 - 4.00	88 - 99
BORG	30	66	0.61 - 0.87	0.0	0.007	0.24 - 0.26	100
BAS44	20	32	0.38 - 0.47	0.001 - 0.003	0.04	0.82 - 0.67	99 - 100

	% groundmass crystals	% Crystal Fractionation	C_{adj} (wt%)	C_{matrix} (wt%)	V_T (km^3)	m_T HCl (Mt)	% degassed
Collier Cone	30	54	0.09 - 0.10	0.05 - 0.06	0.04	0.04 - 0.02	31 - 49
Yapoah Crater	25	52	0.16 - 0.17	0.09 - 0.10	0.04	0.06 - 0.05	37 - 40
Four-In-One Fissure	20	32	0.07 - 0.08	0.06 - 0.07	0.004	$1.6x10^{-3}$ - $9.9x10^{-4}$	14 - 23
Garrison Butte	20	68	0.05	0.04 - 0.05	0.04	$4.5x10^{-3}$ - 0.00	0 - 10
Cinder Cone	10	50	0.06 - 0.07	0.03 - 0.04	0.29	0.21 - 0.17	38 - 43
BORG	30	66	0.10 - 0.08	0.08 - 0.07	0.007	$3.6x10^{-3}$ - $1.8x10^{-3}$	16 - 25
BAS44	20	32	0.03 - 0.04	0.03	0.04	0.01 - $4.5x10^{-3}$	17 - 32

	% groundmass crystals	% Crystal Fractionation	C_{adj} (wt%)	C_{matrix} (wt%)	V_T (km^3)	m_T HF (Mt)	% degassed
Collier Cone	30	54	0.02 - 0.03	0.01 - 0.02	0.04	0.01 - 0.00	0 - 50
Yapoah Crater	25	52	0.03 - 0.04	0.02 - 0.03	0.04	0.01 - $9.3x10^{-5}$	24 - 37
Four-In-One Fissure	20	32	0.02	0.02	0.004	0.00 - $1.9x10^{-3}$	0 - 5
Garrison Butte	20	68	0.03 - 0.04	0.02 - 0.03	0.04	0.02 - 0.00	6 - 49
Cinder Cone	10	50	0.04 - 0.05	0.02 - 0.03	0.29	0.20 - 0.14	40 - 50
BORG	30	66	0.03 - 0.04	0.03 - 0.04	0.007	0.00 - 0.00	0 - 0
BAS44	20	32	0.02	0.01 - 0.02	0.04	0.01 - $2.8x10^{-3}$	13 - 42

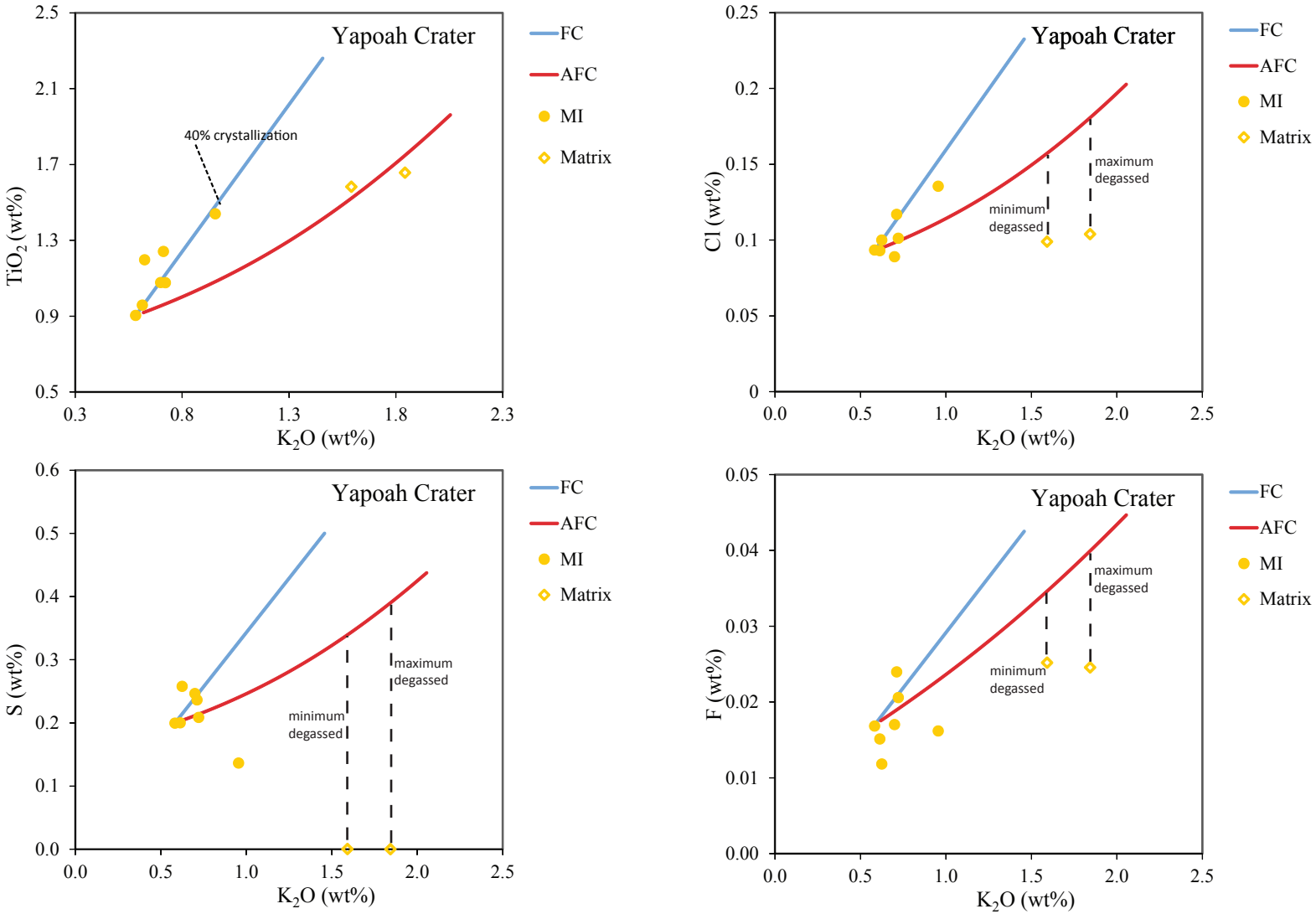

Figure 23: An example of volatile evolution and degassing from Yapoah Crater. The melt inclusion with the lowest TiO_2 and K_2O concentration was used to calculate the percent fractional crystallization and assimilation of the magma. Using these values, a volatile concentration of the evolved melt was calculated. This calculated evolved melt concentration represents the melt prior to degassing and is used to assess the total amount of S, Cl, and F released during eruption.

concentrations as HF. Matrix glass compositions do show however, that F is more soluble in the melt than Cl, as many cones had matrix glass compositions that showed no degassing at all. Collier Cone lost 0-50% F, Four-in-One Fissure lost 0-5% F, and BORG experienced no degassing of F.

The volatiles Cl and F have very high solubility in mafic melts and thus behave as incompatible elements during fractional crystallization. Even at near surface pressures F remains quite soluble, but Cl can begin to partition into the vapor phase at low pressures as large amounts of H_2O and CO_2 begin to exsolve (Metrich and Wallace, 2008). Dissolved CO_2 and H_2O will exsolve into the vapor phase relatively early and become completely separated from the melt. This can cause S, Cl, and sometimes F to diffuse into the exsolved bubbles as pressure within the conduit decreases. These vapors can then readily escape from the magma during eruption or passive degassing through bubble coalescence and bubble rise or through the permeable flow of gas through pathways within a magmatic foam or crystal-rich magma (Belien, 2011; Pioli et al., 2012). Sulfur, in contrast to Cl and F, is somewhat less soluble and can begin to partially partition into a vapor phase at middle to upper crustal pressures (4.5- <1 km) (Wallace, 2005; Metrich and Wallace, 2008). Thus, sulfur shows more degassing at near surface pressures.

It is important to note that because cinder cone systems are characterized by polybaric crystallization, i.e. crystallization at multiple pressures, variable degassing of the melt may have occurred before melt inclusions were formed. Even though I use a calculated melt inclusion representative of an evolved melt that has experienced no degassing, the volatile concentrations captured by the olivine-hosted melt inclusions may not have recorded the initial concentration of the less soluble volatiles, as they degas

readily at lower pressures. Olivine-hosted melt inclusions may also reflect lower concentrations of the higher solubility volatiles if crystallization occurred at very low pressures (Metrich, 1990; Metrich and Wallace, 2008).

Using the modified Thordarson et al. (1996) method to calculate the total volatile species mass released during eruption, I show that each cone released between 0.05 to 4.5 Mt of SO_2, $9.9x10^{-4}$ to 0.2 Mt of HCl, and $9.3x10^{-5}$ to 0.2 Mt of HF (Table 6). Even though the CAB lavas and the transitional LKT lavas share similar concentrations of S, Cl, and F, the eruptive volumes of the cones drastically influence the mass of volatile species released from the vent. Cinder Cone has the highest predicted mass of volatiles released because the eruption volume of Cinder Cone was by far the largest (0.29 kg/km^3) compared to other cones analyzed in central Oregon and northern California. It is important to note that I focus on the degassing of volatiles at the vent; however additional dissolved volatiles can be lost from lava flows during transport and cooling.

Significant degassing of Cl and F occurs passively as lava is extruded from the base of the cone because increased crystallization of the flow decreases of the amount of melt that contains the dissolved volatiles. Fluorine is very soluble at atmospheric pressures (~1 atm) and can remain dissolved in the lava flow. However, no F can remain dissolved in a lava flow that is 100% crystalline. Therefore during transport, F and other high melt soluble volatiles like Cl should degas as the lava cools and crystallizes. Documented gaseous fogs emanating from degassing Hawaiian lava flows as they reach the ocean have been shown to be harmful to nearby residents (e.g. Heliker et al., 2003). I attempted to analyze glassy matrix within lava samples from each respective cone to understand the possible risk to nearby communities. Petrographic slides were assembled

from lava samples collected in the field, however, after observation of the thin sections under a petrographic microscope it was determined that only the lava flow sample from Cinder Cone had a sufficient percentage of glassy matrix to analyze with the Cameca SX100 electron microprobe. The lava sample was analyzed under the same conditions previously presented for olivine-hosted melt inclusions and matrix glass (major and minor element compositions can be found in Appendix D). The data shows considerable loss of S during emplacement and moderate losses of Cl and F (Figure 24). Applying the degassing calculations outlined in Chapter IV to the lava matrix glass yields degassing percentages of SO_2 (99%), HCl (51%), and HF (28-44%) from a calculated melt inclusion that represents the concentration in the magma before the lava was erupted to the surface. These degassing percentages equate to a release of 7.49 Mt SO_2, 0.31 Mt HCl, and 0.16-0.25 Mt HF during effusive eruption activity.

A similarly designed experiment by Thordarson et al. (1996) on the 1783-1784 AD fissure eruption of Laki estimated that ~25 Mt SO_2 (~20%), ~3 Mt HCl (~25%), and ~7 Mt F (~25%) were liberated during and after lava emplacement and crystallization. The Laki fissure eruption is considered to be one the greatest atmospheric pollution events as the eruption released a combined 110 Mt of SO_2, HCl, and HF during its year-long eruptive episode. Though Cinder Cone released a much greater percentage of gas during its eruption compared to Laki, its relatively small eruption volume constrains the total potential amount of gas to be lost during eruption. If I combine the maximum release of SO_2, HCl, and HF during lava transport and explosive activity at Cinder Cone, the amount released into the troposphere is ~11 Mt SO_2, ~0.5 Mt HCl, and ~0.5 Mt HF.

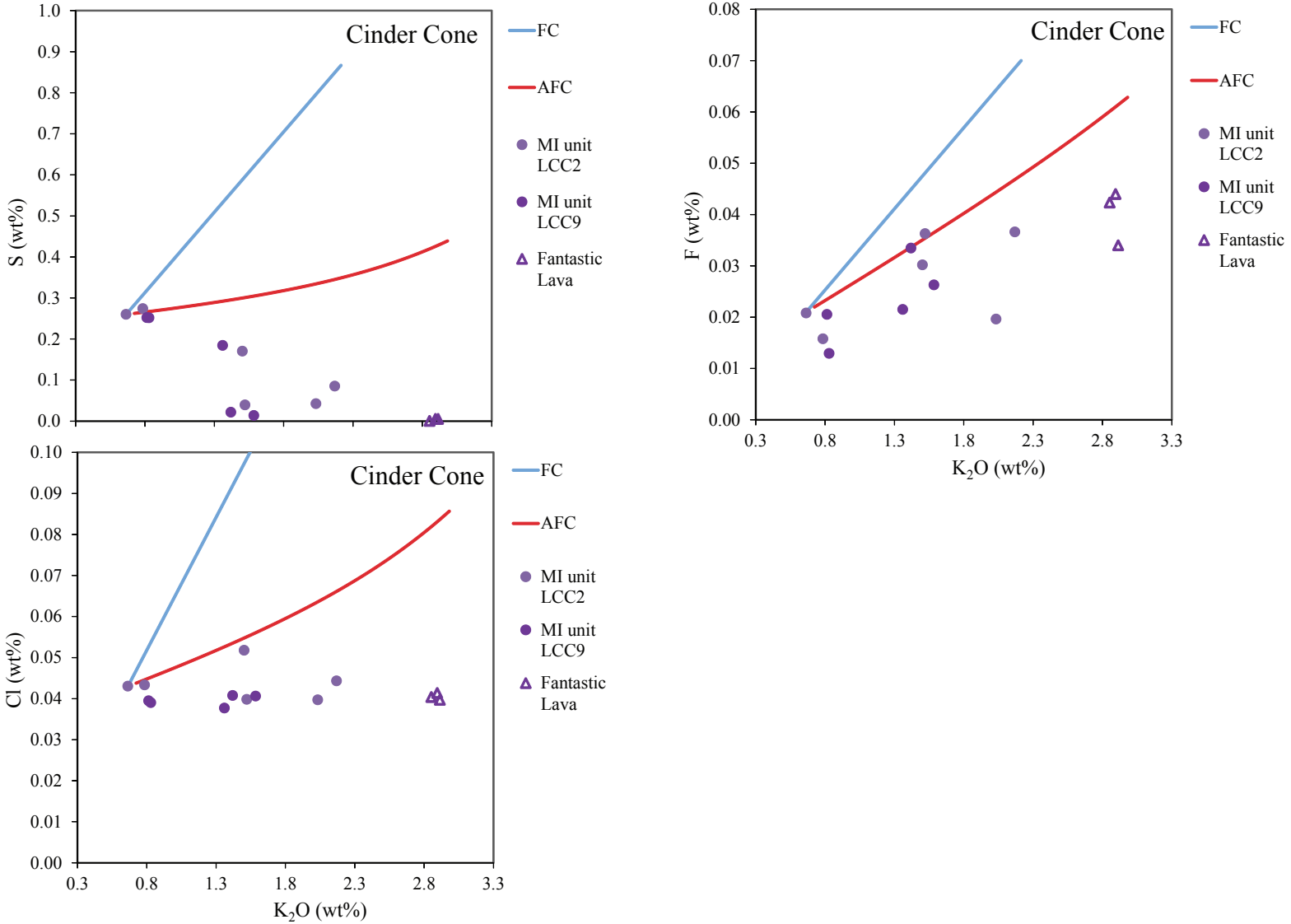

Figure 24: Volatile contents for Cinder Cone (northern California) from olivine-hosted melt inclusions (filled circles) and lava glass (open triangles). The lowest K_2O and TiO_2 concentration melt inclusion was chosen as the best representative of the parental magma composition. FC denotes pure fractionation of crystals; AFC denotes crystal fractionation with assimilation.

The amount of volatile lost during lava flow emplacement is considerable, and greatly increases the exposure risk to volcanic gases during eruption.

6.5. Volatile dispersal within a Gaussian plume

The steady-state Gaussian plume model reveals varying gas concentrations downwind of the vent depending on the instability of the plume. The predominant form of sulfur released during an eruption is SO_2. Both SO_2 and H_2S are released from the magma and their relative abundance largely depends of the oxidation state of the magma. It has been documented during some eruptions that some of the S released from the magma as H_2S oxidizes in the atmosphere to SO_2 (Carroll and Rutherford, 1985, Metrich and Wallace, 2008). In the case of Cl and F, both combine with hydrogen to produce the highly acidic HCl and HF gases, respectively. HCl and HF are highly soluble in water, and thus are of great concern for human, livestock, and agricultural communities.

Figure 25 illustrates how the maximum and minimum SO_2, HCl, and HF concentrations at ground level change with distance from the plume origin. Values for the maximum curves represent a cone with the largest degassed total for a particular volatile. Minimum curve values represent a cone with the least degassed total for a particular volatile. At a distance representative of the length between susceptible communities in central Oregon and northern California and a cinder cone on or near the arc axis, predictions of maximum SO_2 concentrations 25 km downwind of the vent range from 0.006 ppm (unstable) to 1.1×10^{-10} ppm (neutral). Minimum predictions of SO_2 concentrations 25 km downwind of the vent range from 0.005 ppm (unstable) to 8.7×10^{-11} ppm (neutral). Maximum predictions of HCl concentrations 25 km downwind of the vent

range from $2.7x10^{-4}$ ppm (unstable) to $5.0x10^{-11}$ ppm (neutral). Minimum predictions of HCl concentrations 25 km downwind of the vent range from $9.3x10^{-5}$ ppm (unstable) to $1.7x10^{-11}$ ppm (neutral). Maximum predictions of HF concentrations 25 km downwind of the vent range from $9.3x10^{-5}$ ppm (unstable) to $4.8x10^{-11}$ ppm (neutral). Minimum predictions of HF concentrations 25 km downwind of the vent range from $2.9x10^{-5}$ ppm (unstable) to $1.7x10^{-11}$ ppm (neutral). From Figure 25 it is obvious that a highly unstable plume produces overall higher concentrations of gases with distance from the vent than a stable plume, but the maximum concentrations are located within 2 km of the vent.

6.6. Implications for hazards

To date, few investigations in the Cascades have focused on the hazards human, animal, and agriculture populations experience as a result of volcanic degassing during an

---

Figure 25: (next two pages) Predicted ground level volatile concentrations downwind of the vent for the central Oregon and northern California cinder cones for plumes of varying instabilities (a, b). The red line represents the cone with the maximum dissolved volatile content and highest percent degassing. The blue line represents the cone with the minimum dissolved volatile content and lowest percent degassing (excluding 0% degassing). Volatile mass eruption rate (MER) was calculated using the average magmatic MER of Violent Strombolian eruptions (Pioli et al., 2010) and the mass of volatile released during eruption (Equation 5).

a.

"UNSTABLE"

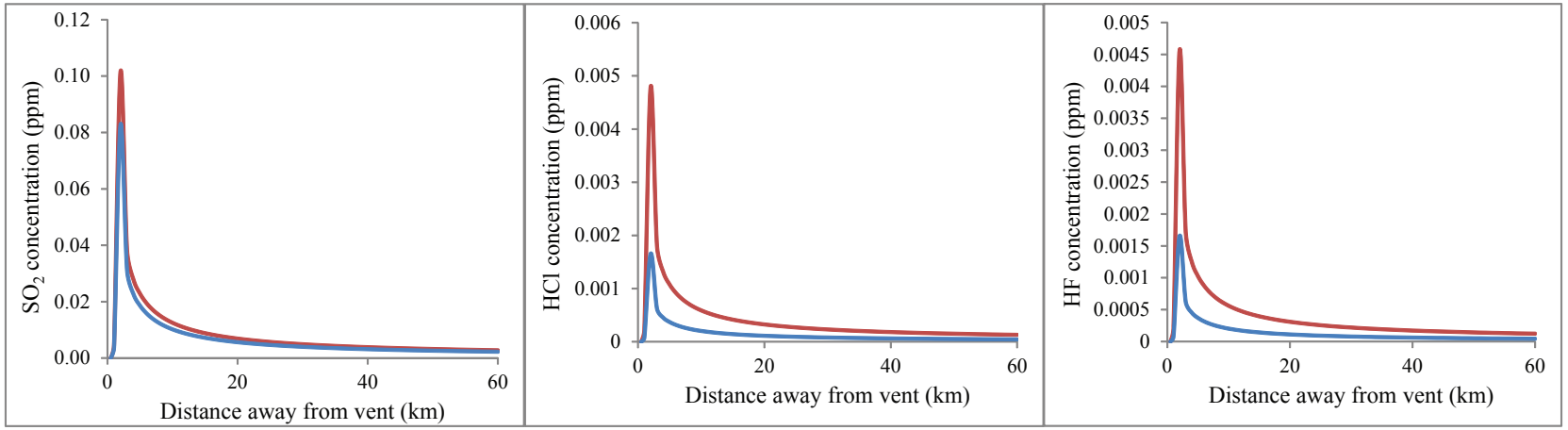

"MODERATELY UNSTABLE"

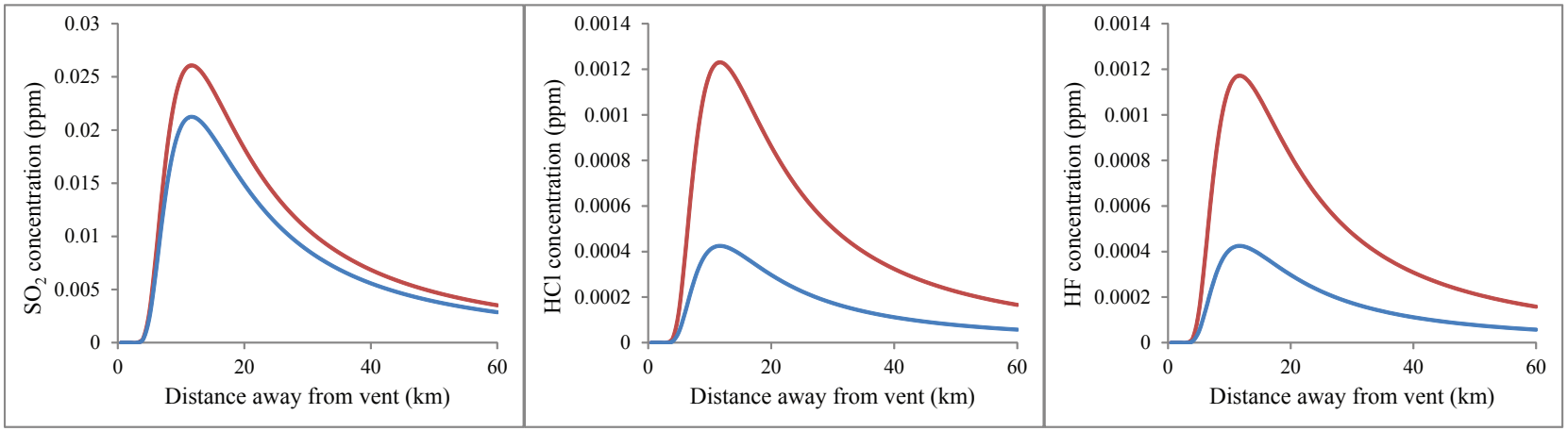

b.

"SLIGHTLY UNSTABLE"

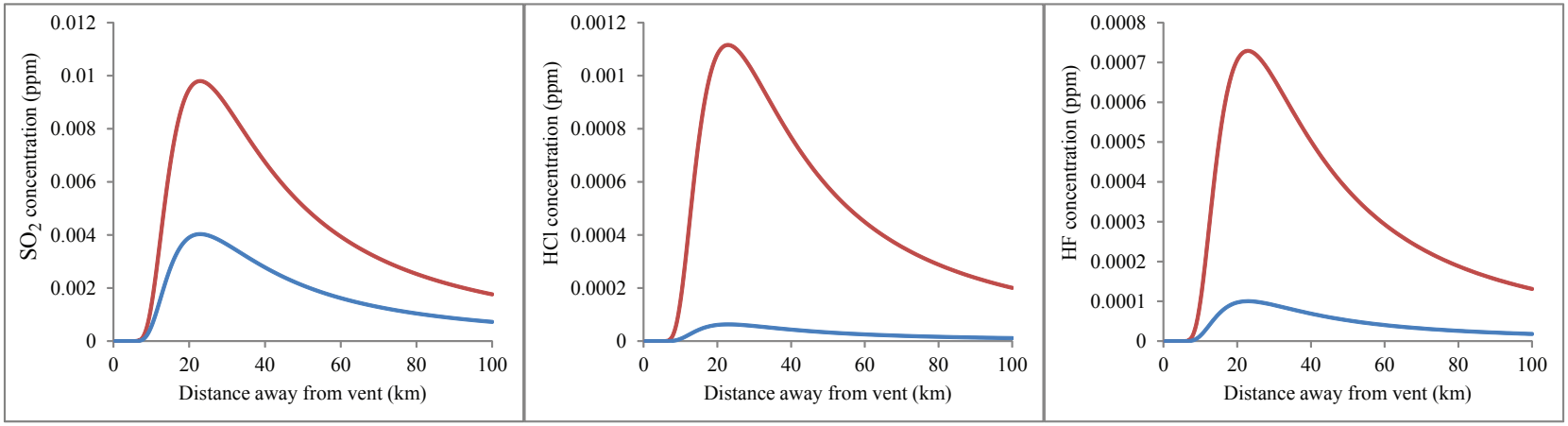

"NEUTRAL"

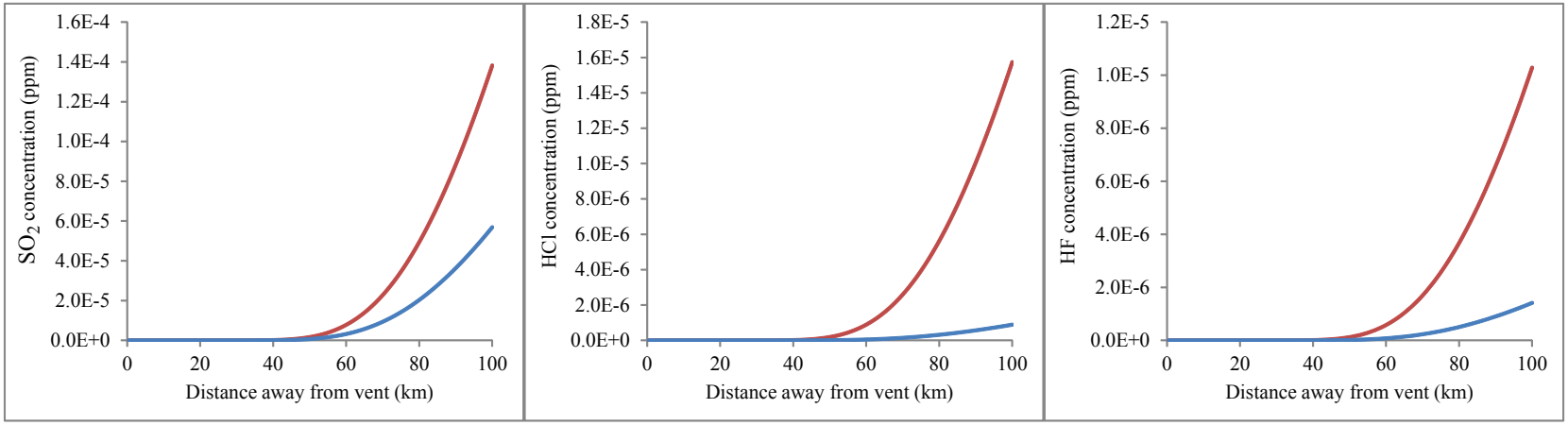

explosive mafic eruption. Assessing emissions released into the atmosphere is essential to the understanding and mitigation of their potential effects on local communities and ecosystems (Sawyer and Oppenheimer, 2006).

Volcanoes and their eruptions can result in a wide range of health impacts, arguably more varied than in any other kind of natural disaster (Hansell et al., 2006). Now more than ever, as cities spread into active volcanic areas, human populations are at risk of experiencing volcanic emissions from a range of eruptions of varying size and explosivity. Areas hundreds of kilometers away can also be affected as a result of strong prevailing winds and airborne dispersal of gases and ash (Hansell et al. 2006). Principal studies concerning health hazards from volcanic gases are not well-represented in the literature. Few principal studies have conducted health tests in response to volcanic gas exposure and those that do exist are limited in terms of exposure assessment (Hansell and Oppenheimer, 2004). Most research to date relates to exposures to CO_2, H_2S, and SO_2 from volcanic and geothermal sources. The studies that concentrate on exposure to HCl and HF focus on the complications associated with inhalation or ingestion of ash-adsorbed aerosol particles or highly acidic waters by sheep and other livestock. A literature review of health hazards associated with volcanic gases by Hansell and Oppenheimer (2004) found that <1 to 4% of all volcano-related mortality was due to volcanic gases. A similar review of volcanic incidents by Witham (2005) reported that out of 491 global events, 11% referred to volcanic gases, accounting for 2,016 (2% of the total) of the killed and 2,860 (18%) of the injured people. However, these estimates are only minimum values- the majority of the reports neglected degassing that occurs passively through lava flow transport.

The most common risk of exposure to volcanic gas in humans is respiratory. A portion of all volcanic gases condense and adsorb onto tephra particles within the plume during transport if atmospheric conditions are favorable for gas-liquid phase reactions (Oskarsson, 1980; Gilbert et al., 1991). These gases react with the silicate glass and form acidic salts, which can easily dissolve with water, or in the case of livestock, in their digestive system (Oskarsson, 1980; Cronin et al., 2003; Horwell and Baxter, 2006). Table 7 shows a compilation of hazardous SO_2, HCl, and HF levels. Human intake values reported for SO_2 were gathered during active eruptions and assessed using the World Health Organization (WHO) air quality standards (WHO, 1984), whereas values for HCl and HF are a combination of hazardous drinking levels from Cronin and Sharp (2002) and concentrations of maximum occupational exposure limits set by the Occupational Safety and Health Administration (OSHA) (OSHA, 1989). SO_2, HCl, and HF can all cause acute irritations to the membrane lining of the eyes, nose and throat. More seriously, these volcanic gases can cause symptoms such as headaches, dizziness, vomiting, visual disturbances, bronchitis, pulmonary edema, and in grave situations, asphyxiation (Heggie, 2009).

Plants and animals can also be affected by volcanic gases, but by other means than in humans. Animal contact with volcanic gases often occurs through ingestion. Cronin et al. (2003) documented the relationship between grazers and fluorides adsorbed onto the ash particles that has fallen onto the pastures. Ingestion of these fluoride salts caused symptoms of dental fluorosis and in total killed at least 2,000 grazing animals. Like humans, fluorosis in livestock causes deterioration in teeth as the enamel fails to mineralize and causes dissolution of bones or abnormal bone growth (Suttle, 2010).

Table 7: Compilation of published exposure limits and medical symptoms of SO_2, HCl, and HF contamination in humans, livestock, and agricultural crops

	life form	*maximum exposure limit	**specific symptoms	references
SO 2	human	177 ppm for 10 min; 7 ppm for a 24-hr period	1 ppm induces asthmatic reponse; 6-12 ppm immediate irritation to the nose and throat	* World Health Organization **World Health Organization; Heggie (2009)
	livestock	unknown	3-4 g S kg^{-1} per day reduction in appetite and growth rate	**Suttle (2010)
	crops	>60 ppbv	<6 ppbv no visible damage; <40 ppbv observable necrosis to trees and shrubs; >62 ppbv fatallity	*Delmelle et al. (2002) **Delmelle et al. (2002); Davidson and Weinstein (2006)
HCl	human	5 ppm for a 24-hr period	>35 ppm irritation to the nose, throat and larynx; >70 ppm acute laryngeal spasm and pulmonary edema	*OSHA ** Heggie (2009)
	livestock	>60 mg Cl kg^{-1} per day	unknown	* Suttle (2010)
	crops	unknown	unknown	
HF	human	3 ppm for 10-hr period; 1.5 ppm in drinking water	50-250 ppm lethal for a 5 min period; drinking water > 1.5 ppm mottling of teeth, 20-40 ppm skeletal fluorosis	*OSHA; Cronin and Sharp (2002) **OSHA
	livestock	>60 mg F kg^{-1} per day	40-100 µg per body weight chronic fluorosis; >100 µg per body weight fatal;	*Suttle (2010) **Cronin et al. (2003)
	crops	unknown	0.25-0.3 µg/m^3 visible necrosis	**Davidson and Weinstein (2006)

Fluorine is absorbed into the livestock's milk and ingestion can be harmful to calves/lambs and humans. Plants can be affected by leaf or fruit injury due to direct contact with gaseous vogs (aerosol fog) or ingestion by uptake through roots. Once inside of a leaf, fluorine ions are transported to the cell walls where they accumulate in the tips of leaves or fruits (Davidson and Weinstein, 2006). This leads to yellowing and possible death of cell membranes. Animal and plant intake values reported for SO_2, HCl, and HF were gathered after eruptive episodes and hazardous intake levels were gathered through trace analysis of bones, teeth, and plant tissues. The danger from drifting volcanic gases is commonly a short-range one (within the vicinity of the cinder cone), but father away damage is mostly caused by aerosols transported by tephra (Thordarson, 1979). However, vegetation and livestock can experience long lasting affects as the acidic aerosols and salts are incorporated into soils (Delmelle et al., 2003) and dissolved into accessible water sources (streams, ponds, groundwater, etc.).

The Gaussian plume model predicts volatile concentrations downwind from the vent to be dilute enough to not pose a significant hazard to surrounding communities (Figure 25). Based on the distal tephra deposits from isopachs of McKay (2012) (Figure 5) and evaluation of smoke stake plume stabilities (Hanna et al., 1981; EPA, 2012), I suggest the moderately unstable plume stabilities best describe the plume behavior of cinder cones in central Oregon and northern California. Gas concentrations for these plumes fall far below the accepted exposure limits listed in Table 7. For the purpose of hazard prediction, I also calculated the gas concentrations downwind of the vent for a MER of $10^{\wedge 5}$ kg/s. Pioli et al. (2009) shows that this MER is representative of Violent Strombolian to Subplinian eruptions, characterized by voluminous and sustained ash

columns ~10-20 km in height. The predicted S, Cl, and F concentrations downwind of the vent for an eruption of MER of $10^{\wedge 5}$ kg/s are a magnitude greater than the concentrations initially calculated, however these concentrations are still below the maximum exposure limits (Figure 26).

Evaluation of the Laki eruption from 1783-1784 reveals concentrations of S, Cl, and F downwind of the vent that far exceed the concentrations released during the Cascades cinder cone eruptions (Figure 27). I estimated the magmatic fluxes of the Cascades cinder cones to be 10^4 kg/s, such that explosive and effusive activity was sustained (Pioli et al., 2008). Unlike the Cascades eruptions, the magmatic flux of Laki has been extrapolated from physical assessments of tephra fall and averages 2.0×10^6 kg/s (total eruption volume) and 5.3×10^4 kg/s (tephra volume) for the 8 month duration of activity. However, 90% of the eruption volume was released during the first 5 months of explosive activity (Thordarson et al., 1996). Crystallization was minimal (<4%) at Laki, therefore Thordarson et al. (1996) did not adjust their volatile concentrations based on crystal percentages of the matrix glasses. Parental volatile concentrations between Laki

---

Figure 26: (next two pages) Predicted ground level volatile concentrations downwind of the vent for the central Oregon and northern California cinder cones for plumes of varying instabilities (a, b) using an eruptive volume of 10^5 kg/s and 10^4 kg/s. The dashed red line represents maximum gas concentration and the blue dashed line represents the minimum gas concentration using 10^5 kg/s. The other symbols are the same as in Figure 25. Refer to Figure 25 for a more detailed explanation of volatile MER.

a.

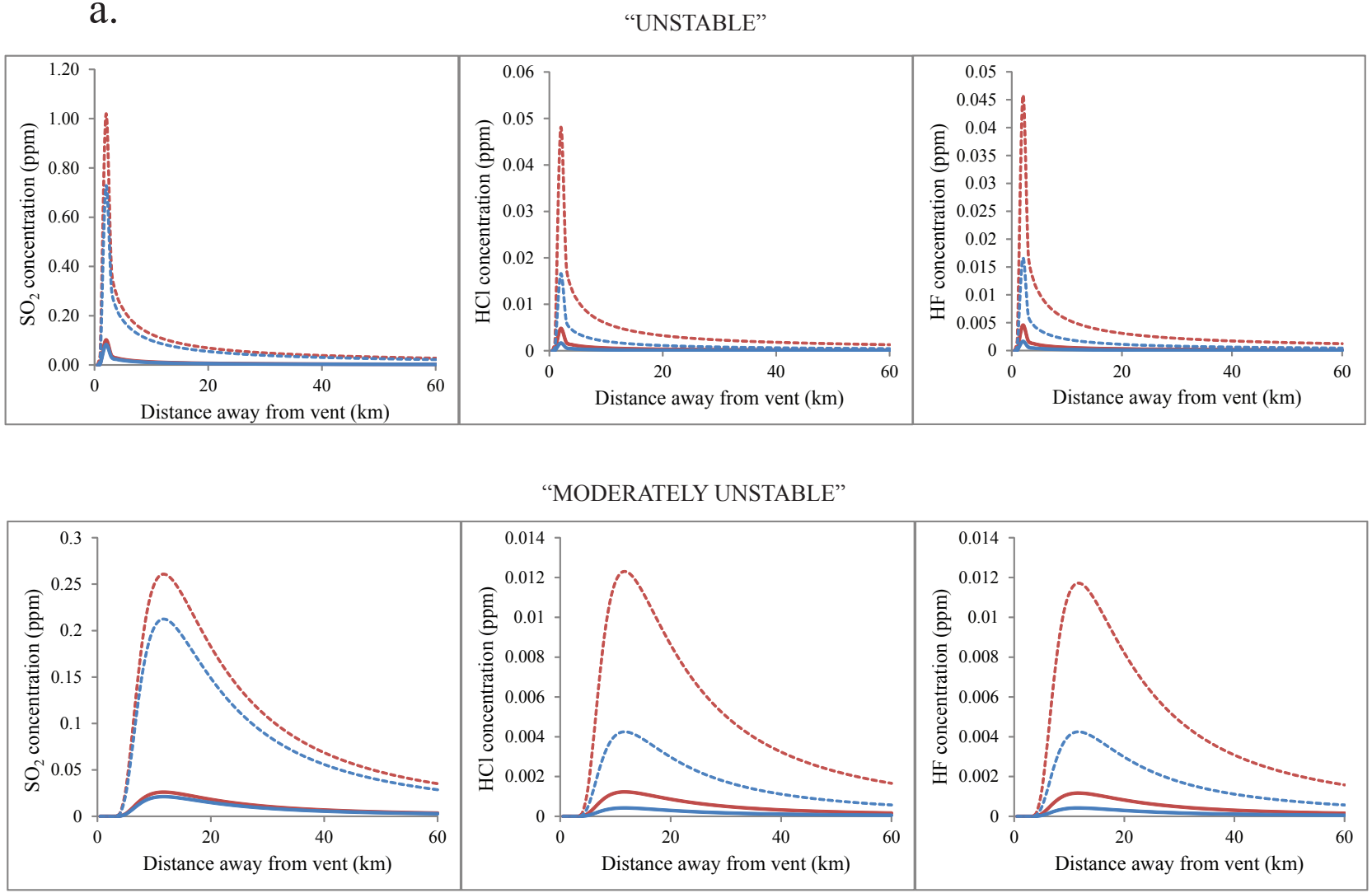
"UNSTABLE"
SO2 concentration (ppm)
1.20
1.00
0.80
0.60
0.40
0.20
0.00
0
20
40
60
Distance away from vent (km)
HCl concentration (ppm)
0.06
0.05
0.04
0.03
0.02
0.01
0
0
20
40
60
Distance away from vent (km)
HF concentration (ppm)
0.05
0.045
0.04
0.035
0.03
0.025
0.02
0.015
0.01
0.005
0
0
20
40
60
Distance away from vent (km)
"MODERATELY UNSTABLE"
SO2 concentration (ppm)
0.3
0.25
0.2
0.15
0.1
0.05
0
0
20
40
60
Distance away from vent (km)
HCl concentration (ppm)
0.014
0.012
0.01
0.008
0.006
0.004
0.002
0
0
20
40
60
Distance away from vent (km)
HF concentration (ppm)
0.014
0.012
0.01
0.008
0.006
0.004
0.002
0
0
20
40
60
Distance away from vent (km)

b.

"SLIGHTLY UNSTABLE"

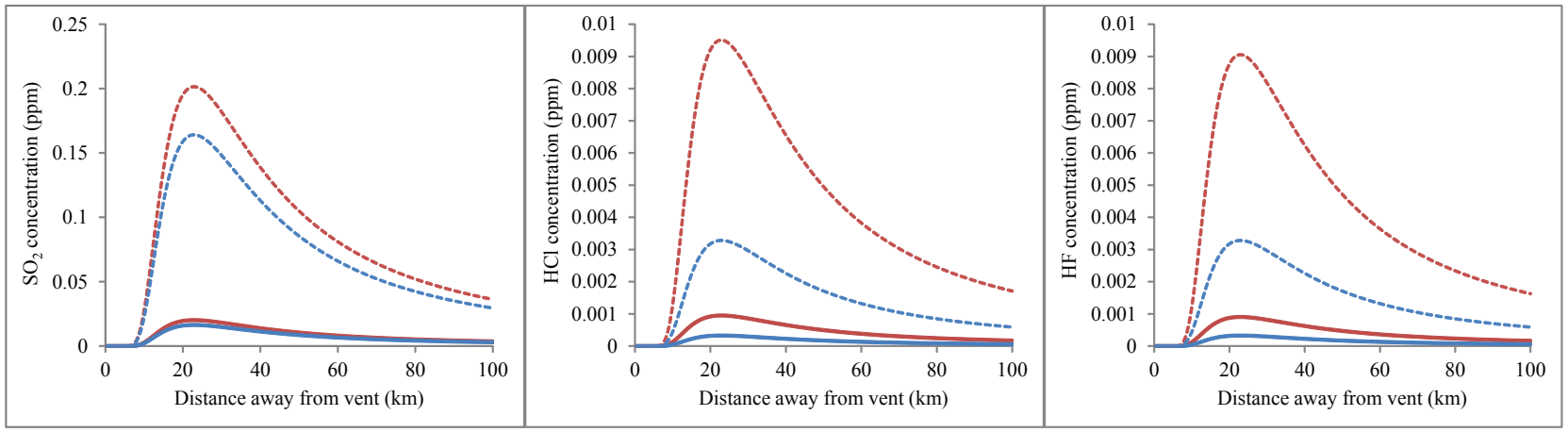

"NEUTRAL"

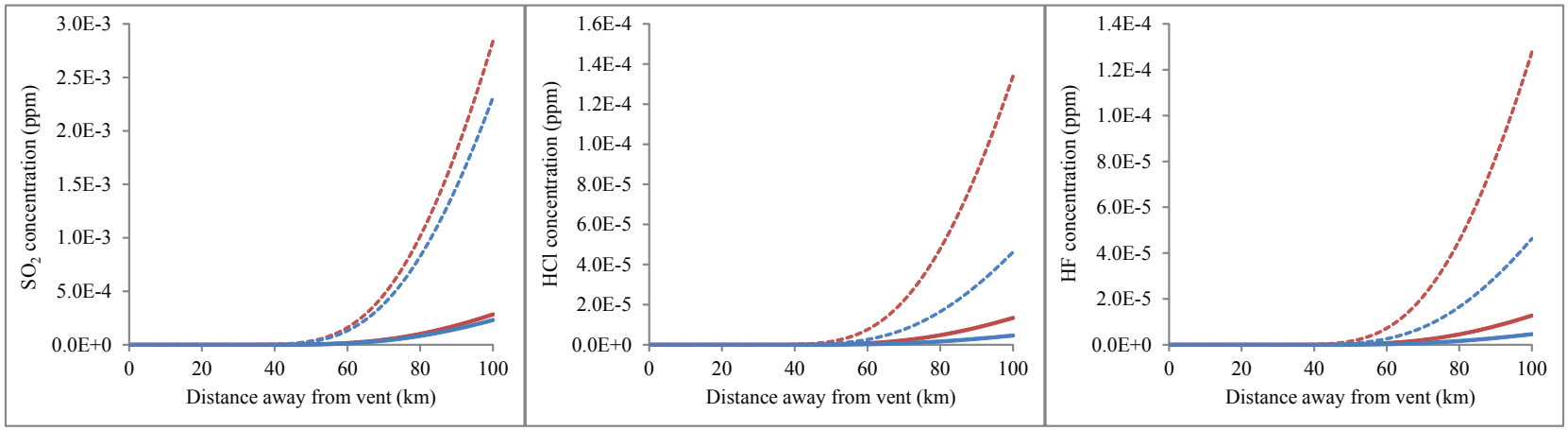

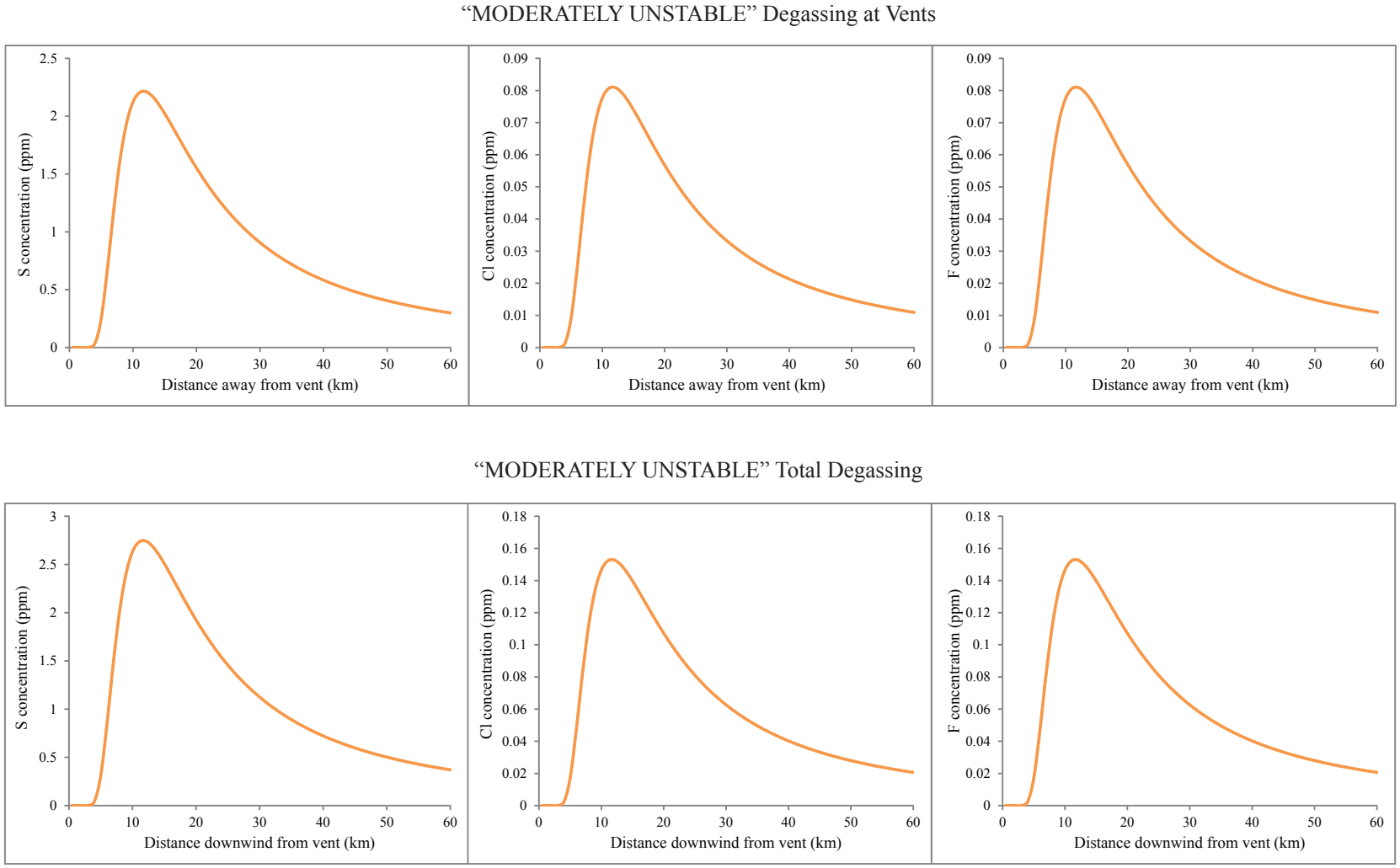

Figure 27: Predicted volatile concentrations downwind of the vent for the 1783-1784 Laki eruption for a plume of moderate unstability that degassed solely at the vent (top) and both at the vent and passively via lava emplacement (bottom). The curves are average concentrations downwind of the vent based on the mass of volatiles released and the total DRE erupted volumes for tephra and all erupted products (Thordarson et al., 1996).

and the Cascades cinder cones are relatively similar, so if a higher volume mafic eruption ever occurs in Cascades in the future, residents of nearby communities may experience seriously harmful concentrations of volcanic gases.

Previous physical analysis by McKay (2012) has shown the occurrence of a Subplinian in character eruption from a mafic cone, Sand Mountain, in the central Oregon Cascades. Though I was unable to match melt inclusion compositions to tephra compositions because of a complex history of compositionally different melt batches mixing in the system, if I assume homogeneity for the different melt batches, I can speculate at the maximum possible release of volatiles during eruption. Olivine-hosted melt inclusions from Sand Mountain recorded volatile concentrations of S (2220-430 ppm), Cl (1860-610 ppm), and F (710-310 ppm). Matrix glass recorded up to ~99% degassing of S, ~73% degassing of Cl, and ~23% degassing of F during the explosive phase of eruption. Using the maximum eruptive volume estimated by McKay (2012), this equates to a release of 7.6 Mt SO_2, 2.9 Mt HCl, and 0.28 Mt release of HF (Appendix G). These release values are roughly an order of magnitude larger than those released by the cinder cones in central Oregon and northern California. The geochemical and physical analysis on Sand Mountain shows that future mafic eruptions in the central Oregon Cascades may have the eruptive power and exsolved volatile concentrations capable of creating a regional hazard.

While not the focus of this study, it is important to note the hazardous effects from tephra fallout that future mafic activity poses to (1) public health, (2) agriculture, and (3) local transportation and infrastructure. Volcanic ash is the most widely distributed eruption product, affecting regions km's away. Airborne ash particles <10

μm can be inhaled in the upper lungs and cause acute asthmatic conditions or bronchitis. Particles <4 μm in diameter are referred to as "respirable" and have the greatest toxic potential, yet diseases such as silicosis or lung cancer often require high levels of cristobalite (3-5 wt%), something mafic eruptions are incapable of crystallizing (Horwell and Baxter, 2006; Hillman et al., 2012). Epidemiological studies established that areas with high levels of airborne ash (daily average total suspended particulates (TSP) of 3000–33000 $\mu g/m^3$) experienced a 2–3-fold increase in hospital admissions and 3–5-fold increase in emergency room visits for respiratory conditions (Hansell et al., 2006). Agriculture can experience heavy impacts from tephra dispersal. The effects of cinder cone eruptions upon nearby agricultural communities were studied by Ort et al. (2008) and their findings indicate a complete disruption to agricultural lands immediately after eruption with >30 cm deposition of tephra. In semi-arid regions, natural processes to breakdown tephra and incorporate it into the soil can take up to 1,000 years. This process can be hastened to a few decades in a more humid environment (Ort et al., 2008). Lastly, airfall can greatly affect the public sector by causing power outages, decreasing water quality through acidification or turbidity, clogging drainage networks, collapsing infrastructure, and reducing visibility, traction, and functionality of major roads and air traffic (Ort et al., 2008; Heggie, 2009; Wilson et al., 2012).

CHAPTER VII

CONCLUSIONS

I have investigated the degassing history of seven prehistoric mafic eruptions in central Oregon and northern California. The eruptions are characterized by Strombolian to Violent Strombolian eruptive activity, and produced ~0.03-0.36 km^3 of basalt to basaltic andesite scoria, tephra, and lava. Olivine-hosted melt inclusions constrain the melt compositions, including volatile content, at each cone. Analysis of olivine-hosted melt inclusions allowed me to compare and contrast the crystallization and degassing history of each cone, and the data reveal a complicated history of magma evolution through fractional crystallization and crustal assimilation. The melt inclusions also show volatile values elevated above MORB concentrations (Wallace, 2005). Compared to matrix glass, the individual eruptions degassed 88-100% sulfur, 0-49% chlorine, and 0-50% fluorine during explosive activity. S was efficiently lost during all eruptions, but Cl and F degassed to a much lesser extent due to their relatively high solubility, allowing them to largely remain in the magma. Three of the seven cones did showed no degassing of F. When converted into megatonnes released into the atmosphere in gas form, each cone emitted $\leq$4.5 Mt SO_2, $\leq$0.2 Mt HCl, and $\leq$0.2 Mt HF. Maximum volatile contents for eruptions in central Oregon and northern California are similar to volatile contents from the mafic eruptions of Laki and Cerro Negro (Thordarson et al., 1996; Portnyagin et al., 2012; Roggensack et al., 1997). Degassing calculations and a Gaussian plume model predicts a Laki eruption to emit hazardous levels of S, Cl, and F considerable distances downwind from the vent. Hazards documented at Laki and Cerro Negro are extensive,

and risk ranges in form of agriculture and livestock fatality, atmospheric pollution, and accumulation of tephra fall on agricultural crops, roads, and infrastructures (Thordarson et al., 1996; Hill et al., 1998; Thordarson and Self, 2003; Delmelle et al., 2002).

My results of volatile degassing from prehistoric mafic volcanism in the Cascades provides reassurance that the levels of volcanic gases in neighboring cities were not high enough at time of the eruption to present an acute or severe health hazard to nearby residents. If future eruptions present themselves like those of the cinder cones of this study there will be no need to evacuate residents on grounds of harmful gas concentrations. However, if future eruptions behave like that of Sand Mountain or Laki, then mitigation for increased airborne concentrations of SO_2, HCl, and HF and high volumes of tephra should be planned accordingly.

APPENDIX A

DETAILED LIST OF SAMPLE LOCATIONS AND DESCRIPTIONS

Collier Cone (Collier33B, Collier33D)

Collier Cone is located on the NW flank of the North Sister stratovolcano, ~3km NNW of the summit, on the axis of the High Cascades arc in Central Oregon (Figure 3). The eruption that built the 150 m high scoria cone occurred 1600 ±100 years B.P (based on ^{14}C dating) (McKay, 2012; Sherrod et al., 2004). The cone is breached to the west and flows of basaltic andesite, andesite, and dacite lava (Sherrod et al., 2004) exited the breach and flowed down valley to White Branch Valley, ~13 km away. The lavas contain troctolite xenoliths that are interpreted to be mafic cumulates, as well as silicic xenoliths similar in composition to the Obsidian Cliffs, a dacitic to rhyolitic flow originating from Middle Sister (Schick, 1994). Addition of a silicic contaminant can explain much of the compositional variation of Collier Cone melt inclusions (Ruscitto, 2011). Table 2 lists the major and minor element concentrations for the silicic xenoliths near North Sister (Schick, 1994). The lava flows partially cover the western edge of the nearby Four-in-One Fissure tephra blanket, stratigraphically placing the eruption of Collier Cone after that of Four-in-One Fissure. The tephra blanket is exposed east of the vent where it lies stratigraphically above a tephra unit from the Yapoah eruption (Sherrod et al., 2004). The total volume of the tephra is 0.037 km^3 over a 14.7 km^2 area. The total volume of lava erupted from Collier Cone is 0.154 km^3. The total DRE eruptive volume for Collier Cone is 0.154 km^3 (McKay, 2012). Based on volume and areal dispersal

calculations by McKay (2012), the eruption style of Collier Cone was mainly Strombolian, but had episodes of Violent Strombolian activity.

Yapoah Crater (Yo061E)

Yapoah Crater is located ~6 km N from the summit of North Sister and ~3km N of Collier Cone (Figure 3). The cone is approximately 85 m high and a small breach to the NW side of the cone fed basaltic andesite lava flows that extended ~12 km NNE around the flank of Belknap shield volcano. No absolute age date exists for Yapoah Crater, but a relative age date (based on stratigraphy) from the eruptions of Little Belknap Crater and Four-in-One Fissure brackets the age for the Yapoah eruption at 2883±175 B.P. to 1980±160 B.P (based on ^{14}C dating; Sherrod et al., 2004). Small lenses of tephra are visible to the east of Yapoah Crater, but to date no isopach has been constructed for Yapoah. Therefore, the volume of tephra, lava and total eruptive products are not known. Because no isopach exists for Yapoah Crater, no inference about eruption style can be made. However, based on grain size and grain sorting work by McKay (2012) for other cinder cones in the High Cascades and the Oregon Cascades back arc, I propose Yapoah Crater may have erupted with similar Strombolian-like characteristics.

Four-in One Fissure (Fo0803D3)

Four-in-One Fissure is a 75 m series of cones located ~6 km NNW of the summit of North Sister and ~2 km WSW of Yapoah Crater (Figure 3). It consists of four contiguous cones erupted from a linear fissure system, trending N 10° E (Sherrod et al., 2004). The best eruption age estimate is based on radiocarbon dating and places the

onset of activity to be 1980±160 years B.P. The basaltic-andesite to andesite flows of Four-in-One Fissure (Sherrod et al., 2004) breached the cone to the NW and flowed a short distance of ~4 km towards Belknap Crater. Tephra is again exposed to the east of the vent where it is overlain by Collier Cone lava. The tephra east of the vent stratigraphically lies above a tephra sequence from the Yapoah Crater eruption. McKay (2012) calculates the extent of the tephra blanket to be 0.002 km^3 over an area of 1.36 km^2, but these are minimum estimates as a complete isopach has yet to be obtained. The volume of lava erupted is estimated to 0.036 km^3. The minimum total eruptive DRE volume for Four-in-One Fissure is 0.032km^3. Based on volume and areal dispersal calculations by McKay (2012), the eruption style of Four-in-One Fissure was likely Hawaiian to Strombolian.

Garrison Butte (GB072)

Garrison Butte is a 41 m high cone located ~30 km NE of the North Sister summit, and ~7 km E of Black Butte shield volcano (Figure 4). Garrison Butte lies along strike of a closely clustered chain of cinder cones trending N 40° W. Unlike Collier Cone, Yapoah Crater, and Four-in-One Fissure, Garrison Butte resides in the Cascade back arc, off-axis of the arc by ~24 km to the east. No physical, petrological or radiogenic studies have been conducted on Garrison Butte, therefore eruptive volume and age are not known. The cone of Garrison Butte and its associated lava flows are heavily vegetated, and therefore I would expect Garrison Butte to be older than Yapoah Crater.

Cinder Cone (LCC2, LCC9)

Cinder Cone is an aptly named cinder cone standing ~160 m tall and located in the Lassen Volcanic Field in Northern California (Figure 5). It lies adjacent to Pilot Butte and ~17 km ENE of Lassen Peak. The cone sits atop an older, destroyed cone, thought to be the primary vent in the earlier stages of eruption. The eruption of Cinder Cone is thought to be segmented into three distinct episodes that spanned a 300-year period (USGS, 2000). These periods are labeled by their associated lava flow (oldest to youngest) - Old Bench lava flow, Painted Dunes lava flow, and Fantastic lava beds. Radiocarbon dating by Clynne et al. (2002) dates the time of eruption at 264±28 B.P (based on ^{14}C dating). The composition of lavas at Cinder Cone are basalt to basaltic-andesite and contain quartz phenocrysts and granitic xenoliths. The quartz xenocrysts and granitic xenoliths are suggested to be from a Mesozoic granite, possibly akin to the Sierra Nevadas, buried beneath the Lassen region. The granitic xenoliths have major and trace element compositions that are typical of the Sierra Nevada granitoids (Borg and Clynne, 1998). Table 2 lists the major and minor element concentrations for the Lassen granitic xenoliths (Borg and Clynne, 1998). The lavas damned a prehistoric lake, which formed the current Snag and Butte Lakes. Because of Cinder Cone's young age the tephra deposit is well-preserved. Tephra is exposed mainly NE of the vent, but can be found radially around the cone. The total volume of tephra is 0.043 km^3 while the total eruptive volume of lava is 0.08km^3 (Clynne AGU 2011, Marks, 2012). The total eruptive DRE volume for Cinder Cone is estimated to be 0.36 km^3 (Clynne AGU 2011). Based on the isopach, grains size, and grain sorting Cinder Cone erupted in a Strombolian to Violent Strombolian style (Marks, 2012).

Basalt of Old Railroad Grade (BORG)

Basalt of Old Railroad Grade (BORG) is a cinder cone within a larger chain of cones trending N 35° W, known as the Basalts of old railroad grade, and is located in the Caribou Volcanic field of Northern California (Figure 5). The cone edifice of BORG is roughly ~80 m high and is located ~14 km NNE from Cinder Cone and ~30 km NE from the summit of Lassen Peak. The cone is relatively intact; a vegetated lava flow is visible to the NW of the vent and tephra is exposed in small lenses NW of the vent. The Basalts of old railroad grade include four eruptive units (bg1-bg4), of which BORG is considered a sub unit within bg3. The Basalts of old railroad grade are classified into a larger eruptive group known as the Poison Lake Chain (Muffler et al., 2011). A complicated stratigraphic history of the Poison Lake Chain reveals the chain most likely erupted in two short periods, separated by movement on a normal fault associated with the Hat Creek fault system. The earliest eruptions of the Basalts of old railroad grade are suggested to have begun at ~100 Kya (based on $^{40}Ar/^{39}Ar$ dating; Muffler et al., 2011). The commencement and termination of eruptions that formed BORG have yet to be determined, but $^{40}Ar/^{39}Ar$ dating by Muffler et al. (2011) on unit bg4 of the Basalts of old railroad grade and the next stratigraphically youngest unit, the Bidwell Spring Chain, reveal a potential eruption age that ranges from 102.4 ± 11.4 to 46.3 ± 3.4 Kya. No description of distal tephra exits, however, the total volume of erupted lava is 0.059 km^3 over a 2.97 km^2 area. The total erupted DRE volume, excluding tephra volume, erupted from BORG is estimated to be 0.07 km^3 (Muffler et al., 2011). Because distal tephra has not been described, the erupted style for BORG is unknown.

Basalt of Highway 44 (BAS44)

Basalt of Highway 44 (BAS44) is located in the back arc basin of Northern California. BAS44 is situated ~10 km WSW from BORG and ~21 km NE of the Lassen Peak summit (Figure 5). BAS44 stands ~40 m high and a breach on the SE side of the cone is visible. A small, vegetated lava flow is present flowing from the SE breach, but it is overlain by a visibly younger lava flow erupted from a cinder cone situated on the SE flank of West Prospect Peak shield volcano (not dated). The flows are also bounded to the west by the western edge of the Hat Creek Graben. No physical, petrological or radiogenic studies have been conducted on BAS44, therefore eruptive volume, eruptive style, and age are not known.

APPENDIX B

OLIVINE-HOSTED MELT INCLUSION MAJOR, MINOR ELEMENT, AND VOLATILE DATA FOR CENTRAL AND SOUTHERN CASCADES CINDER CONES

	(wt%) SiO_2	TiO_2	Al_2O_3	FeO^T	MnO	MgO	CaO	Na_2O	K_2O	P_2O_5	S	Cl
Collier33B												
e1	54.00	0.88	19.46	6.80	0.11	5.27	8.83	4.05	0.52	0.09	0.07	0.06
e2	54.39	0.90	19.11	6.80	0.10	5.28	8.71	4.09	0.53	0.10	0.07	0.07
d	54.28	0.86	19.36	6.76	0.08	5.14	8.22	4.54	0.65	0.13	0.08	0.07
b	53.70	0.87	19.64	6.73	0.10	5.27	8.91	3.95	0.64	0.19	0.08	0.06
a	53.00	0.90	19.94	6.75	0.11	5.40	9.45	3.84	0.46	0.14	0.07	0.07
avg.	*53.87*	*0.88*	*19.50*	*6.77*	*0.10*	*5.27*	*8.82*	*4.09*	*0.56*	*0.13*	*0.07*	*0.06*
Collier33D												
a	57.31	1.13	17.48	7.31	0.13	3.28	6.71	5.46	0.97	0.22	0.08	0.07
d	55.00	0.97	18.29	8.03	0.15	4.07	8.20	4.54	0.65	0.11	0.07	0.06
e	55.22	1.00	18.71	6.61	0.12	4.65	8.48	4.49	0.61	0.11	0.07	0.07
b1	54.22	0.94	19.55	6.46	0.08	4.97	8.97	4.12	0.56	0.12	0.07	0.06
b3	53.72	0.95	19.75	6.57	0.09	5.02	9.03	4.23	0.52	0.12	0.07	0.07
avg.	*55.09*	*1.00*	*18.76*	*7.00*	*0.11*	*4.40*	*8.28*	*4.57*	*0.66*	*0.14*	*0.07*	*0.07*
Yo016E												
1E-h	54.51	0.92	18.16	7.43	0.09	5.24	8.55	4.1	0.65	0.16	0.09	0.09
1E-I	52.93	0.96	19.07	7.44	0.1	5.25	9.1	4.15	0.65	0.16	0.09	0.09
avg.	*53.72*	*0.94*	*18.62*	*7.435*	*0.095*	*5.245*	*8.825*	*4.125*	*0.65*	*0.16*	*0.09*	*0.09*
Fo0803D3												
Xb	54.85	0.99	17.23	8.62	0.15	5.36	8.68	3.19	0.73	0.21	0.08	0.11
c1	53.84	1.12	17.91	8.39	0.16	5.65	9.12	2.90	0.65	0.23	0.09	0.09
f	54.09	1.10	17.66	8.41	0.11	5.68	8.79	3.21	0.72	0.24	0.09	0.08

e	53.13	1.18	17.63	8.39	0.13	5.81	9.16	3.62	0.70	0.25	0.09	0.09
g	53.66	1.14	17.12	8.40	0.12	5.95	9.35	3.35	0.67	0.24	0.10	0.08
a	53.21	1.16	18.08	8.38	0.13	6.00	9.11	3.00	0.67	0.25	0.09	0.08
m	53.82	1.10	16.83	8.39	0.14	6.11	9.47	3.27	0.64	0.23	0.09	0.08
i	53.84	1.24	17.08	8.40	0.12	6.16	8.91	3.22	0.69	0.35	0.09	0.08
k	53.06	1.13	17.47	8.41	0.14	6.14	9.49	3.28	0.63	0.25	0.09	0.08
L	53.69	1.10	17.35	8.40	0.12	6.22	9.15	3.09	0.67	0.23	0.09	0.08
avg.	*53.72*	*1.13*	*17.44*	*8.42*	*0.13*	*5.91*	*9.12*	*3.21*	*0.68*	*0.25*	*0.09*	*0.08*
GB072												
1-g	50.21	1.47	16.52	10.51	0.18	6.66	9.82	3.4	0.64	0.34	0.13	0.07
1-i	48.86	1.57	17.67	10.52	0.15	6.7	10.14	3.29	0.46	0.4	0.12	0.04
1-a	49.59	1.54	17.22	10.47	0.13	6.85	9.95	3.06	0.51	0.42	0.12	0.09
1-b	49.4	1.48	17.43	10.49	0.18	6.91	9.73	3.22	0.56	0.34	0.13	0.05
1-h	50.01	1.39	16.4	10.47	0.2	7.31	9.52	3.5	0.62	0.33	0.13	0.08
1-f	50.07	1.5	16.08	10.47	0.16	7.56	9.66	3.33	0.58	0.34	0.14	0.05
1-k1	49.07	1.42	17.56	10.5	0.16	7.27	9.91	3.02	0.43	0.41	0.12	0.04
1-k2	48.88	1.49	17.61	10.48	0.13	7.16	9.87	3.22	0.48	0.43	0.12	0.05
1-c	48.99	1.49	17.4	10.47	0.17	7.43	9.77	3.16	0.49	0.38	0.12	0.05
1-L	49.05	1.56	16.97	10.53	0.14	7.49	9.91	3.2	0.48	0.41	0.12	0.06
1-d	48.17	1.39	17.94	10.51	0.14	7.47	9.95	3.22	0.49	0.46	0.12	0.06
avg.	*49.30*	*1.48*	*17.16*	*10.49*	*0.16*	*7.16*	*9.84*	*3.24*	*0.52*	*0.39*	*0.12*	*0.06*
LCC2												
LCC-2-02	51.75	1.02	18.10	5.12	0.09	5.59	9.85	3.16	1.03	0.21	0.09	0.04
LCC-2-04	51.52	1.03	18.09	5.07	0.09	5.46	10.09	3.52	0.98	0.22	0.10	0.04
LCC-2-01	51.36	1.02	17.69	4.93	0.10	5.68	10.20	3.83	0.95	0.20	0.10	0.04
LCC-2-05	50.85	1.04	18.24	5.16	0.09	5.71	10.05	3.66	0.98	0.22	0.10	0.04
LCC-2-08	50.62	0.98	17.81	5.68	0.09	5.64	9.93	3.58	0.95	0.21	0.10	0.04
LCC-2-07	50.76	1.02	17.99	5.35	0.09	5.56	10.12	3.73	0.97	0.21	0.10	0.04

LCC-2-10	50.69	0.99	18.11	5.22	0.09	5.57	10.18	3.68	0.96	0.21	0.10	0.04
LCC-2-09	51.20	1.01	17.99	5.22	0.09	5.75	10.10	3.69	0.97	0.21	0.10	0.04
LCC-2-11	53.82	1.07	19.45	5.53	0.10	4.29	8.85	3.70	1.48	0.22	0.04	0.04
avg.	*51.40*	*1.02*	*18.16*	*5.25*	*0.09*	*5.47*	*9.93*	*3.62*	*1.03*	*0.21*	*0.09*	*0.04*
LCC9												
LCC-9-01	51.04	0.91	17.42	5.34	0.10	5.71	10.57	3.39	0.90	0.17	0.09	0.04
LCC-9-02	49.89	0.95	18.12	5.39	0.09	7.15	9.49	3.46	0.85	0.18	0.09	0.04
LCC-9-06	50.48	0.93	17.82	4.99	0.09	5.72	11.48	3.11	0.77	0.18	0.10	0.04
LCC-9-07	50.57	0.83	16.72	5.18	0.09	8.59	10.17	2.78	0.82	0.16	0.09	0.03
LCC-9-09(1)	51.04	0.85	17.20	4.94	0.09	5.80	10.73	3.19	0.83	0.16	0.09	0.04
LCC-9-09(2)	51.44	0.86	17.73	5.05	0.09	5.88	10.46	3.06	0.88	0.16	0.06	0.04
LCC-9-04	50.89	0.89	17.72	5.30	0.09	5.77	10.76	3.34	0.85	0.17	0.10	0.04
LCC-9-04(2)	51.28	0.88	17.61	5.25	0.09	5.58	10.51	3.22	0.93	0.16	0.09	0.04
LCC-9-10	51.15	0.86	17.95	5.18	0.09	5.67	10.79	3.23	0.87	0.17	0.10	0.04
LCC-9-13	53.14	0.85	17.70	6.21	0.11	4.87	8.92	3.72	1.35	0.16	0.08	0.04
LCC-9-16(1)	49.96	0.87	17.27	5.46	0.10	6.03	11.20	3.12	0.71	0.17	0.10	0.04
LCC-9-16(2)	50.10	0.89	17.45	5.31	0.10	6.05	11.32	3.09	0.72	0.16	0.10	0.04
LCC-9-18(1)	51.18	0.87	17.39	5.21	0.10	5.94	10.77	3.24	0.83	0.16	0.09	0.04
avg.	*50.94*	*0.88*	*17.55*	*5.29*	*0.09*	*6.06*	*10.55*	*3.23*	*0.87*	*0.16*	*0.09*	*0.04*
BORG												
A1	48.78	0.73	18.72	6.65	0.13	7.05	10.78	2.90	0.55	0.11	0.11	0.06
A5	49.23	0.77	17.66	6.57	0.13	6.88	10.86	2.70	0.56	0.09	0.13	0.06
A6	50.74	0.90	21.11	7.16	0.13	3.94	9.56	3.66	0.60	0.14	0.16	0.05
A9	48.79	0.70	17.80	6.62	0.11	7.17	10.92	2.63	0.53	0.08	0.13	0.05
A10	50.03	0.78	20.82	5.93	0.12	3.62	10.75	3.48	0.60	0.10	0.15	0.07
A18	50.36	0.81	17.63	6.27	0.11	6.17	11.37	2.70	0.54	0.12	0.13	0.06
A23	49.78	0.82	18.54	6.37	0.11	4.59	11.39	2.91	0.57	0.11	0.14	0.06
A24	49.63	0.81	18.19	6.05	0.09	6.31	12.28	2.70	0.44	0.10	0.13	0.07

A28	49.53	0.78	19.49	6.26	0.12	5.15	11.89	2.82	0.53	0.10	0.14	0.06
AA1	50.90	0.90	18.45	7.11	0.13	5.30	9.55	3.65	0.62	0.12	0.11	0.04
AA4	49.33	0.89	18.73	7.42	0.13	6.34	9.12	3.36	0.57	0.11	0.22	0.04
AA5	50.80	0.84	17.99	6.29	0.10	5.55	11.31	2.80	0.54	0.12	0.13	0.06
avg.	*49.91*	*0.82*	*18.67*	*6.46*	*0.12*	*5.70*	*10.79*	*3.04*	*0.58*	*0.11*	*0.14*	*0.05*
BAS44												
B1	49.66	0.03	17.73	8.00	0.14	7.78	11.16	3.00	0.28	1.01	0.04	0.12
B2	48.00	0.99	19.02	7.50	0.14	7.34	11.19	3.01	0.31	0.15	0.11	0.03
B3	48.83	1.04	18.19	7.83	0.12	7.51	11.43	2.94	0.28	0.17	0.12	0.03
B6	50.17	1.01	16.98	8.04	0.14	7.58	11.10	3.12	0.34	0.17	0.12	0.03
B7	49.59	0.99	17.60	7.82	0.13	7.72	11.27	2.71	0.29	0.17	0.12	0.03
B17	48.91	1.01	17.46	7.80	0.13	7.90	11.09	3.01	0.31	0.16	0.12	0.03
B18	49.67	0.99	17.15	7.94	0.13	8.33	10.72	3.21	0.29	0.17	0.12	0.03
B20	49.27	1.01	17.15	7.76	0.13	7.39	11.24	3.06	0.31	0.17	0.12	0.03
B23	49.53	0.99	17.40	7.91	0.13	7.39	11.13	2.95	0.31	0.17	0.12	0.03
B24	49.00	1.03	17.68	7.66	0.11	7.43	11.26	2.98	0.30	0.17	0.12	0.03
B25	50.50	1.03	17.61	8.22	0.14	7.74	11.48	1.58	0.29	0.17	0.11	0.03
BB3	49.22	1.00	17.29	8.12	0.13	7.75	11.15	3.15	0.31	0.17	0.11	0.03
avg.	*49.26*	*0.88*	*17.66*	*7.84*	*0.13*	*7.69*	*11.15*	*3.01*	*0.30*	*0.27*	*0.11*	*0.04*

**Collier33B, Collier33D, Yo016E, Fo0803D3, GB072 data from Ruscitto (2011)*
***LCC2, LCC9 data from Walowski (unpublished)*
****BORG, BAS44 data from Rasmussen (unpublished)*

APPENDIX C

MATRIX GLASS MAJOR AND MINOR ELEMENT DATA FOR CENTRAL AND SOUTHERN CASCADES CINDER CONES

	(wt%) SiO_2	TiO_2	Al_2O_3	FeO^T	MnO	MgO	CaO	Na_2O	K_2O	P_2O_5
Collier33B	56.40	0.85	18.93	6.53	0.12	4.87	7.33	3.94	0.89	0.13
Collier33D	56.54	1.09	18.50	7.44	0.13	3.78	7.27	4.27	0.84	0.15
Yo061E	53.81	0.82	20.00	6.85	0.12	5.88	8.29	3.37	0.72	0.15
Fo0803D3	52.68	1.11	19.25	7.84	0.14	5.52	8.96	3.62	0.64	0.23
GB072	49.71	1.33	16.42	10.30	0.18	9.09	9.33	2.80	0.54	0.29
LCC2										
ash unit 2 base	54.78	0.72	16.42	6.62	0.12	8.24	8.51	3.13	1.18	0.15
ash unit 2 middle	53.71	0.74	16.12	6.96	0.13	9.04	8.92	3.00	1.03	0.19
ash unit 2 middle	54.62	0.71	16.42	6.67	0.12	8.40	8.57	3.03	1.15	0.17
ash unit 2 PP Tr	54.68	0.69	16.08	6.69	0.13	8.60	8.67	3.00	1.12	0.19
ash unit 2 PP Tr	55.51	0.71	16.29	6.45	0.12	7.92	8.26	3.17	1.24	0.19
ash unit 2, 74 cm	56.31	0.65	15.90	6.23	0.12	8.01	8.08	3.06	1.33	0.17
ash unit 2, 77 cm	57.96	0.66	15.73	5.83	0.11	7.46	7.16	3.20	1.58	0.18
avg.	*55.37*	*0.70*	*16.14*	*6.49*	*0.12*	*8.24*	*8.31*	*3.08*	*1.23*	*0.18*
LCC9										
ash unit 3, 10 cm	57.72	0.69	15.95	5.92	0.11	7.15	7.35	3.25	1.57	0.15
ash unit 3, 100 cm	54.92	0.83	16.93	6.71	0.12	7.45	8.25	3.23	1.22	0.19
ash unit 3, 11 cm	56.83	0.74	15.98	6.17	0.12	7.73	7.36	3.25	1.50	0.20
ash unit 3, 120-125 cm	55.42	0.80	16.93	6.45	0.12	7.28	8.09	3.28	1.30	0.18
ash unit 3, 120-125 cm	55.63	0.79	16.80	6.43	0.12	7.23	8.06	3.30	1.31	0.18
ash unit 3, 17 cm	56.46	0.78	16.39	6.27	0.12	7.22	7.63	3.30	1.48	0.21

ash unit 3, 20 cm	57.20	0.74	16.13	6.04	0.11	7.12	7.40	3.36	1.55	0.21
ash unit 3, 40 cm	56.29	0.80	16.37	6.33	0.12	7.30	7.70	3.30	1.46	0.19
ash unit 3, 58 cm	55.67	0.79	16.86	6.46	0.12	7.12	8.06	3.26	1.32	0.19
ash unit 3, 73 cm	55.20	0.80	16.92	6.57	0.12	7.39	8.16	3.24	1.27	0.17
ash, unit 3, near top	55.06	0.83	16.45	6.73	0.12	7.70	8.15	3.29	1.31	0.20
avg.	*56.04*	*0.78*	*16.52*	*6.37*	*0.12*	*7.34*	*7.84*	*3.28*	*1.39*	*0.19*
BORG										
LM91-2130	49.96	0.68	16.15	7.94	0.15	12.24	9.64	2.39	0.55	0.13
LM91-2140	50.25	0.69	16.95	7.59	0.14	10.96	10.11	2.50	0.49	0.14
LM91-2116	51.17	0.70	17.09	7.36	0.14	10.15	9.84	2.64	0.60	0.14
LC86-829	51.51	0.71	17.24	7.33	0.13	9.20	10.42	2.57	0.61	0.12
avg.	*50.72*	*0.70*	*16.86*	*7.56*	*0.14*	*10.64*	*10.00*	*2.53*	*0.56*	*0.13*
BAS44										
RNW	49.49	0.98	17.54	1.44	0.16	9.12	10.58	2.76	0.35	0.21
RNW	49.58	0.99	17.57	1.45	0.15	8.71	10.74	2.89	0.36	0.17
RNW	49.97	0.99	18.12	1.40	0.15	8.26	10.41	2.93	0.42	0.18
avg.	*49.68*	*0.99*	*17.74*	*1.43*	*0.15*	*8.70*	*10.58*	*2.86*	*0.38*	*0.19*

**Collier33B, Collier33D, Yo016E, Fo0803D3, GB072 data from Ruscitto (2011)*
***LCC2, LCC9, BORG, BAS44 data from Clynne (2011)*

APPENDIX D

MAJOR AND MINOR ELEMENT DATA FOR CINDER CONE LAVA GLASSES

(wt%)	SiO_2	TiO_2	Al_2O_3	FeO^T	MnO	MgO	CaO	Na_2O	K_2O	P_2O_5
LCC2										
PD2	57.06	0.62	15.64	6.01	0.12	7.92	7.88	3.06	1.41	0.14
PD2	57.57	0.61	15.46	5.88	0.11	7.88	7.67	3.08	1.47	0.14
PD2 knoll n Snag Lake	57.88	0.65	15.79	5.82	0.11	7.29	7.38	3.21	1.57	0.18
PD2	58.27	0.64	15.77	5.70	0.11	7.13	7.16	3.28	1.61	0.19
PD2	58.74	0.59	15.64	5.55	0.11	7.08	7.16	3.21	1.63	0.17
PD2 bomb on knoll	58.83	0.59	15.59	5.51	0.11	7.07	7.15	3.19	1.67	0.16
PD2	58.97	0.59	15.57	5.49	0.11	6.98	7.03	3.26	1.69	0.18
PD2 SE edge	59.00	0.53	15.08	5.60	0.10	7.56	7.14	3.08	1.66	0.13
PD2 Snag lake	59.10	0.57	15.49	5.40	0.11	7.17	7.03	3.19	1.69	0.13
PD2 Snag Lake	59.16	0.56	15.33	5.42	0.11	7.24	7.13	3.12	1.67	0.13
PD2 n of Snag Lake	59.16	0.57	15.30	5.44	0.11	7.18	7.13	3.15	1.68	0.15
PD2	59.55	0.55	15.35	5.29	0.11	6.94	6.95	3.23	1.74	0.16
PD2	59.67	0.54	15.27	5.31	0.11	7.01	6.93	3.14	1.73	0.16
FL2 Butte Lakeshore	55.65	0.82	16.80	6.50	0.12	7.03	8.04	3.34	1.33	0.22
FL2 Butte Lakeshore	55.78	0.82	16.84	6.46	0.12	6.96	8.00	3.33	1.35	0.19
FL2 Butte Lakeshore	56.09	0.80	16.79	6.37	0.12	6.81	7.95	3.35	1.37	0.21
FL1 Butte Lakeshore	56.11	0.78	16.26	6.49	0.12	7.32	7.96	3.22	1.42	0.18
FL2 PD to 1144 trav	56.16	0.80	16.74	6.32	0.12	6.90	7.88	3.35	1.39	0.21
FL2 S of Devils Thrt	56.25	0.78	16.66	6.29	0.12	6.99	7.89	3.31	1.38	0.19
FL2 east flow edge	56.33	0.75	16.44	6.37	0.12	7.08	7.98	3.23	1.39	0.17
FL1 NW cor Butte Lake	56.35	0.79	16.29	6.30	0.12	7.31	7.69	3.34	1.45	0.22

FL1 6235' kipuka	56.47	0.78	16.29	6.25	0.12	7.26	7.64	3.35	1.52	0.19
FL1 east of PD	56.51	0.79	16.46	6.26	0.12	6.99	7.77	3.29	1.47	0.21
FL1 1409 to Is trav	56.70	0.78	16.24	6.23	0.12	7.19	7.58	3.31	1.48	0.22
FL1 east of PD	56.75	0.77	16.37	6.19	0.12	6.93	7.70	3.32	1.49	0.21
FL1 E side Butte Lake	56.80	0.80	16.37	6.18	0.12	6.94	7.61	3.30	1.53	0.21
FL1 Butte Lakeshore	56.84	0.79	16.40	6.15	0.12	6.87	7.59	3.34	1.53	0.23
FL1 east side	57.07	0.80	16.19	6.22	0.12	6.74	7.67	3.32	1.55	0.19
FL1 flow leeve	57.17	0.74	16.13	6.07	0.12	7.17	7.46	3.29	1.52	0.19
FL1 "the Island"	57.32	0.79	16.32	6.06	0.12	6.69	7.44	3.32	1.60	0.20
avg.	*58.52*	*0.59*	*15.51*	*5.62*	*0.11*	*7.32*	*7.26*	*3.17*	*1.61*	*0.16*
LCC9										
Old Bench east	54.08	0.70	15.99	6.88	0.12	8.89	8.92	3.05	1.07	0.15
Old Bench west	53.53	0.72	16.00	7.04	0.13	9.28	9.07	2.93	1.00	0.16
PD1 under PD	54.45	0.69	16.07	6.80	0.12	8.51	8.80	3.11	1.14	0.15
PD1	54.51	0.71	15.95	6.75	0.13	8.79	8.76	2.97	1.11	0.16
PD1 under PD	54.86	0.68	15.83	6.71	0.12	8.63	8.73	3.03	1.12	0.14
PD1 under PD	55.03	0.70	16.44	6.61	0.13	8.03	8.49	3.06	1.20	0.16
PD1 kipuka	55.26	0.68	15.90	6.52	0.12	8.52	8.48	3.00	1.18	0.19
PD1	55.84	0.66	16.00	6.31	0.12	8.23	8.15	3.10	1.28	0.15
PD1 under PD	55.97	0.63	15.79	6.28	0.12	8.18	8.26	3.20	1.30	0.14
avg.	*54.84*	*0.69*	*16.00*	*6.66*	*0.12*	*8.56*	*8.63*	*3.05*	*1.15*	*0.16*

**LCC2* , *LCC9* data from Clynne (2011)

APPENDIX E

GAUSSIAN PLUME STABILITY CONSTANTS AND DEFINITIONS

Definitions of plume stability from Hanna et al. (1982)

A: Extremely unstable conditions
B: Moderately unstable conditions
C: Slightly unstable conditions
D: Neutral conditions†
E: Slightly stable conditions
F: Moderately stable conditions

Surface wind speed, m/sec	Daytime insolation			Nighttime conditions‡	
	Strong	Moderate	Slight	Thin overcast or >4/8 low cloud	≤3/8 cloudiness
<2	A	A–B	B		
2	A–B	B	C	E	F
4	B	B–C	C	D	E
6	C	C–D	D	D	D
>6	C	D	D	D	D

*From F. A. Gifford, Turbulent Diffusion-Typing Schemes: A Review, *Nucl. Saf.*, 17(1): 71 (1976).

†Applicable to heavy overcast day or night.

‡The degree of cloudiness is defined as that fraction of the sky above the local apparent horizon that is covered by clouds.

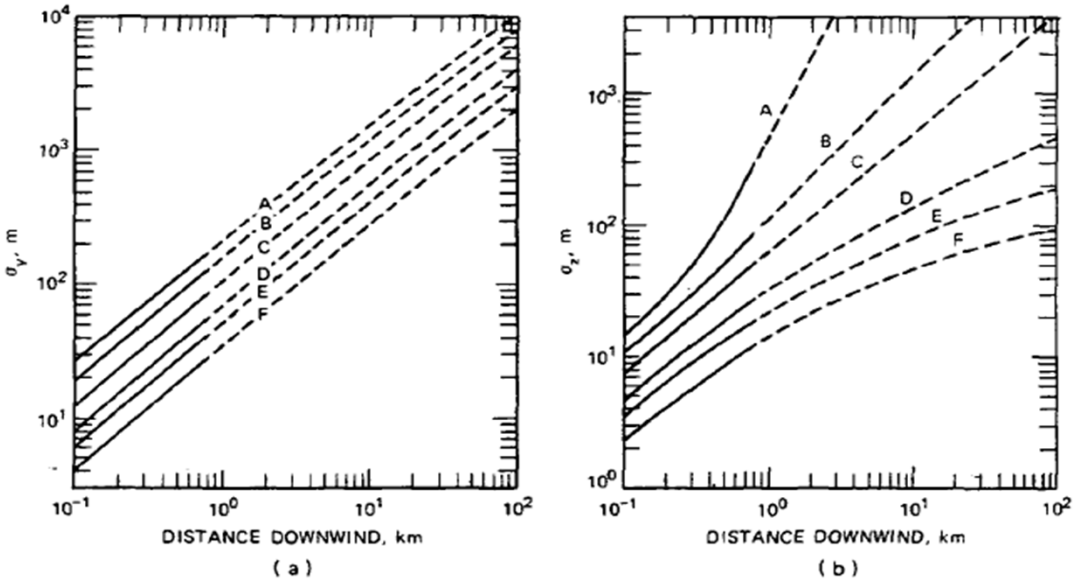

Gaussian plume constants for varying plume stability from Guenther (2010)

Plume Stability	x (km)	a	b	c	d
Unstable	<0.1	122.80	0.94	24.17	2.53
	0.10-0.15	158.08	1.05	24.17	2.53
	0.16-0.20	170.22	1.09	24.17	2.53
	0.21-0.25	179.52	1.13	24.17	2.53
	0.26-0.30	217.41	1.26	24.17	2.53
	0.31-0.4	258.89	1.41	24.17	2.53
	0.41-0.5	346.75	1.73	24.17	2.53
	0.51-3.11	453.85	2.12	24.17	2.53
	>3.11	+	+	24.17	2.53
Moderately Unstable	<0.20	90.67	0.93	18.33	1.81
	0.21-0.40	98.48	0.98	18.33	1.81
	>0.40	109.30	1.10	18.33	1.81
Slightly Unstable	All	61.14	0.91	12.50	1.09
Neutral	<0.30	34.46	0.87	8.33	0.72
	0.31-1.00	32.09	0.81	8.33	0.72
	1.01-3.00	32.09	0.64	8.33	0.72
	3.01-10.00	33.50	0.60	8.33	0.72
	10.01-30.00	36.65	0.57	8.33	0.72
	>30.00	44.05	0.51	8.33	0.72

+ if σ_z >5000 m, σ_z is set to 5000 m

APPENDIX F

SULFUR, CHLORINE, AND FLUORINE EVOLUTION AND DEGASSING

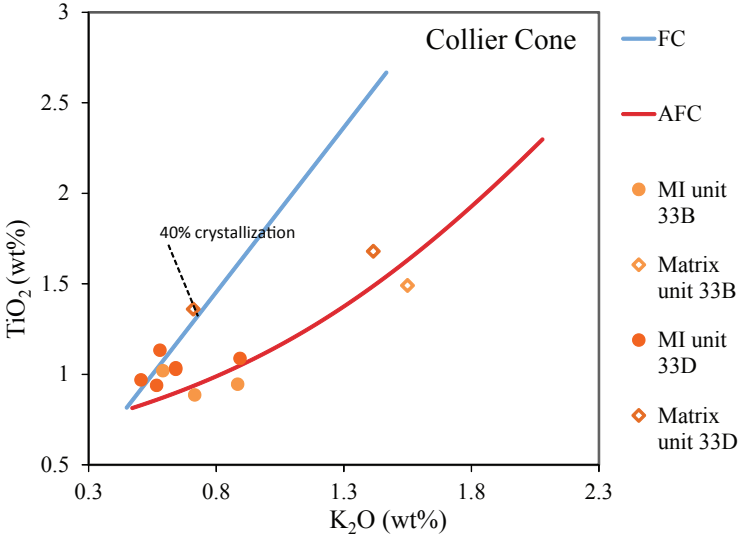

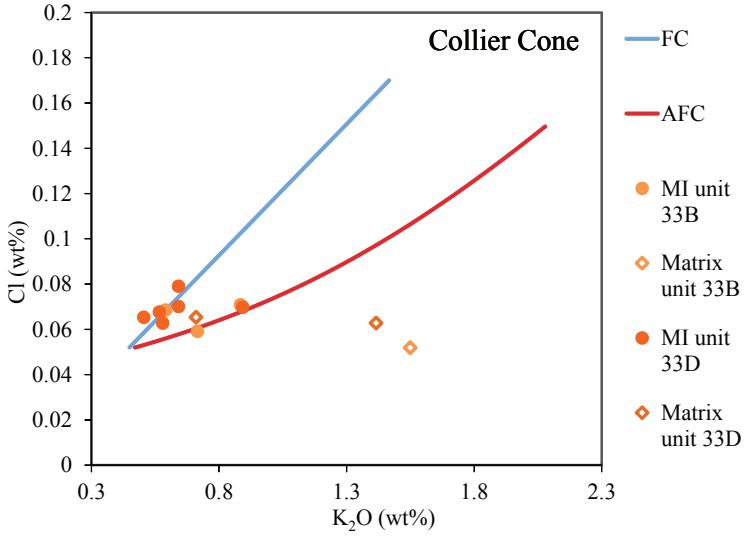

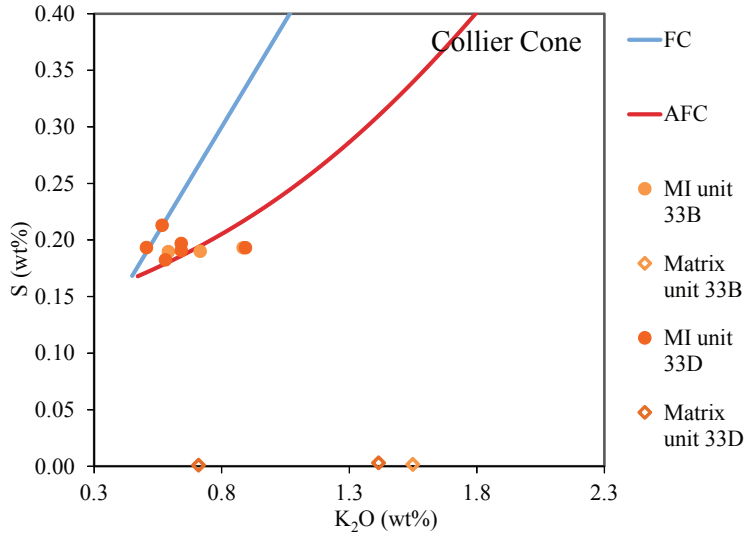

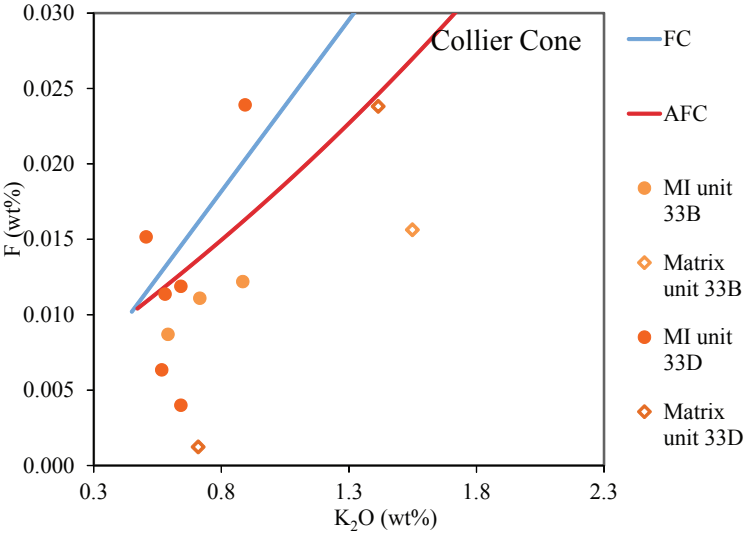

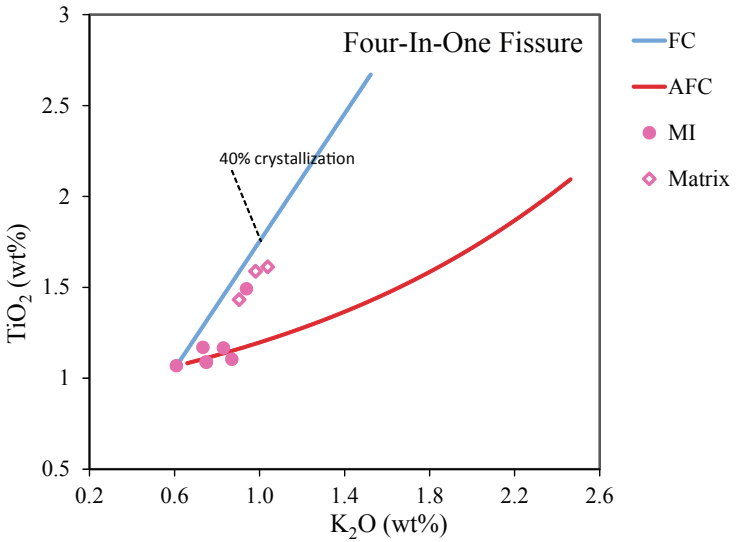
Four-In-One Fissure
40% crystallization
FC
AFC
MI
Matrix
TiO2 (wt%)
K2O (wt%)
3
2.5
2
1.5
1
0.5
0.2
0.6
1.0
1.4
1.8
2.2
2.6

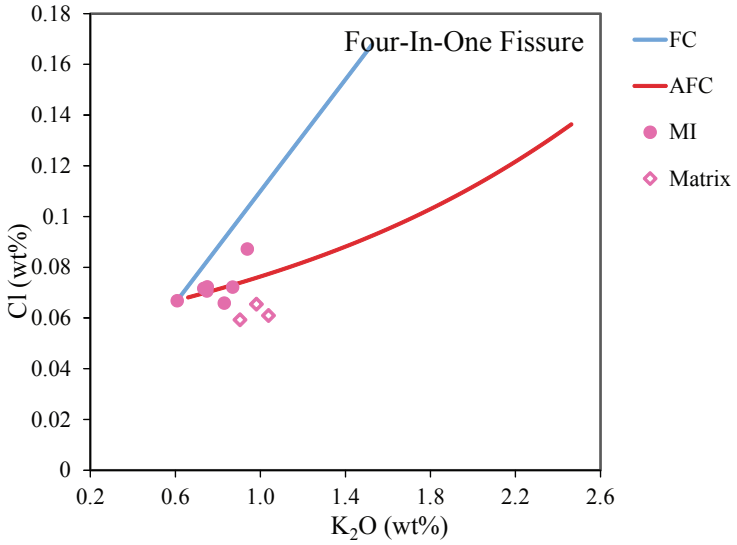
Four-In-One Fissure
FC
AFC
MI
Matrix
Cl (wt%)
K2O (wt%)
0.18
0.16
0.14
0.12
0.1
0.08
0.06
0.04
0.02
0
0.2
0.6
1.0
1.4
1.8
2.2
2.6

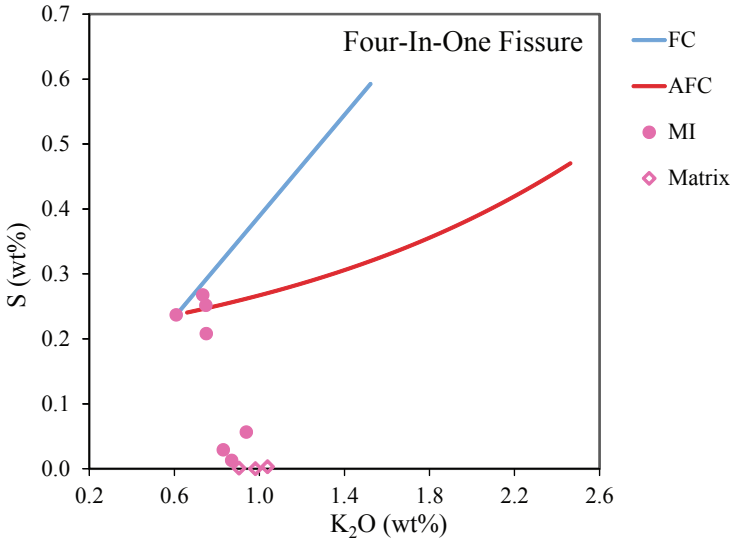
Four-In-One Fissure
FC
AFC
MI
Matrix
S (wt%)
K2O (wt%)
0.7
0.6
0.5
0.4
0.3
0.2
0.1
0.0
0.2
0.6
1.0
1.4
1.8
2.2
2.6

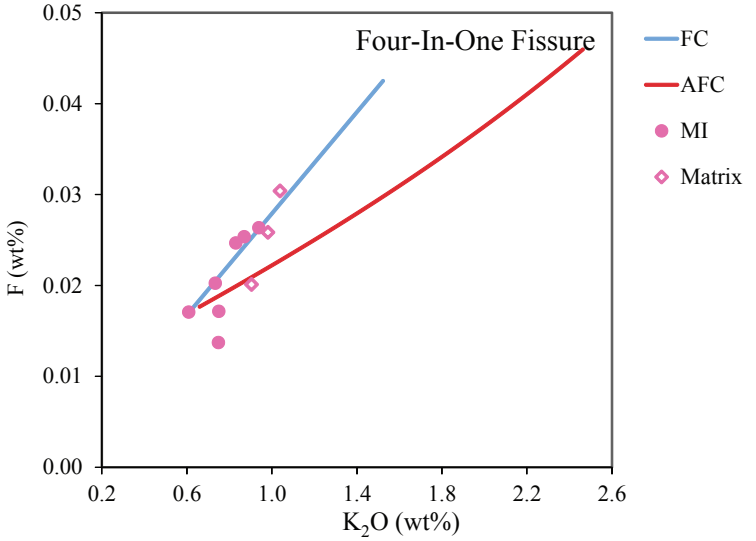
Four-In-One Fissure
FC
AFC
MI
Matrix
F (wt%)
K2O (wt%)
0.05
0.04
0.03
0.02
0.01
0.00
0.2
0.6
1.0
1.4
1.8
2.2
2.6

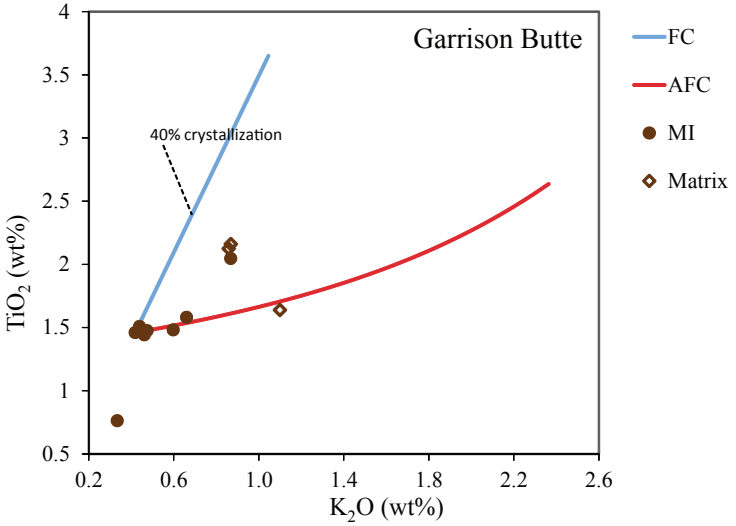
Garrison Butte
40% crystallization
TiO2 (wt%)
K2O (wt%)
FC
AFC
MI
Matrix

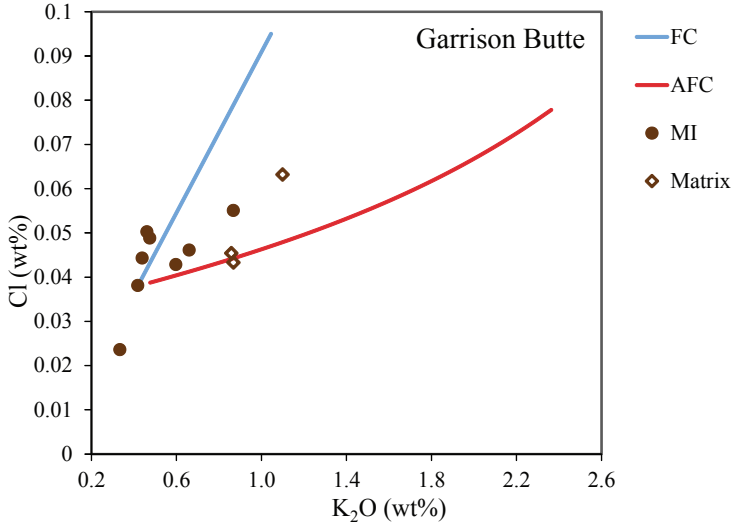
Garrison Butte
Cl (wt%)
K2O (wt%)
FC
AFC
MI
Matrix

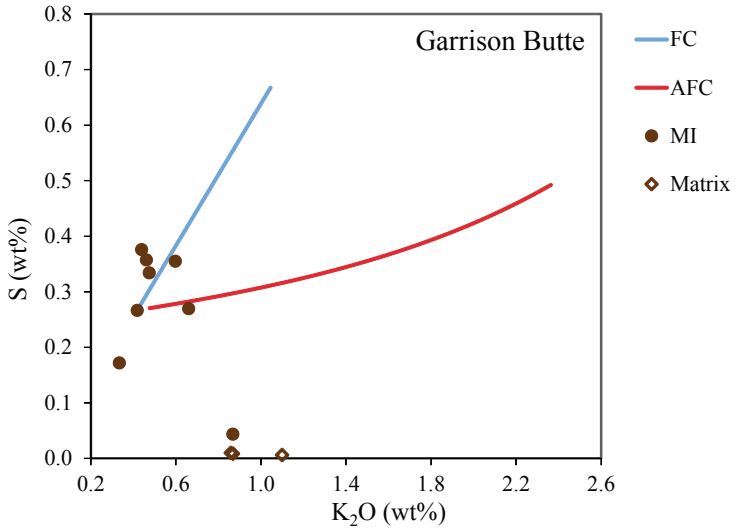
Garrison Butte
S (wt%)
K2O (wt%)
FC
AFC
MI
Matrix

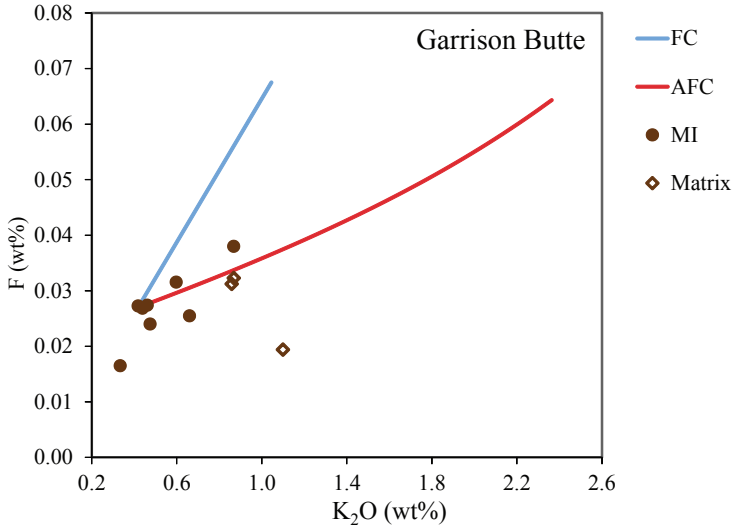
Garrison Butte
F (wt%)
K2O (wt%)
FC
AFC
MI
Matrix

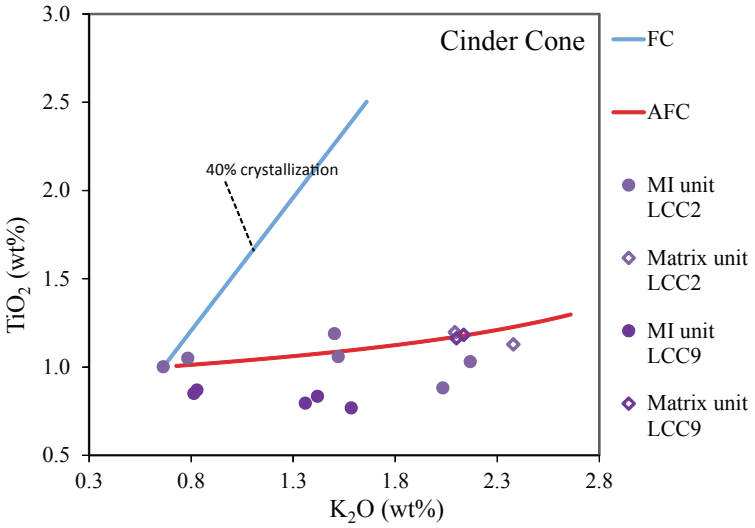
Cinder Cone
40% crystallization
FC
AFC
MI unit LCC2
Matrix unit LCC2
MI unit LCC9
Matrix unit LCC9
TiO2 (wt%)
K2O (wt%)
3.0
2.5
2.0
1.5
1.0
0.5
0.3
0.8
1.3
1.8
2.3
2.8

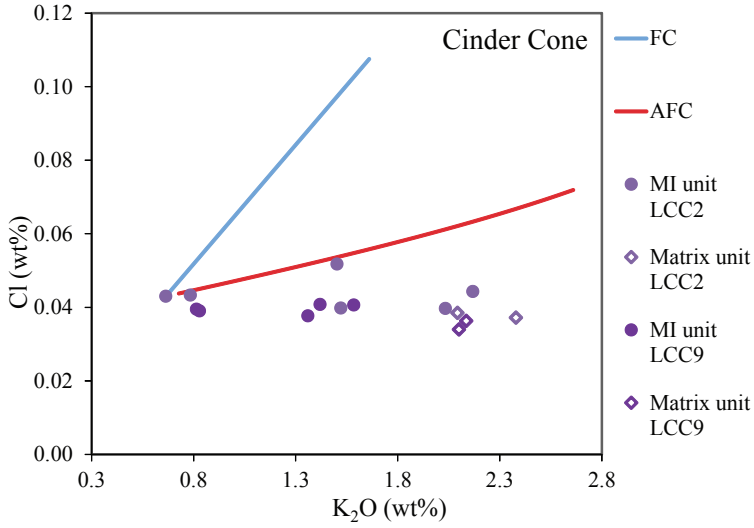
Cinder Cone
FC
AFC
MI unit LCC2
Matrix unit LCC2
MI unit LCC9
Matrix unit LCC9
Cl (wt%)
K2O (wt%)
0.12
0.10
0.08
0.06
0.04
0.02
0.00
0.3
0.8
1.3
1.8
2.3
2.8

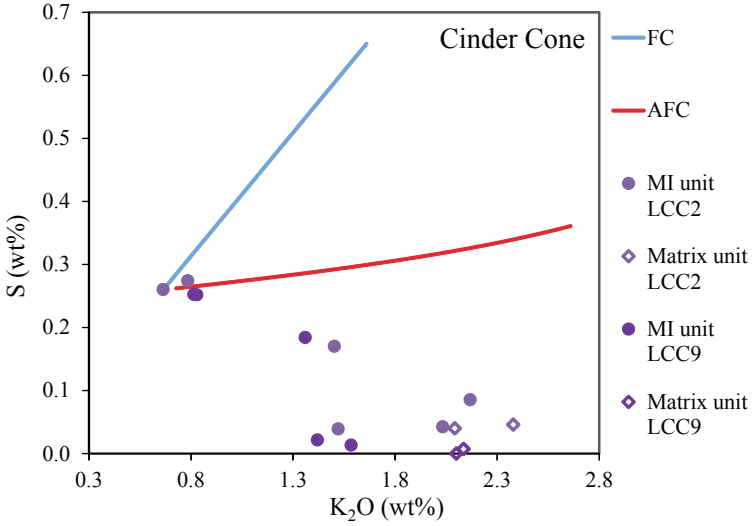
Cinder Cone
FC
AFC
MI unit LCC2
Matrix unit LCC2
MI unit LCC9
Matrix unit LCC9
S (wt%)
K2O (wt%)
0.7
0.6
0.5
0.4
0.3
0.2
0.1
0.0
0.3
0.8
1.3
1.8
2.3
2.8

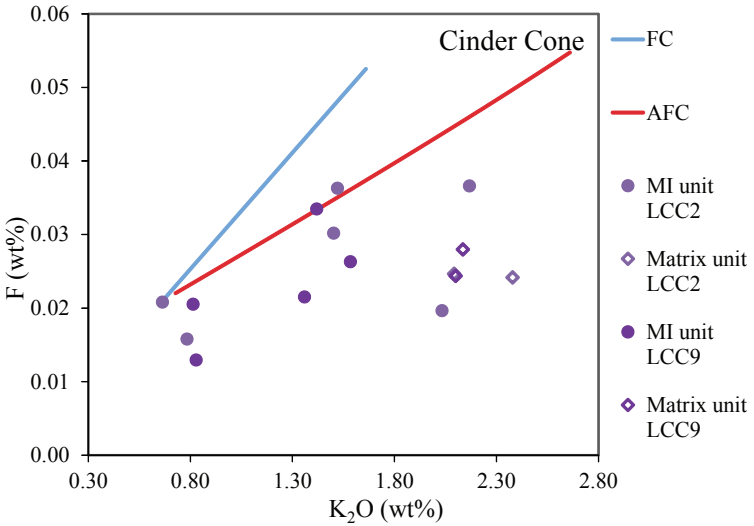
Cinder Cone
FC
AFC
MI unit LCC2
Matrix unit LCC2
MI unit LCC9
Matrix unit LCC9
F (wt%)
K2O (wt%)
0.06
0.05
0.04
0.03
0.02
0.01
0.00
0.30
0.80
1.30
1.80
2.30
2.80

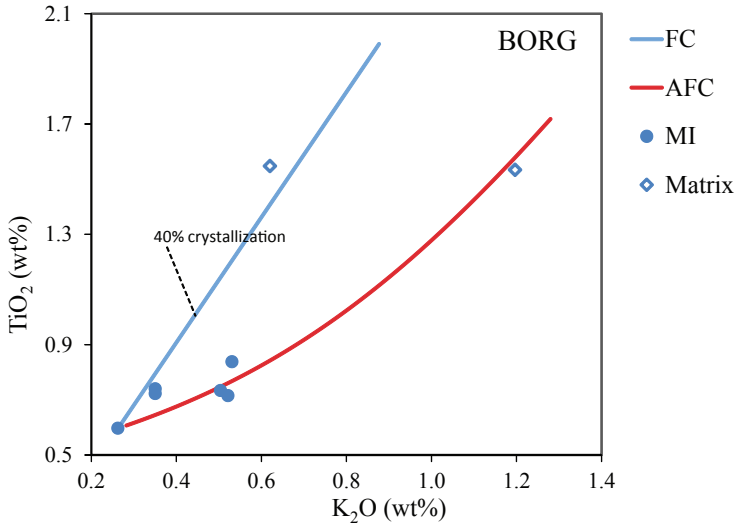
BORG
FC
AFC
MI
Matrix
40% crystallization
TiO2 (wt%)
K2O (wt%)
2.1
1.7
1.3
0.9
0.5
0.2
0.4
0.6
0.8
1.0
1.2
1.4

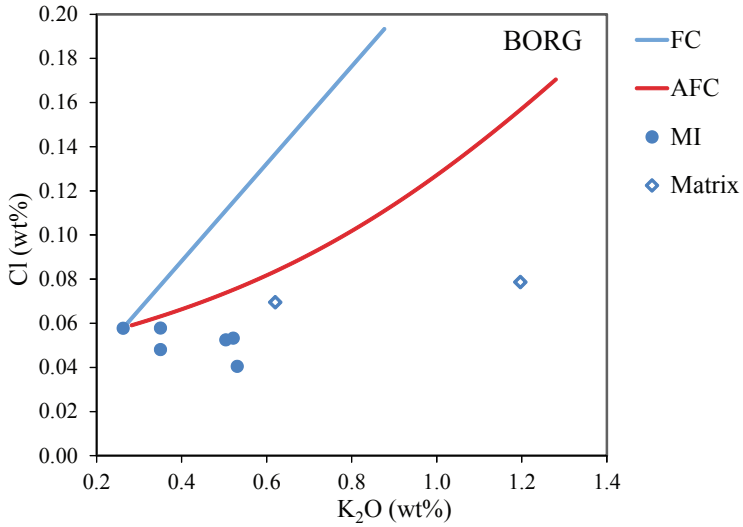
BORG
FC
AFC
MI
Matrix
Cl (wt%)
K2O (wt%)
0.20
0.18
0.16
0.14
0.12
0.10
0.08
0.06
0.04
0.02
0.00
0.2
0.4
0.6
0.8
1.0
1.2
1.4

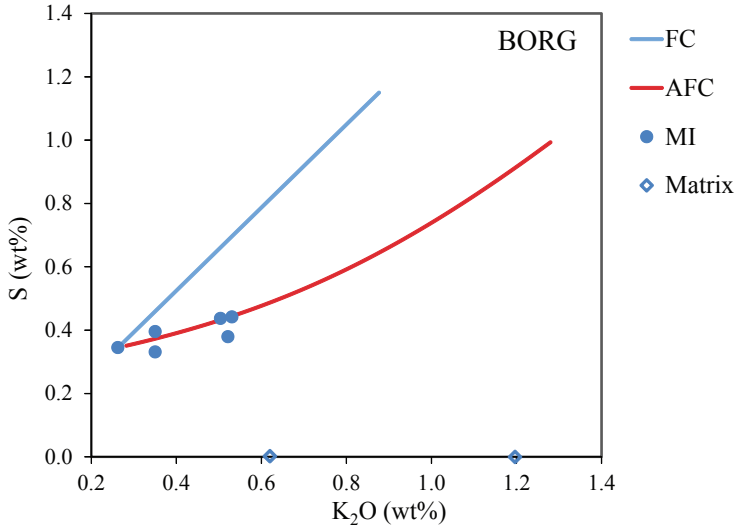
BORG
FC
AFC
MI
Matrix
S (wt%)
K2O (wt%)
1.4
1.2
1.0
0.8
0.6
0.4
0.2
0.0
0.2
0.4
0.6
0.8
1.0
1.2
1.4

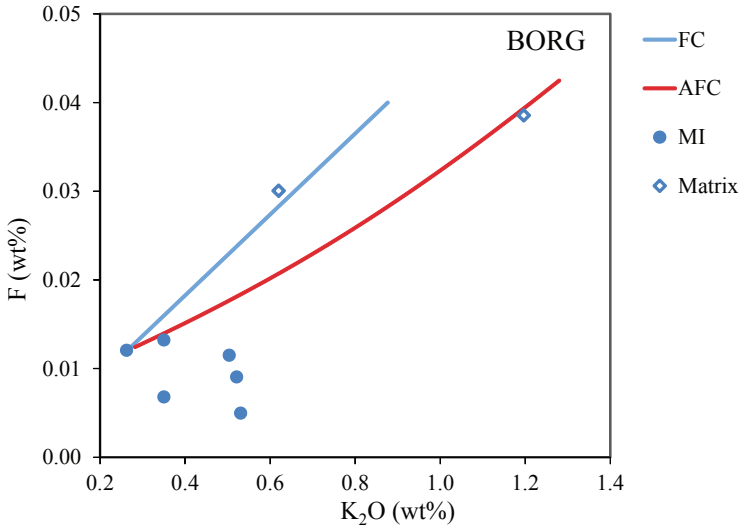
BORG
FC
AFC
MI
Matrix
F (wt%)
K2O (wt%)
0.05
0.04
0.03
0.02
0.01
0.00
0.2
0.4
0.6
0.8
1.0
1.2
1.4

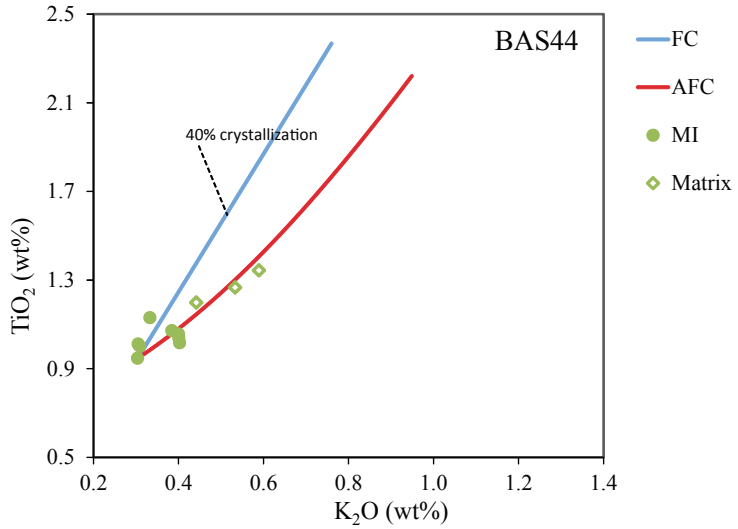
BAS44
40% crystallization
TiO2 (wt%)
K2O (wt%)
2.5
2.1
1.7
1.3
0.9
0.5
0.2
0.4
0.6
0.8
1.0
1.2
1.4

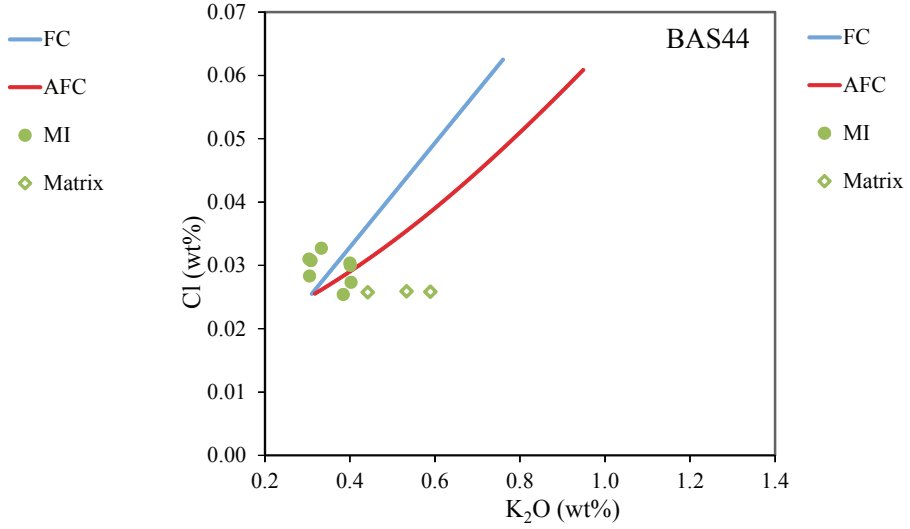
FC
AFC
MI
Matrix

BAS44
Cl (wt%)
K2O (wt%)
0.07
0.06
0.05
0.04
0.03
0.02
0.01
0.00
0.2
0.4
0.6
0.8
1.0
1.2
1.4

FC
AFC
MI
Matrix

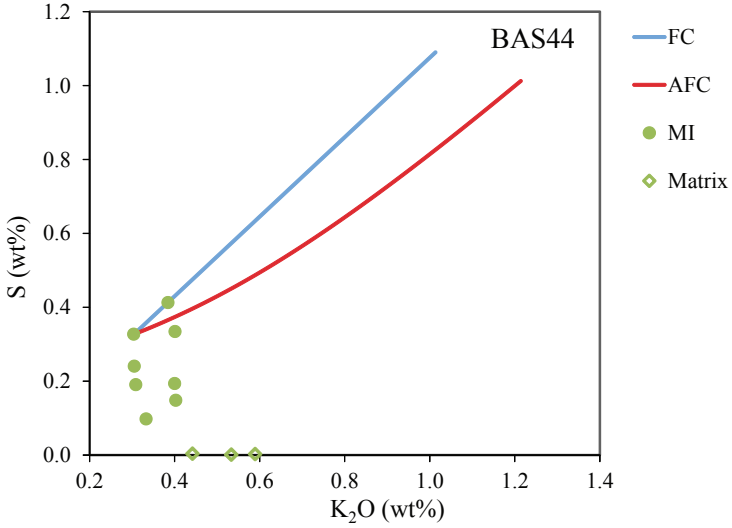
BAS44
S (wt%)
K2O (wt%)
1.2
1.0
0.8
0.6
0.4
0.2
0.0
0.2
0.4
0.6
0.8
1.0
1.2
1.4

FC
AFC
MI
Matrix

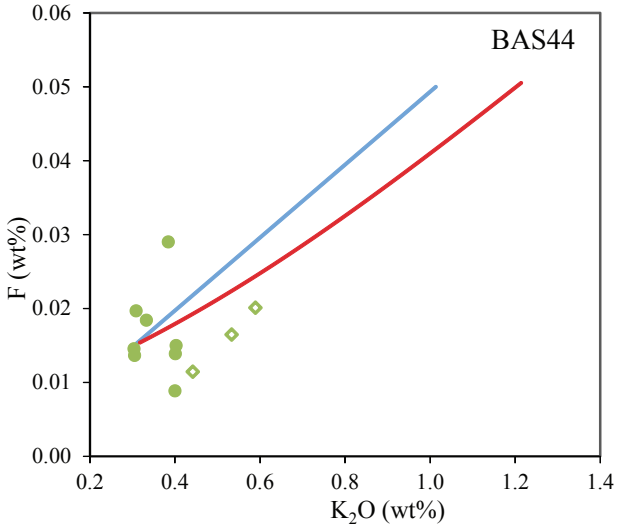
BAS44
F (wt%)
K2O (wt%)
0.06
0.05
0.04
0.03
0.02
0.01
0.00
0.2
0.4
0.6
0.8
1.0
1.2
1.4


FC
AFC
MI
Matrix

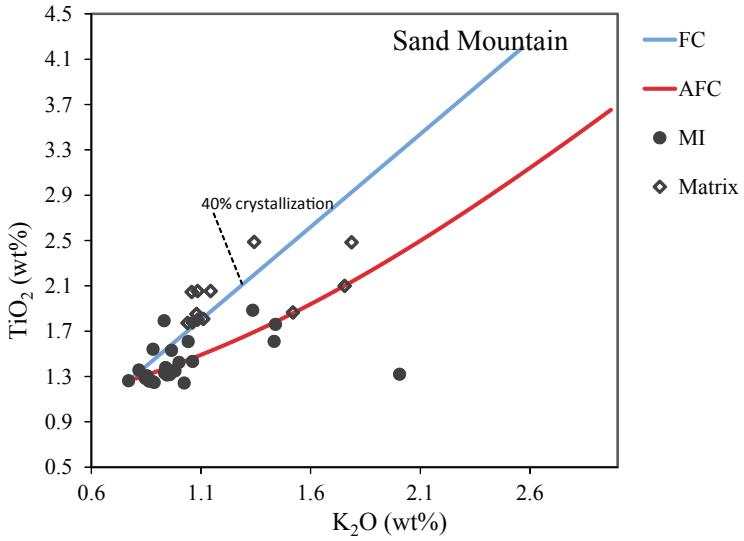
Sand Mountain
40% crystallization
TiO2 (wt%)
K2O (wt%)
FC
AFC
MI
Matrix

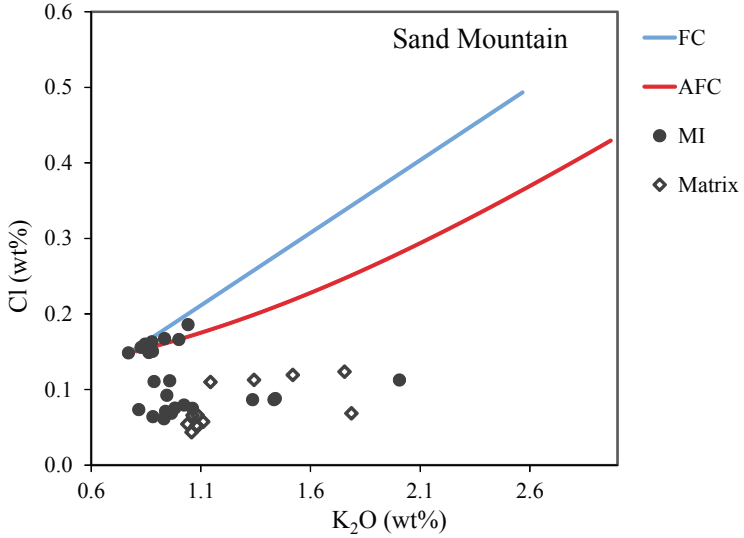
Sand Mountain
Cl (wt%)
K2O (wt%)
FC
AFC
MI
Matrix

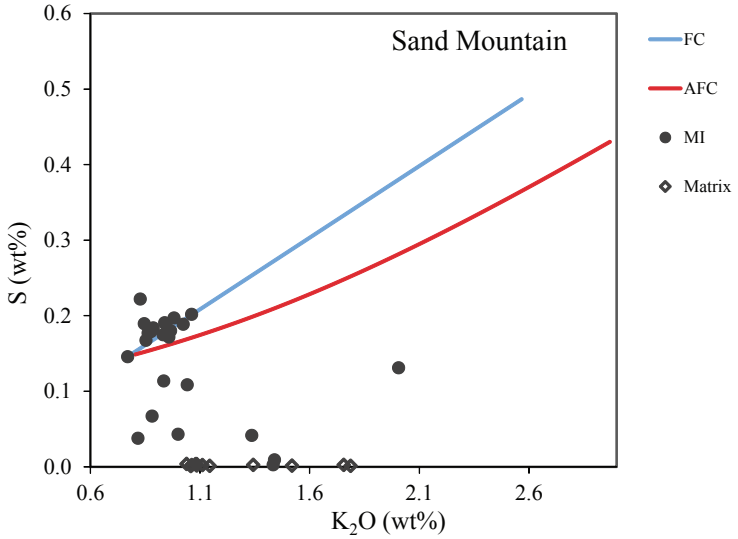
Sand Mountain
S (wt%)
K2O (wt%)
FC
AFC
MI
Matrix

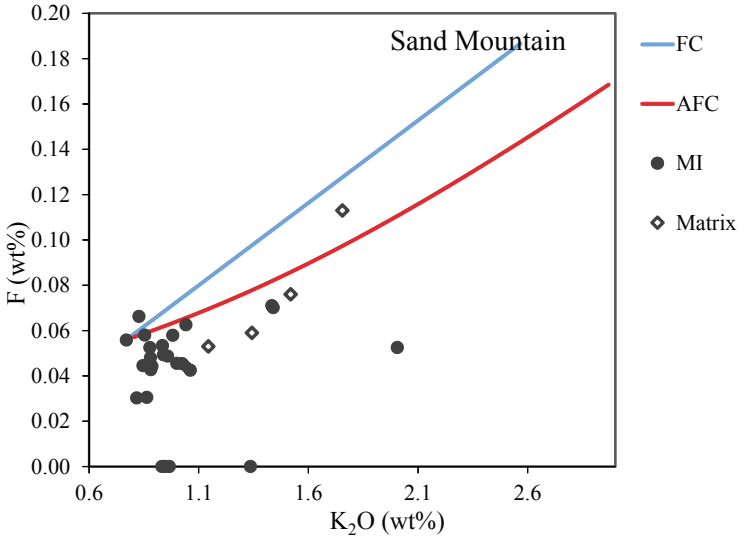
Sand Mountain
F (wt%)
K2O (wt%)
FC
AFC
MI
Matrix

APPENDIX G

MASS OF SO_2, HCL, AND HF DEGASSED DURING EXPLOSIVE ACTIVITY AT SAND MOUNTAIN

	C_{adj} (*wt %*)	C_{matrix} (*wt %*)	V_T (km^3)	**m_T SO_2 (Mt)**	**% degassed**
Sand Mountain	0.253	0.001	0.75	**7.55**	100

	C_{adj} (*wt %*)	C_{matrix} (*wt %*)	V_T (km^3)	**m_T HCl (Mt)**	**% degas**
Sand Mountain	0.252	0.068	0.75	**2.93**	73

	C_{adj} (*wt %*)	C_{matrix} (*wt %*)	V_T (km^3)	**m_T HF (Mt)**	**% degas**
Sand Mountain	0.068	0.053	0.75	**0.28**	23

	% Crystallinity	% Crystal Fractionation
Sand Mountain	25	40

REFERENCES CITED

Aiuppa, A., Franco, A., Von Glasow, R., Allen, A. G., D'Alessandro,W., Mather, T. A., Pyle, D. M., Valenza, M., 2006. The tropospheric processing of acidic gases and hydrogen sulphide in volcanic gas plumes as inferred from field and model investigations. Atmospheric Chemistry and Physics. http://hal.archives-ouvertes.fr/hal-00296172.

Bacon, C. R., Bruggman, P. E., Christiansen, R. L., Clynne, M. A., Donnelly-Nolan, J. M., Hildret, W., 1997. Primitive magmas at five Cascades volcanic fields: Melts from hot, heterogeneous sub-arc mantle. Canadian Mineralogist. 35, 397-424.

Bebbington, M., Cronin, S., 2011. Spatio-temporal hazard estimation in the Auckland Volcanic Field, New Zealand, with a new event-order model. Bulletin of Volcanology. 73, 55-72

Belin, I. L.M.B., 2010. Gas Migration through crystal-rich mafic volcanic systems and application to Stromboli Volcano, Aeolian Islands, Italy. University of Oregon, PhD Dissertation.

Borg, L. E., Clynne, M. A., 1998. The petrogenesis of felsic calc-alkaline magmas from the southernmost Cascades, California: Origin by partial melting of basaltic lower crust. Journal of Petrology. 39, 1197-1222.

Carroll, M.R., Rutherford, M.J., 1985. Sulfide and sulfate stability in hydrous silicate melts. Journal of Geophysical Research. 90, C601-C612.

Cashman, K., Sturtevant, B., Papale, P., Navon, O., 2000. Magmatic Fragmentation, in Sigurdsson, H., Houghton, B.F., McNutt, S.R., Rymer, S.R., Stix, J., McBirney, A.R. (eds), Encyclopedia of Volcanoes. Academic Press, San Diego. 421-430.

Clynne, M. A., 2008. Radiocarbon dates from volcanic deposits of the Chaos Crags and Cinder Cone eruptive sequences and other deposits, Lassen Volcanic National Park and vicinity, California. United States Department of the Interior, U.S. Geological Survey, Reston, Va,. http://purl.access.gpo.gov/GPO/LPS96692.

Clynne, M., 2011. Stratigraphy and compositional evolution of Cinder Cone, a composite monogenetic cone in Lassen Volcanic National Park, California, Abstract V13C-2621presented at 2011 Fall Meeting, AGU, San Francisco, Calif., 5-9 Dec.

Connor, C. B., Hill, B. E., Winfrey, B., Franklin, N. M., Femina, P. C. L., 2001. Estimation of Volcanic Hazards from Tephra Fallout. Natural Hazards Review. 2, 33-42.

Connor, C.B., Conway, F.M., 2000. Basaltic Volcanic Fields, in Sigurdsson, H., Houghton, B.F., McNutt, S.R., Rymer, S.R., Stix, J., McBirney, A.R. (eds), Encyclopedia of Volcanoes. Academic Press, San Diego. 331-343.

Conrey, R. M., Sherrod, D. R., Hooper, P. R., Swanson, D. A., 1997. Diverse primitive magmas in the Cascade arc, northern Oregon and southern Washington. The Canadian Mineralogist. 35, 367-396.

Coote, G. E., Cutress, T. W., Suckling, G. W., 1997. Uptake of fluoride into developing sheep teeth, following the 1995 volcanic eruption of Mt Ruapehu, New Zealand. Nuclear Instruments and Methods in Physics Research. Section B, Beam Interactions with Materials and Atoms. 130, 571-575.

Cronin, S. J., Neall, V., Le Cointre, J., Hedley, M., Loganathan, P., 2003. Environmental hazards of fluoride in volcanic ash: a case study from Ruapehu volcano, New Zealand. Journal of Volcanology and Geothermal Research. 121, 271-291.

Cronin, S., Sharp, D., 2002. Environmental impacts on health from continuous volcanic activity at Yasur (Tanna) and Ambrym, Vanuatu. International Journal of Environmental Health Research. 12, 109-123.

Davidson, A.W., Weinstein, L.H., 2006. Some problems relating to fluorides in the environment: Effects on plants and animals, in Tressaud, A. (ed), Fluorine and the environment: atmospheric chemistry, emissions, and lithosphere. Elsevier, Amsterdam, 251-298.

Deligne, N. I., 2012. After the flow: Landscape response to the emplacement of Holocene lava flows, central Oregon Cascades, USA. University of Oregon, PhD Dissertation.

Delmelle, P., Delfosse, T., Delvaux, B., 2003. Sulfate, chloride and fluoride retention in Andosols exposed to volcanic acid emissions. Environmental Pollution. 126, 445-457.

Delmelle, P., Stix, J., Baxter, J., Garcia-Alvarez, J., Barquero, J., 2002. Atmospheric dispersion, environmental effects and potential health hazard associated with the low-altitude gas plume of Masaya volcano, Nicaragua. Bulletin of Volcanology. 64, 423-434.

Di Traglia, F., Cimarelli, C., De Rita, D., Gimento Torrente, D., 2009. Changing eruptive styles in basaltic explosive volcanism: Examples from Croscat complex scoria cone, Garrotxa Volcanic Field (NE Iberian Peninsula). Journal of Volcanology and Geothermal Research. 180, 89-109.

Donovan ,J.J., Lowers, H.A., Rusk, B.G., 2011. Improved electron probe microanalysis of trace elements in quartz. American Mineralogist. 96, 274-282.

EPA (Environmental Protection Agency), 2012. Vertical Motion and Atmospheric Stability. Air Pollution Training Institute.

http://yosemite.epa.gov/oaqps/eogtrain.nsf/ae20ef1becae534385256b4100770781/1c9d492b7ccef4fe85256b6d0064b4ee/$FILE/Lesson%204.pdf. Accessed September 20, 2012.

Erlund, E.J., Cashman, K.V., Wallace, P.J., Rosi, M., Johnson, E., Delgado Granados, H., 2010. Compositional evolution of magma from Parícutin Volcano, Mexico: The tephra record. Journal of Volcanology and Geothermal Research. 197, 167-187.

Gilbert, J. S., Lane, S. J., Sparks, R. S. J., Koyaguchi, T., 1991. Charge measurements on particle fallout from a volcanic plume. Nature. 349, 598-600.

Guenther, C.F.K., 2010. Guassian Point Source. Universidad de São Paulo. http://www.lete.poli.usp.br/Guenther/aula_4/Plumes.pdf. Accessed September 17, 2012.

Guffanti, M., Clynne, M., Smith, J., Muffler, L., Bullen, T., 1990. Late Cenozoic volcanism, subduction, and extension in the Lassen region of California, southern Cascade Range. Journal of Geophysical Research. 95:B12, 19,453-19,464.

Hanna, S. R., 1981. Handbook on atmospheric diffusion models. Oak Ridge, TN, National Oceanic and Atmospheric Administration.

Hansell, A. L., Horwell, C.J., Oppenheimer, C., 2006. The health hazards of volcanoes and geothermal areas. Occupational and Environmental Medicine. 63, 149-156.

Hansell, A, Oppenheimer, C., 2004. Health hazards from volcanic gases: a systematic literature review. Archives of Environmental Health. 59, 628-39.

Hartmann, G., Wedepohl, K., 1993. The composition of peridotite tectonites from the Ivrea Complex, northern Italy: Residues from melt extraction. Geochimica Et Cosmochimica Acta. 57:8, 1761-1782.

Heggie, T., 2009. Geotourism and volcanoes: Health hazards facing tourists at volcanic and geothermal destinations. Travel Medicine and Infectious Disease. 7, 257-261.

Heliker, C. C., Swanson, D. A., & Takahashi, T. J., 2003. The Pu‘u ‘Ō‘ō-Kūpaianaha eruption of Kīlauea Volcano, Hawai‘i: The first 20 years. U.S. Dept. of the Interior, U.S. Geological Survey, Reston, Va.

Hildreth, W., 2007. Quaternary magmatism in the Cascades: Geologic perspectives. U.S. Department of the Interior, U.S. Geological Survey, Reston, Va.

Hill, B. E., Connor, C. B., 1998. 1995 eruptions of Cerro Negro volcano, Nicaragua, and risk assessment for future eruptions. Geological Society of America Bulletin. 110, 1231-1241.

Hillman, S. E., Horwell, C. J., Densmore, A. L., Damby, D. E., Fubini, B., Ishimine, Y., Tomatis, M., 2012. Sakurajima volcano: a physico-chemical study of the health

consequences of long-term exposure to volcanic ash. Bulletin of Volcanology. 74, 913-930.

Hintz, A.R., Valentine, G.A., 2012. Complex plumbing of monogenetic scoria cones: New insights from the Lunar Crater Volcanic Field (Nevada, USA). Journal of Volcanology and Geothermal Research. 239-240, 19-32.

Horwell, C., Baxter, P., 2006. The respiratory health hazards of volcanic ash: A review for volcanic risk mitigation. Bulletin of Volcanology. 69, 1-24.

Hughes, S., 1990. Mafic magmatism and associated tectonism of the central High Cascade Range, Oregon. Journal of Geophysical Research. 95, 19,623-19,638.

Hughes, S. S., Taylor, E. M., 1986. Geochemistry, petrogenesis, and tectonic implications of central High Cascade mafic platform lavas. Geological Society of America Bulletin. 97, 1024-1046.

Jambon, A., 1994 Earth degassing and large-scale geochemical cycling of volatile elements in Carroll M.R., Holloway, J.R (eds), Volatiles in Magmas. Reviews in Mineralogy. 30, 479-517.

Johnson, E.R., Wallace, P.J., Cashman, K.V., Granados, H.D., Kent, A.J.R., 2008. Magmatic volatile contents and degassing-induced crystallization at Volcán Jorullo, Mexico: Implications for melt evolution and the plumbing systems of monogenetic volcanoes. Earth and Planetary Science Letters. 269, 477-486.

Keating, G., Valentine, G., Krier, D., Perry, F., 2008. Shallow plumbing systems for small-volume basaltic volcanoes. Bulletin of Volcanology. 70, 563-582.

Kirby, S. H., Wang, K., Dunlop, S., 2002. The Cascadia subduction zone and related subduction systems: Seismic structure, intraslab earthquakes and processes, and earthquake hazards. U.S. Dept. of the Interior, U.S. Geological Survey, Menlo Park. U.S. Geological Survey open-file report, 02-328.

Kirby, S.H., Wang, K., 2002. Introduction to a global systems approach to Cascadia slab processes and associated earthquake hazards in Kirby, S. H., Wang, K., Dunlop, S (eds), The Cascadia subduction zone and related subduction systems seismic structure, intraslab earthquakes and processes, and earthquake hazards. U.S. Dept. of the Interior, U.S. Geological Survey, Menlo Park, CA. 5-8.

Le Voyer, M.L., Rose-Koga, E.F., Laubier, M., Schiano, P., 2008. Petrogenesis of arc lavas from the Rucu Pichincha and Pan de Azucar volcanoes (Ecuadorian arc): Major, trace element, and boron isotope evidences from olivine-hosted melt inclusions. Geochemistry, Geophysics, Geosystems. 9, 1-27.

Le Voyer, M., 2009. Rôle des fluides dans la genèse des magmas d'arcs: analyses in situ des éléments volatils et des isotopes du bore dans les inclusions magmatiques des

olivines primitives. Université Blaise Pascal – Clermont-Ferrand II, PhD Dissertation.

Le Voyer, M., Rose-Koga, E.F., Schiano, P., Shimizu, N., Grove, T.L., 2010. Two contrasting H_2O-rich components in primary melt inclusions from Mount Shasta. Journal of Petrology. 51, 1571-1595.

Leeman, W. P., Lewis, J. F., Evarts, R. C., Conrey, R. M., Streck, M. J., 2005. Petrologic constraints on the thermal structure of the Cascades arc. Journal of Volcanology and Geothermal Research. 140, 19,561-19,582.

Leeman, W., Smith, D., Hildreth, W., Palacz, Z., Rogers, N., 1990. Compositional diversity of Late Cenozoic basalts in a transect across the southern Washington Cascades: Implications for subduction zone magmatism. Journal of Geophysical Research. 95:B12, 19,561-19,582.

Love, G., Scott, V. D., 1983. Quantitative electron-probe microanalysis. Halsted Press, Chichester, West Sussex, England.

Marks, J. K., 2012. Physical volcanology of the 1666 C.E. Cinder Cone eruption, Lassen Volcanic National Park, CA. University of Oregon, Masters Thesis.

Mather, T. A., Pyle, D. M., Oppenheimer, C., 2003. Tropospheric volcanic aerosol. Geophysical Monograph. 139, 189-212.

McKay, D., 2012. Recent mafic eruptions at Newberry Volcano and in the central Oregon Cascades: Physical volcanology and implications for hazards. University of Oregon, PhD Dissertation.

McKnight, S. B., Williams, S. N., 1997. Old cinder cone or young composite volcano?: The nature of Cerro Negro, Nicaragua. Geology. 25, 339-342.

Metrich, N., 1990. Chlorine and fluorine in tholeiitic and alkaline lavas of Etna (Sicily). Journal of Volcanology and Geothermal Research. 40, 133-148.

Metrich, N., Wallace, P., 2008. Volatile abundances in basaltic magmas and their degassing paths tracked by melt inclusions. Reviews in Mineralogy and Geochemistry. 69, 363-402.

Miyashiro, A., 1974. Volcanic rock series in island arcs and active continental margins. American Journal of Science. 274, 321-355.

Muffler, L.J.P., Clynne, M.A., Calvert, A.T., Champion, D.E., 2011. Diverse, discrete, mantle-derived batches of basalt erupted along a short normal fault zone: The poison lake chain, southernmost Cascades. Bulletin of the Geological Society of America. 123, 2177-2200.

Münker, C., Wörner, G., Yogodzinski, G., Churikova, T., 2004. Behaviour of high field strength elements in subduction zones: Constraints from Kamchatka–Aleutian arc lavas. Earth and Planetary Science Letters. 224, 275-293.

Occupational Health and Safety Administration (OSHA), 1989. OSHA--Final rule. Air contaminants--permissible exposure limits, (Title 29 Code of Federal Regulations Part 1910.1000). U.S. Department of Labor, Occupational Safety and Health Administration. American Industrial Hygiene Association Journal. 50, 257-93.

Ort, M.H., Elson, M.D., Anderson, K.C., Duffield, W.A., Hooten, W.A., Champion, D.E., Waring, G., 2008. Effects of scoria-cone eruptions upon nearby human communities. Geological Society of America Bulletin. 120, 476-486.

Óskarsson, N., 1980. The interaction between volcanic gases and tephra: Fluorine adhering to tephra of the 1970 Hekla eruption. Journal of Volcanology and Geothermal Research. 8, 251-266.

Parfitt, E. A., Wilson, L., 1995. Explosive volcanic eruptions-IX. The transition between Hawaiian-style lava fountaining and Strombolian explosive activity. Geophysical Journal International. 121, 226-232.

Pioli, L., Erlund, E., Johnson, E., Cashman, K., Wallace, P., Rosi, M., Delgado Granados, H. 2008. Explosive dynamics of Violent Strombolian eruptions: The eruption of Parícutin Volcano 1943-1952 (Mexico). Earth and Planetary Science Letters. 271, 359-368.

Pioli, L., Azzopardi, B.J., Cashman, K.V., 2009. Controls on the explosivity of scoria cone eruptions: Magma segregation at conduit junctions. Journal of Volcanology and Geothermal Research. 186, 407-415.

Pioli, L., Bonadonna, C., Azzopardi, B., Phillips, J., Ripepe, M., 2012. Experimental constraints on the outgassing dynamics of basaltic magmas. Journal of Geophysical Research. 117, B03204 1-17.

Portnyagin, M., Hoernle, K., Plechov, P., Mironov, N., Khubunaya, S., 2007. Constraints on mantle melting and composition and nature of slab components in volcanic arcs from volatiles (H2O, S, Cl, F) and trace elements in melt inclusions from the Kamchatka Arc. Earth and Planetary Science Letters. 255, 53-69.

Portnyagin, M. V., Hoernle, K., Mironov, N. L., 2012. Contrasting compositional trends of rocks and olivine-hosted melt inclusions from Cerro Negro volcano (Central America): implications for decompression-driven fractionation of hydrous magmas. International Journal of Earth Sciences. DOI: 10.1007/s00531-012-0810-3

Rhoades, D. A., Dowrick, D. J., Wilson, C. J. N., 2002. Volcanic hazard in New Zealand: Scaling and attenuation relations for tephra fall deposits from Taupo Volcano. Natural Hazards. 26, 147-174.

Roedder, E., 1984. Fluid Inclusions. Chelsea, MI, BookCrafters, Inc.

Roggensack, K., Hervig, R. L., McKnight, S. B., Williams, S. N., 1997. Explosive Basaltic Volcanism from Cerro Negro Volcano: Influence of Volatiles on Eruptive Style. Science. 277, 1639-1642.

Rowe, M. C., Kent, A. J. R., Nielsen, R. L., 2009. Subduction influence on oxygen fugacity and trace and volatile elements in basalts across the Cascade Volcanic Arc. Journal of Petrology. 50, 61-91.

Rubin, C.H., Noji, E.K., Seligman, P.J., Holtz, J.L., Grande, J., Vittani, F., 1994. Evaluating a fluorosis hazard after a volcanic eruption. Archives of Environmental Health. 49, 395-401.

Rudnick R. L., Gao S., 2003. Composition of the continental crust in Rudnick, R. L., Holland, H.D., Turekian, K.K. (eds.), The Crust, Treatise on Geochemistry. Elsevier, Oxford. 3, 1-64.

Ruscitto, D.M., Wallace, P.J., Johnson, E.R., Bindeman, I.N., Kent, A.J.R., 2010. Volatile contents of mafic magmas from cinder cones in the central Oregon High Cascades: Implications for magma formation and mantle conditions in a hot arc. Earth and Planetary Science Letters. 298, 153-161.

Ruscitto, D.M., 2011. Magmatic volatile contents and explosive cinder cone eruptions in the High Cascades: Recent volcanism in central Oregon and northern California. University of Oregon, PhD Dissertation.

Sawyer, G.M., Oppenheimer, C., 2006. Volcanic fluorine emissions: Observations by Fourier Transform Infrared Spectroscopy, in Tressaud, A. (ed), Fluorine and the environment: atmospheric chemistry, emissions, and lithosphere. Amsterdam, Elsevier, 165-185.

Schick, J. D., 1994. Origin of compositional variability of the lavas at Collier Cone, High Cascades, Oregon. University of Oregon, Masters Thesis.

Schmidt, M.E., Grunder, A.L., 2009. The evolution of North Sister: A volcano shaped by extension and ice in the central Oregon Cascade Arc. Bulletin of the Geological Society of America. 121, 643-662.

Sherrod, D.R., Taylor, E.M., Ferns, M.L., Scott, W.E., Conrey, R.M., Smith, G.A., 2004. Geologic map of the Bend 30- x 60-Minute Quadrangle, Central Oregon. United States Department of the Interior, U.S. Geological Survey, Geologic Investigations Series I-2683.

Spilliaert, N., Metrich, N., Allard, P., 2006. S-Cl-F degassing pattern of water-rich alkali basalt: Modelling and relationship with eruption styles on Mount Etna volcano. Earth and Planetary Science Letters. 248, 772-786.

Stern, R. J., 2002. Subduction zones. Reviews of Geophysics. 40, 3.1-3.38.

Stoiber, R. E., Rose, W. I., 1973. Cl, F, and SO_2 in Central American volcanic gases. Bulletin Volcanologique. 37, 454-460.

Sisson, S. M., Layne, G. D., 2003. The systematics of chlorine, fluorine, and water in Izu arc front volcanic rocks: Implications for volatile recycling in subduction zones. Geochimica Et Cosmochimica Acta. 67, 4179-4203.

Strong, M., Wolff, J., 2003. Compositional variations within scoria cones. Geological Society of America Bulletin. 31, 143-146.

Suttle, N., 2010. Mineral nutrition of livestock. CABI, Wallingford, UK.

Taylor, E. M., 1990. Volcanic history and tectonic development of the central High Cascade Range, Oregon. Journal of Geophysical Research. 95, 19611-19622.

Textor, C., Sachs, P. M., Graf, H.F., Hansteen, T. H., 2003. The 12900 years BP Laacher See eruption: Estimation of volatile yields and simulation of their fate in the plume. Geological Society Special Publication. 213, 307-328.

Thordarson, T., 1979. On the damage caused by volcanic eruptions with special reference to tephra and gases, in Sheets, P. D., Grayson, D. K., Volcanic activity and human ecology. New York, Academic Press, pp. 125-159

Thordarson, T., Self, S., Oskarsson, N., Hulsebosch, T., 1996. Sulfur, chlorine, and fluorine degassing and atmospheric loading by the 1783-1784 AD Laki (Skaftar Fires) eruption in Iceland. Bulletin of Volcanology. 58, 205-225.

Till, C. B., Grove, T. L., Withers, A. C., 2012. The beginnings of hydrous mantle wedge melting. Contributions to Mineralogy and Petrology. 163, 669-688.

Trehu, A. M., Asudeh, I., Brocher, T. M., Luetgert, J. H., Mooney, W. D., Nabelek, J. L., Nakamura, Y., 1994. Crustal Architecture of the Cascadia Forearc. Science. 266, 237-243.

United States Geological Survey, 2000. How old is "Cinder Cone"?: Solving a mystery in Lassen Volcanic National Park, California. United States Department of the Interior, U.S. Geological Survey, Reston, Va,.

Vergniolle, S., Mangan, M., 2000. Hawaiian and Strombolian Eruptions, in Sigurdsson, H., Houghton, B.F., McNutt, S.R., Rymer, S.R., Stix, J., McBirney, A.R. (eds), Encyclopedia of Volcanoes. Academic Press, 447-461.

Vespermann, D., Sschmincke, H., 2000. Scoria cones and tuff rings, in Sigurdsson, H., Houghton, B.F., McNutt, S.R., Rymer, S.R., Stix, J., McBirney, A.R. (eds), Encyclopedia of Volcanoes. Academic Press, 683-694.

Vigouroux, N., Wallace, P. J., Kent, A. J. R., 2008. Volatiles in high-K magmas from the Western Trans-Mexican Volcanic Belt: Evidence for fluid fluxing and extreme enrichment of the mantle wedge by subduction processes. Journal of Petrology. 49, 1589-1618.

Wade, J. A., Plank, T., Melson, W. G., Soto, G. J., Hauri, E. H., 2006. The volatile content of magmas from Arenal volcano, Costa Rica. Journal of Volcanology and Geothermal Research. 157, 94-120.

Wallace, P.J., 2003. From mantle to atmosphere: Magma degassing, explosive eruptions, and volcanic volatile budgets in De Vivo, B. Bodnar, R.J. (eds), Melt inclusions in volcanic systems: methods, applications, and problems. Elsevier, Amsterdam, 105.

Wallace, P. J., 2005. Volatiles in subduction zone magmas: concentrations and fluxes based on melt inclusion and volcanic gas data. Journal of Volcanology and Geothermal Research. 140, 217-240.

Wallace, P., Anderson Jr., A.T., 2000. Volatiles in magmas, in Sigurdsson, H., Houghton, B.F., McNutt, S.R., Rymer, S.R., Stix, J., McBirney, A.R. (eds), Encyclopedia of Volcanoes. Academic Press, 149-170.

Wallace, P. J., Carmichael, I. S. E., 1994. S speciation in submarine basaltic glasses as determined by measurements of S K-alpha X-ray. American Mineralogist. 79, 161-167.

Wallace, P., Edmonds, M., 2011. The sulfur budget in magmas: Evidence from melt inclusions, submarine glasses, and volcanic gas emissions. Reviews in Mineralogy and Geochemistry. 73, 215-246.

Wedepohl, K. H., 1995. The composition of the continental crust. Geochimica Et Cosmochimica Acta. 59, 1217-1232.

Wells, R.E., Blakely, R.J., Weaver, C.S., 2002. Cascadia microplate models and within-slab earthquakes in Kirby, S. H., Wang, K., Dunlop, S (eds), The Cascadia subduction zone and related subduction systems seismic structure, intraslab earthquakes and processes, and earthquake hazards. United States Department of the Interior, U.S. Geological Survey, Menlo Park, CA, 17-23.

Wilson, T.M., Cole, J.W., Wardman, J., Wilson, G., Barnard, S.T., Stewart, C., Leonard, G.S., Johnston, D.M., Sword-Daniels, V., 2012. Volcanic ash impacts on critical infrastructure. Physics and Chemistry of the Earth. 45-46, 5-23.

Witham, C., 2005. Volcanic disasters and incidents: A new database. Journal of Volcanology and Geothermal Research. 148, 191-233.

WHO Study Group on recommended health-based occupational exposure limits for respiratory irritants, (1984). Recommended health-based occupational exposure limits for respiratory irritants. World Health Organization Technical Report Series. World Health Organization, Geneva. 707, 1-154.

Wohletz, K., Heiken, G., 1992. Volcanology and geothermal energy. University of California Press, Berkeley.